The Dissertation Committee for Benjamin Peirce Holder
certifies that this is the approved version of the following dissertation:

Coherent control of cold atoms in a optical lattice

Committee:

Linda Reichl, Supervisor

Qian Niu

Mark Raizen

Jack B. Swift

Robert E. Wyatt

Coherent control of cold atoms in a optical lattice

by

Benjamin Peirce Holder, BA

Dissertation

Presented to the Faculty of the Graduate School of

The University of Texas at Austin

in Partial Fulfillment

of the Requirements

for the Degree of

Doctor of Philosophy

The University of Texas at Austin

May 2007

Acknowledgments

I am extremely grateful for the guidance and support of my advisor, Linda Reichl. She has given me great freedom in my research, patiently allowing me to seek out the topics which I found most interesting and fully supporting me in that venture. When I have encountered obstacles, she has always been available to talk and has often provided the key insight to get me started again. Perhaps most importantly, she has helped to guide my work in a direction that gives it context within the greater scientific community. In short, Linda has been all I could have hoped for in an advisor.

I owe a great debt to Vladimir Strelnitski of the Maria Mitchell Observatory, for setting me on this course. Ten years ago, during a summer undergraduate research program, he ignited my interest in physics research with projects on astrophysical turbulence. He is the most curious and passionate scientist I have met, the most patient and inspiring teacher, and a tireless advocate for his students. I hope that I may live a fraction of my life by his example.

I would also like to thank my friends and colleagues here in Austin and elsewhere. Saša has not only been a great friend, but also a great teacher, from whom I learned how to "do physics". Regina has been a dependable reassuring presence for me since our first days "on island." And to Biny, Brian, César, Kavan, Mandi, Rachel, Rosie, Riva, the Tees Family ... thanks a bunch. The environment at the Center for Complex Quantum Systems has been a great place to work over

the past four years. Annie Harding has always provided invaluable and friendly assistance. I'm also grateful to Professors Antoniewicz, Gleeson, Jogee and Moore for providing me with some wonderful teaching opportunities during my time here in Austin.

Finally, thanks to my family for their support of my endless schooling. My parents have always been supportive of my path and confident in my continued progress. With their lives as an example, I have always believed that I can become whoever I want to be and things will work out. Molly and Sam, you are both a source of pride and inspiration for me. And lastly, thanks to my grandparents, each of whose life has served as a model for my own.

<div align="right">

Benjamin Peirce Holder

</div>

The University of Texas at Austin
May 2007

Coherent control of cold atoms in a optical lattice

Publication No. _____

Benjamin Peirce Holder, Ph.D.

The University of Texas at Austin, 2007

Supervisor: Linda Reichl

The dynamics of non-interacting, ultracold alkali atoms in the presence of counter-propagating lasers (optical lattice systems) is considered theoretically. The center of mass motion of an atom in such a system can be described by an effective Hamiltonian of a relatively simple form. Modulation of the laser fields implies a parametric variation of the effective Hamiltonian's eigenvalue spectrum, under which avoided crossings may occur. We investigate two dynamical processes arising from these near-degeneracies, which can be manipulated to coherently control atomic motion. First, we demonstrate the mechanism for the chaos-assisted, or multiple-state, tunneling observed in recent optical lattice experiments. Second, we propose a new method for the coherent acceleration of lattice atoms using the techniques of

stimulated Raman adiabatic passage (STIRAP). In each case we use perturbation analysis to show the existence of a small, few level, subsystem of the full effective Schrödinger equation that determines the dynamics.

Contents

Chapter 1

Introduction

Over the past twenty years, a wealth of theoretical and experimental techniques have been developed which allow for the coherent manipulation of neutral atoms with laser fields. The techniques of laser cooling and trapping, for which a Nobel Prize was given in 1997 (see [14; 70] and references therein), have allowed for the isolation of atoms from thermal effects which had previously made their study impossible. In fact, modern techniques allow for the preparation of a non-interacting cloud of alkali atoms with an effective temperature well below the single photon recoil temperature $k_B T_r \equiv (\hbar k_L)^2/2M$ (k_L is the wavevector of the laser used for cooling and trapping and M is the mass of the atom) [40; 6]. Once cooled and trapped, pairs of laser fields can be applied to the cloud of atoms to form a one-dimensional "optical lattice" in which the center of mass dynamics of an individual atom is described by an effective Hamiltonian with a relatively simple form [27]. This system is therefore a laboratory, or more precisely an *ensemble* of laboratories, for studying the dynamics of a single quantum particle. It is this laboratory which will be the focus of the theoretical work presented here.

   The effective Hamiltonians we will study in this dissertation, and the optical lattice systems which they describe, will be one-dimensional and time-dependent,

consisting of a kinetic energy term for the center of mass atomic motion plus an effective potential describing the atom-lattice interaction (see Chapter 2). Because of the harmonic nature of the laser fields creating the optical lattice, the effective potentials will be periodic in both space and time. Additionally, the cooling techniques mentioned above allow for the preparation of a cloud of atoms with very nearly zero momentum when compared to the two-photon interaction with the lattice lasers. Therefore, solutions of the effective Schrödinger equation will be spatially-periodic functions which can be written in the Floquet form of a time-periodic function multiplied by an exponential in time (see Chapter 3). It will be shown that the dynamics can then be described by a "time-independent" Floquet Hamiltonian, which acts in an extended Hilbert space with time considered to be an additional *coordinate*. The eigenvectors and eigenvalues of this Floquet Hamiltonian will serve as the dynamical structure in which we study atoms trapped in the optical lattice.

The focus of this dissertation will be on the quantum dynamics of systems for which the eigenvalues of the Floquet Hamiltonian are nearly degenerate. These near degeneracies can occur at chance avoided crossings, where the adiabatic variation of a parameter in the Floquet Hamiltonian (induced by variation of the laser amplitudes) brings two or more eigenvalues into near intersection. Alternatively, a near degeneracy can be consciously created by harmonically coupling the eigenvalues of an "unperturbed" system (e.g. Rabi oscillations). These two types of eigenvalue interactions provide the underlying mechanism for the two quantum phenomena we analyze in this work; the former allows for "chaos-assisted tunneling" and the latter for the coherent acceleration of atoms by stimulated Raman adiabatic passage (STIRAP).

The dissertation is organized as follows. The derivation of an effective Hamiltonian for atoms in an optical lattice is given in Chapter 2, with a description of some experimentally achievable effective potentials. Chapter 3 contains a description

of the primary theoretical tools for the quantum and classical analysis of effective Hamiltonians. Floquet theory is presented in detail, including a description of the extended Hilbert space and analysis utilizing the Floquet matrix approach. A brief overview of classical Hamiltonian systems and the approach to chaos is also given in this chapter, as well as a technique for comparing the "phase space dynamics" of quantum systems to their classical counterparts. An example system is used to demonstrate the techniques. The main original results of this dissertation are presented in Chapters 4 and 5, which contain the analysis of chaos-assisted tunneling in an optical lattice experiment and the proposal of a new technique for coherent acceleration of lattice atoms, respectively. A few appendices have been included either to provide reference on a particular subject or to separate a section of the analysis from the main body in the interest of continuity.

In the remaining part of this introductory chapter, we discuss a few simple examples of quantum dynamics in the vicinity of eigenvalue degeneracies. Although the processes are well-known and the presentation is heuristic, reviewing these simple model systems here will allow us to present many concepts essential to the work in the following chapters without the need for much technical machinery. Our purpose in this presentation is to unite the dynamics of three familiar quantum systems: two-state tunneling, avoided crossings of eigenvalues, and Rabi oscillations. Specifically, it will be seen that the model system of an avoided crossing can be used to describe the other two phenomena exactly. The importance of that fact in the context of this dissertation is that the dynamical processes of chaos-assisted tunneling and STIRAP-like transitions for cold atoms have an underlying universality in the near-degeneracy of eigenvalues.

1.1 Dynamics in nearly-degenerate model systems

The simplest investigations of quantum mechanical phenomena involve two and three-level model systems. Without doubt, these are crude approximations of the full energy structure of most quantum mechanical objects. However, for single-particle systems (or collections of non-interacting particles, like the optical lattice systems considered in this dissertation) many interesting quantum mechanical processes observed in the full system dynamics can be reduced to exactly these models in the limit of some small perturbation. For systems which cannot be described with perturbation theory, these models can often be used as an approximate guide for understanding the dynamics.

The connection of these models to degeneracies in eigenvalue spectra is intrinsic. In the perturbation approach, sets of unperturbed eigenstates with degenerate or nearly degenerate eigenvalues must be considered collectively when constructing a zeroth-order eigenstate of the perturbed system (the well-known method of "degenerate perturbation theory"). Thus, the intersection or near-intersection of two or three unperturbed eigenvalues leads to two or three-level Hamiltonian matrices in the perturbed system, which are isolated subsystems of the full dynamics in the limit of small perturbation. In a more general system, not readily described by a perturbation approach, an isolated avoided crossing of two eigenvalue curves under the variation of a parameter can be modeled by a two-level system. Each avoided crossing can be associated to nearby degeneracies (branch points) of the complex energy surface, when the parameter is allowed to take complex values [86; 87; 32; 33].

The focus of this section is on the dynamical evolution of states involved in near-degenerate interaction. It will be seen that the presence of near-degeneracies in the eigenvalue spectrum introduces Schrödinger's cat-like superpositions of underlying basis states. This is most obvious in the case of avoided crossings, where eigenstates in the region of interaction are superpositions of the two associated eigen-
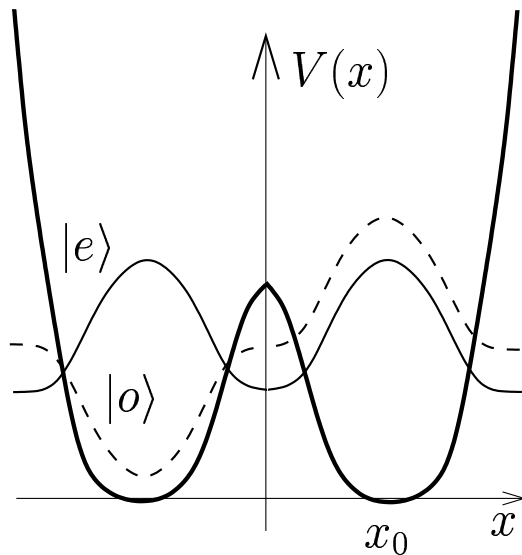
Figure 1.1: An example of two-state tunneling. The two lowest energy eigenstates of a symmetric double well potential are an opposite-parity, nearly-degenerate doublet. A state prepared in either the left or right well, constructed as a superposition of these two eigenstates, will oscillate between the two wells with frequency proportional to the energy spacing Δ.

states asymptotically far from the avoided crossing. What makes these interactions interesting is that the underlying basis states are often of the type easily explained classically (e.g. via semi-classical quantization methods [75; 18; 41; 30]) and the superposition of such states leads to purely quantum behavior. The most familiar dynamics of this type is two-state tunneling (see next section), where the preparation of a state in one-side of a double well potential leads to oscillatory tunneling between the wells. Other examples include chaos-assisted tunneling and stimulated Raman adiabatic passage which are the focus of this dissertation.

1.1.1 Two-state tunneling

Perhaps the most familiar quantum mechanical process related to near-degeneracies in eigenvalue spectra is that of two-state tunneling. This phenomenon is a common

example in elementary studies of quantum mechanics because it provides such a simple description of fundamentally non-classical dynamics: quantum states which can be described classically as "contained" in some region of phase space by energetic or dynamical barriers (i.e. KAM tori) evolve unhindered through these barriers. Our reason for presenting this model here, however, is that its existence is a necessary condition for the process of "chaos-assisted tunneling" described in Chapter 4.

The symmetric double-well potential, shown in Figure 1.1, is a typical system in which two-state tunneling occurs. The lowest energy eigenstates of this system are an opposite-parity doublet $\{|e\rangle, |o\rangle\}$, which have a small energy splitting $\Delta \equiv E_o - E_e$ determined by the height of the barrier at $x = 0$. We can define two states

$$|\pm\rangle = \frac{1}{\sqrt{2}} \left(|e\rangle \pm |o\rangle\right) , \tag{1.1}$$

which are localized primarily in either the right or left well at $\pm x_0$. A quantum state initially localized in the left well ($|\psi(t = 0)\rangle = |-\rangle$), will undergo an oscillatory evolution

$$\begin{aligned}
|\psi(t)\rangle &= \frac{1}{\sqrt{2}} \left(e^{-i\frac{E_e t}{\hbar}} |e\rangle - e^{-i\frac{E_o t}{\hbar}} |o\rangle \right) \\
&= \frac{1}{\sqrt{2}} e^{-i\frac{E_e t}{\hbar}} \left(|e\rangle - e^{-i\frac{\Delta t}{\hbar}} |o\rangle \right) ,
\end{aligned} \tag{1.2}$$

such that $|\psi(t = \hbar\pi/\Delta)\rangle \sim |+\rangle$ and the *tunneling frequency* of complete oscillation is $\omega_{tun} = \frac{\Delta}{\hbar}$.

It will be useful, for comparison to the systems in the following sections, to look at the (two-level) Hamiltonian for this system. In the basis of eigenstates, the Hamiltonian matrix H_t is of course diagonal. A unitary transformation to the basis

$\{|\pm\rangle\}$ can be made, yielding the transformed Hamiltonian

$$
\begin{aligned}
H_t' = U H_t U^\dagger &= \frac{1}{2} \begin{pmatrix} 1 & -1 \\ 1 & 1 \end{pmatrix} \begin{pmatrix} E_e & 0 \\ 0 & E_o \end{pmatrix} \begin{pmatrix} 1 & 1 \\ -1 & 1 \end{pmatrix} \\
&= \frac{1}{2} \begin{pmatrix} 2E_{avg} & \Delta \\ \Delta & 2E_{avg} \end{pmatrix},
\end{aligned}
\tag{1.3}
$$

where $E_{avg} = (E_e + E_o)/2$. When viewed in this basis, one can see that the energy splitting of the two eigenstates may be termed a *tunneling coupling* of the states $|\pm\rangle$.

1.1.2 Avoided crossings

We will now consider avoided crossings of energy eigenvalues. It was first shown by von Neumann and Wigner that the variation of a single parameter in a finite-dimensional, general Hermitian matrix cannot create degeneracies in the eigenvalue spectrum ([84]; an outline of their proof is given in Appendix B). A matrix is considered "general" if there are no relations between the matrix elements other than Hermiticity. For instance, if a Hamiltonian has a discrete symmetry of some kind, i.e. it commutes with a parity operator, then it would not be considered general; eigenvalues of opposite parity may cross freely. The eigenvalues of a quantum system without such symmetries, however, or the subset of eigenvalues with the same symmetry properties, will undergo avoided crossings when a single parameter is varied. We will see in this section that these avoided crossings induce a coherent "mixing" of state character which allows for dynamics very similar to the two-state tunneling considered in the previous section.

The two-level model Hamiltonian of an avoided crossing that we will consider

can be written in some basis $\{|\pm\rangle\}$ as

$$H'_{ac} = \frac{1}{2} \begin{pmatrix} X & \Delta \\ \Delta & -X \end{pmatrix} \quad ; \quad X = a\,\kappa, \qquad (1.4)$$

where a and Δ are positive constants and H' is parameterized by $-\infty < \kappa < \infty$ [88]. We can interpret this system as an unperturbed Hamiltonian under which the two basis states have eigenvalues $\pm \frac{a}{2}\kappa$, plus an off-diagonal constant coupling matrix. The two eigenvalues of H' are strictly positive or negative for all values of κ,

$$E_e \equiv +\frac{1}{2}\sqrt{X^2 + \Delta^2} \quad \text{and} \quad E_o \equiv -\frac{1}{2}\sqrt{X^2 + \Delta^2}, \qquad (1.5)$$

and we will write the associated eigenvectors as $|e(\kappa)\rangle$ and $|o(\kappa)\rangle$, respectively (the designation of these states as "even" and "odd" will become clear in what follows). It is easy to see that the closest approach of the eigenvalues, at $\kappa = 0$, is Δ. We can transform the Hamiltonian into the basis of the eigenvectors at this position $\{|e(\kappa = 0)\rangle, |o(\kappa = 0)\rangle\}$ by the inverse of the unitary transformation performed in the previous section:

$$\begin{aligned} H_{ac} \equiv U H'_{ac} U^\dagger &= \frac{1}{4} \begin{pmatrix} 1 & 1 \\ -1 & 1 \end{pmatrix} \begin{pmatrix} X & \Delta \\ \Delta & -X \end{pmatrix} \begin{pmatrix} 1 & -1 \\ 1 & 1 \end{pmatrix} \\ &= \frac{1}{2} \begin{pmatrix} \Delta & -X \\ -X & -\Delta \end{pmatrix}. \end{aligned} \qquad (1.6)$$

Writing the eigenvectors as

$$\begin{aligned} |e(\kappa)\rangle &= c_1^e(\kappa)|e(\kappa = 0)\rangle + c_2^e(\kappa)|o(\kappa = 0)\rangle \\ |o(\kappa)\rangle &= c_1^o(\kappa)|e(\kappa = 0)\rangle + c_2^o(\kappa)|o(\kappa = 0)\rangle, \end{aligned} \qquad (1.7)$$

and using the eigenvalue equation for H, we find that as $\kappa \to -\infty$

$$\lim_{\kappa \to -\infty} \frac{c_1^e}{c_2^e} = \lim_{\kappa \to -\infty} \frac{X}{\Delta - \sqrt{X^2 + \Delta^2}} = 1$$

$$\lim_{\kappa \to -\infty} \frac{c_1^o}{c_2^o} = \lim_{\kappa \to -\infty} \frac{X}{\Delta + \sqrt{X^2 + \Delta^2}} = -1 \,,$$

(1.8)

and, as $\kappa \to \infty$,

$$\lim_{\kappa \to \infty} \frac{c_1^e}{c_2^e} = -1$$

$$\lim_{\kappa \to \infty} \frac{c_1^o}{c_2^o} = 1 \,.$$

(1.9)

Using the unitary transformation above, we can write

$$|e(\kappa = 0)\rangle = \frac{1}{\sqrt{2}} \left(|+\rangle + |-\rangle \right)$$

$$|o(\kappa = 0)\rangle = \frac{1}{\sqrt{2}} \left(|-\rangle - |+\rangle \right) \,,$$

(1.10)

and, considering the above limits, we find that

$$
\begin{array}{cccccc}
& \kappa \to -\infty & & \kappa = 0 & & \kappa \to \infty \\
|e(\kappa)\rangle : & |-\rangle & \to & \frac{1}{\sqrt{2}} \left(|-\rangle + |+\rangle \right) & \to & |+\rangle \\
|o(\kappa)\rangle : & -|+\rangle & \to & \frac{1}{\sqrt{2}} \left(|-\rangle - |+\rangle \right) & \to & |-\rangle \,.
\end{array}
$$

(1.11)

So we see that, as the eigenstates pass through the avoided crossing, they exchange character (see Figure 1.2).

Given the designation of "even" and "odd" it is easy to see that at $\kappa = 0$ the eigenstates have the same form as the two-state tunneling model (here, these states are an even and odd superposition of the asymptotic eigenstates). Therefore the time evolution of a system at $\kappa = 0$, will be identical to that of two-state tunneling: a state prepared in $|+\rangle$ ($|-\rangle$) will evolve to $|-\rangle$ ($|+\rangle$) in time $\hbar\pi/\Delta$, with a tunneling frequency of oscillations $\omega_{tun} = \Delta/\hbar$. By considering $\kappa \neq 0$, we can

9
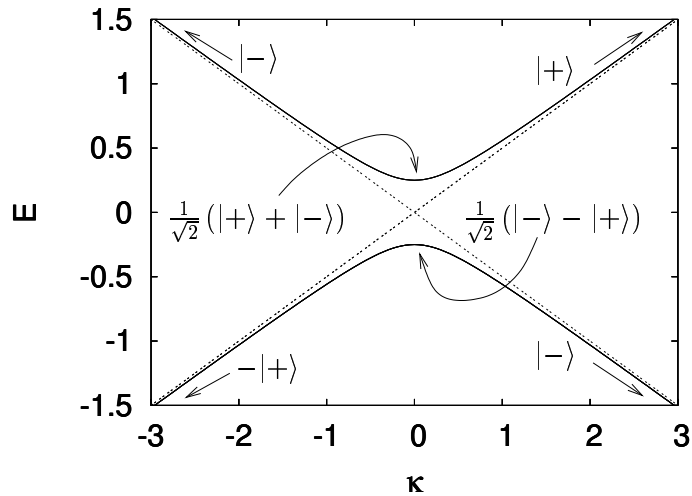
Figure 1.2: The eigenvalues of the avoided crossing model system as a function of the parameter κ ($a = 1; \Delta = 0.5$). The eigenvalues when $\Delta = 0$ are plotted as dotted lines. Eigenstate character, in the basis $\{|+\rangle, |-\rangle\}$ is as indicated by the arrows.

obtain a generalization of the two-state tunneling phenomenon.

The asymptotic behavior seen in Eq. (1.11) suggests assigning an angular dependence to the eigenstates in the $\{|+\rangle, |-\rangle\}$ basis. Specifically, if we write $|e(\kappa)\rangle = c_+^e(\kappa)|+\rangle + c_-^e(\kappa)|-\rangle$, then the functional dependence on κ can be seen as a rotation in this basis:

$$
|e(\kappa)\rangle = \begin{pmatrix} c_+^e(\kappa) \\ c_-^e(\kappa) \end{pmatrix} = R(\theta[\kappa]) \begin{pmatrix} c_+^e(\kappa = 0) \\ c_-^e(\kappa = 0) \end{pmatrix}
$$
$$
\text{with} \quad R(\theta[\kappa]) = \begin{pmatrix} \cos(\theta[\kappa]) & \sin(\theta[\kappa]) \\ -\sin(\theta[\kappa]) & \cos(\theta[\kappa]) \end{pmatrix},
$$

(1.12)

where the dependence $\theta[\kappa]$ is thus far unknown. Using the same rotation to express
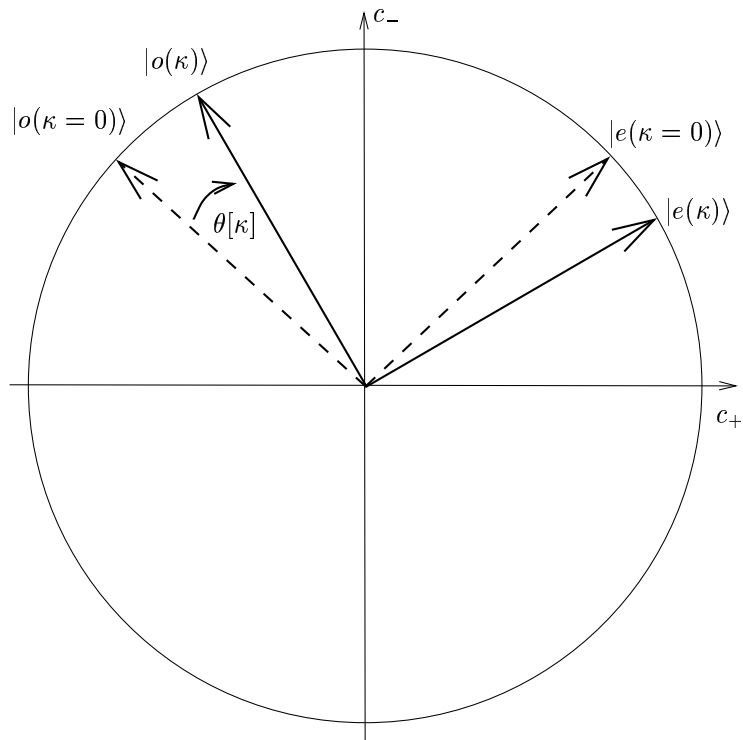
Figure 1.3: Representation of the eigenvectors of the avoided crossing Hamiltonian in the basis $\{|+\rangle, |-\rangle\}$ (plotted on the unit circle). The κ dependence of these eigenvectors can be represented by a rotation $-\pi/4 < \theta < \pi/4$ from the $\kappa = 0$ position.

$|o(\kappa)\rangle$, we obtain

$$
\begin{pmatrix} c_+^e(\kappa) \\ c_-^e(\kappa) \end{pmatrix} = \frac{1}{\sqrt{2}} \begin{pmatrix} \cos(\theta[\kappa]) + \sin(\theta[\kappa]) \\ \cos(\theta[\kappa]) - \sin(\theta[\kappa]) \end{pmatrix} \tag{1.13}
$$

and

$$
\begin{pmatrix} c_+^o(\kappa) \\ c_-^o(\kappa) \end{pmatrix} = \frac{1}{\sqrt{2}} \begin{pmatrix} \sin(\theta[\kappa]) - \cos(\theta[\kappa]) \\ \cos(\theta[\kappa]) + \sin(\theta[\kappa]) \end{pmatrix} . \tag{1.14}
$$

The representation of the eigenvectors in this manner is shown in Figure 1.3. Considering Eq. (1.11), we assume that the dependence takes the following form,

$$
\kappa[\theta] = A \tan(2\theta), \tag{1.15}
$$

implying that $\cos(2\theta) = A/\sqrt{\kappa^2 + A^2}$ and $\sin(2\theta) = \kappa/\sqrt{\kappa^2 + A^2}$. Equating the ratio of the coefficients in Eq. (1.13) to the same ratio determined by solution of the eigenproblem of H', we find

$$
\begin{aligned}
\frac{c_+^e}{c_-^e} &= \frac{1 + \sin(2\theta)}{\cos(2\theta)} = \frac{X + \sqrt{X^2 + \Delta^2}}{\Delta} \\
\frac{\kappa + \sqrt{\kappa^2 + A^2}}{A} &= \frac{\kappa + \sqrt{\kappa^2 + \left(\frac{\Delta}{a}\right)^2}}{\frac{\Delta}{a}} .
\end{aligned} \tag{1.16}
$$

showing that our hypothesis was correct and $A = \Delta/a$. The analogous procedure for the coefficients of $|o(\kappa)\rangle$ confirms this result.

We can now consider the dynamics of a system at $\kappa \neq 0$. Defining the following functions

$$
\begin{aligned}
f(\kappa) &= \frac{1}{\sqrt{2}} \left[\cos(\theta[\kappa]) + \sin(\theta[\kappa]) \right] \\
g(\kappa) &= \frac{1}{\sqrt{2}} \left[\cos(\theta[\kappa]) - \sin(\theta[\kappa]) \right],
\end{aligned} \tag{1.17}
$$

12

and using Eqs. (1.13) and (1.14), we can write the asymptotic eigenstates as

$$|+\rangle = f(\kappa)|e(\kappa)\rangle - g(\kappa)|o(\kappa)\rangle$$
$$|-\rangle = g(\kappa)|e(\kappa)\rangle + f(\kappa)|o(\kappa)\rangle \tag{1.18}$$

for any κ. If we consider a state prepared at $t = 0$ in $|+\rangle$, the time evolution of that state will take the form

$$|\psi(t)\rangle = e^{-\frac{iE_e(\kappa)t}{\hbar}} f(\kappa)|e(\kappa)\rangle - e^{-\frac{iE_o(\kappa)t}{\hbar}} g(\kappa)|o(\kappa)\rangle$$
$$= e^{-\frac{iE_e(\kappa)t}{\hbar}} \left[f(\kappa)|e(\kappa)\rangle - e^{-\frac{i(E_o(\kappa)-E_e(\kappa))t}{\hbar}} g(\kappa)|o(\kappa)\rangle \right] . \tag{1.19}$$

Clearly, this state will have oscillatory evolution with oscillation frequency $\omega_{tun}(\kappa) \equiv \Delta(\kappa)/\hbar$ where $\Delta(\kappa) \equiv E_e(\kappa) - E_o(\kappa)$. However, unlike the two-state tunneling phenomenon, a complete oscillation to $|-\rangle$ will not occur. Rewriting the above equation in terms of $|\pm\rangle$,

$$|\psi(t)\rangle = e^{-\frac{iE_e(\kappa)t}{\hbar}} \left\{ \left[f^2(\kappa) + g^2(\kappa)e^{\frac{i\Delta(\kappa)t}{\hbar}} \right] |+\rangle \right.$$
$$\left. + \left[f(\kappa)g(\kappa) - f(\kappa)g(\kappa)e^{\frac{i\Delta(\kappa)t}{\hbar}} \right] |-\rangle \right\} , \quad (1.20)$$

we see that the occupation probability of state $|-\rangle$,

$$|c_-|^2 = 2f^2(\kappa)g^2(\kappa) \left[1 - \cos\left(\frac{\Delta(\kappa)t}{\hbar} \right) \right]$$
$$= \frac{1}{2} \cos^2(2\theta[\kappa]) \left[1 - \cos\left(\frac{\Delta(\kappa)t}{\hbar} \right) \right] \tag{1.21}$$
$$= \frac{1}{2} \frac{\Delta^2}{(a\kappa)^2 + \Delta^2} \left[1 - \cos\left(\frac{\Delta(\kappa)t}{\hbar} \right) \right] ,$$

has an maximum value which is less than unity for $\kappa \neq 0$. Some examples of this evolution are shown in Figure 1.4.
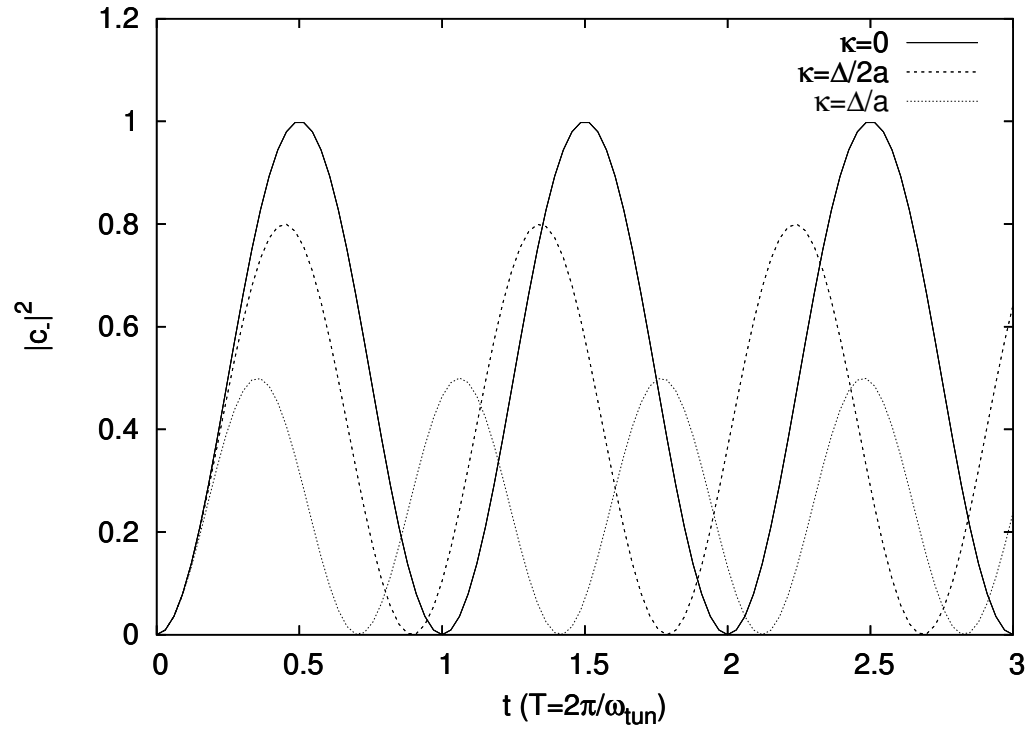
Figure 1.4: Evolution of the occupation probability of $|-\rangle$ for a state initially prepared as $|\psi(t = 0)\rangle = |+\rangle$, plotted as a function of time measured in units of $2\pi/\omega_{tun}(\kappa = 0)$. Full oscillation between the two states is observed at $\kappa = 0$ (solid line), while the dynamics of a system at $|\kappa| = \frac{\Delta}{2a}, \frac{\Delta}{a}$ allows for only an incomplete inversion.

1.1.3 Rabi Oscillations

As a final section of this introductory chapter, we briefly consider the phenomenon of Rabi tunneling, i.e. periodic oscillations in a two-level system, induced by a coherent, mono-chromatic coupling field which has been tuned to the energy spacing of the levels. The Hamiltonian for such a system can be written in the dipole approximation as

$$H_R(t) = E_+|+\rangle\langle+| + E_-|-\rangle\langle-| - d\mathcal{E}_0 \cos(\Omega t)\left[|+\rangle\langle-| + |-\rangle\langle+|\right], \qquad (1.22)$$

where $\mathcal{E}_0$ is the electric field amplitude of the coupling laser field, d is the matrix element of the dipole operator $d \equiv \langle+|\hat{d}|-\rangle = \langle-|\hat{d}|+\rangle$, and Ω is the frequency of the laser's electric field. The energy spacing of the two levels will be written in terms of the frequency $\omega_0 = (E_+ - E_-)/\hbar$. In what follows, we show that this Hamiltonian can be written in exactly the form of the avoided crossing Hamiltonian of the previous section.

A time-dependent unitary transformation,

$$i\hbar\frac{\partial}{\partial t}|\psi(t)\rangle = \hat{H}|\psi(t)\rangle$$
$$\rightarrow i\hbar\frac{\partial}{\partial t}\left[\hat{U}(t)|\psi(t)\rangle\right] = \left[\hat{U}(t)\hat{H}\hat{U}^\dagger(t) + i\hbar\frac{\partial\hat{U}}{\partial t}\hat{U}^\dagger\right]\left[\hat{U}(t)|\psi(t)\rangle\right],$$
$$(1.23)$$

yields a transformed Hamiltonian of the form

$$\hat{H}' \equiv \hat{U}(t)\hat{H}\hat{U}^\dagger(t) + i\hbar\frac{\partial\hat{U}}{\partial t}\hat{U}^\dagger. \qquad (1.24)$$

Thus, by using $\hat{U}_1(t) = \exp\left[i/\hbar\left(E_+|+\rangle\langle+| + E_-|-\rangle\langle-|\right)t\right]$, we can eliminate the

zero-field evolution, resulting in a new Hamiltonian

$$\hat{H}'_R = -d\mathcal{E}_0 \cos(\Omega t) \left[e^{i\omega_0 t}|+\rangle\langle-| + e^{i\omega_0 t}|+\rangle\langle-| \right]$$
$$= -\frac{d\mathcal{E}_0}{2} \left[\left(e^{i(\omega_0+\Omega)t} + e^{i(\omega_0-\Omega)t} \right)|+\rangle\langle-| + \left(e^{-i(\omega_0-\Omega)t} + e^{-i(\omega_0+\Omega)t} \right)|-\rangle\langle+| \right] .$$

$$(1.25)$$

At this point it is customary to make the rotating wave approximation and disregard the rapidly oscillating terms (see Section C.1.2). We can then write the Hamiltonian as

$$\hat{H}'_R = -\frac{d\mathcal{E}_0}{2} \left[e^{i\delta t}|+\rangle\langle-| + e^{-i\delta t}|-\rangle\langle+| \right] .$$

$$(1.26)$$

where we have defined the detuning of the laser from the transition frequency as $\delta = \omega_0 - \Omega$. One final time-dependent unitary transformation, using $\hat{U}_2(t) = \exp\left[i\left(\frac{\delta}{2}|-\rangle\langle-| - \frac{\delta}{2}|+\rangle\langle+| \right) t \right]$, results in a *time-independent* Hamiltonian of the form

$$\hat{H}''_R = \frac{\hbar\delta}{2}|+\rangle\langle+| - \frac{\hbar\delta}{2}|-\rangle\langle-| - \frac{d\mathcal{E}_0}{2} \left[|+\rangle\langle-| + |-\rangle\langle+| \right] .$$

$$(1.27)$$

Writing this in matrix form, in the basis $\{|+\rangle, |-\rangle\}$, we obtain

$$H_R = \frac{\hbar}{2} \begin{pmatrix} \delta & -\frac{d\mathcal{E}_0}{\hbar} \\ -\frac{d\mathcal{E}_0}{\hbar} & -\delta \end{pmatrix} ,$$

$$(1.28)$$

which is equivalent to the avoided crossing model when $\kappa a = \hbar\delta$ and $\Delta = -d\mathcal{E}_0$. The "tunneling frequency" of oscillations for resonant tuning of the laser ($\delta = 0$) is called the *Rabi oscillation frequency*, $\omega_R \equiv \frac{d\mathcal{E}_0}{\hbar}$. For near-resonant tuning of the laser, the dynamics of a particle prepared in either the ground or excited state will be the same as that shown in Figure 1.4. When $\delta = \omega_R$ (the case of $\kappa a = \Delta$ in Figure 1.4), the inversion of population is only $\sim$50 % efficient.

16

Floquet analysis of the Rabi system

As a final remark, we mention that the Rabi model system in Eq. (1.28) can be derived from Eq. (1.26) by means of Floquet theory. Thus, this system can be used to demonstrate a technique which will be used throughout our analysis in Chapters 4 and 5: the transformation of a time-periodic Hamiltonian system to a time-independent one, by the consideration of time as a coordinate rather than a parameter. We present the method briefly here, reserving a more complete description for Chapter 3.

The Hamiltonian H'_R is periodic in time with period $T = 2\pi/\delta$ and therefore any solution to its associated Schrödinger equation can be written in the form

$$|\psi_\alpha(t)\rangle = \mathrm{e}^{-i\frac{\epsilon_\alpha t}{\hbar}}|\phi_\alpha(t)\rangle \quad \text{with} \quad |\phi_\alpha(t+T)\rangle = |\phi_\alpha(t)\rangle\,, \tag{1.29}$$

where ϵ_α is called the Floquet eigenvalue and $|\phi_\alpha\rangle$ the Floquet eigenstate. If this solution is plugged into the Schrödinger equation, we obtain an eigenvalue equation for the *Floquet Hamiltonian*:

$$\hat{H}_{F,R}|\phi_\alpha\rangle = \left[\hat{H}_R + \hat{q}\right]|\phi_\alpha\rangle = \epsilon_\alpha|\phi_\alpha\rangle\,, \tag{1.30}$$

where the operator $\hat{q}$ and its normalized eigenvectors are defined by the equation

$$\langle t|\hat{q}|q\rangle = -i\hbar\frac{\partial}{\partial t}\langle t|q\rangle = q\hbar\delta\langle t|q\rangle \quad \to \quad \langle t|q\rangle = \frac{1}{\sqrt{T}}\mathrm{e}^{iq\delta t}\,(q \in \mathbb{Z})\,. \tag{1.31}$$

The Floquet Hamiltonian is a Hermitian operator in an extended Hilbert space which includes time as a coordinate. Defining $|n = \pm1\rangle \equiv |\pm\rangle$, the states $\{|n, q\rangle = |n\rangle \otimes |q\rangle\}$ form a basis in the extended space. In this basis, the Floquet Hamiltonian matrix

has the form

$$\langle\langle n, q | \hat{H}_{F,R} | n', q' \rangle\rangle = \hbar q \delta \; \delta_{n,n'} \delta_{q,q'}$$
$$- d\mathcal{E}_0 \left[\delta_{n',-1} \delta_{n,+1} \delta_{q-q',1} + \delta_{n',+1} \delta_{n,-1} \delta_{q-q',-1} \right] , \quad (1.32)$$

where it is customary to write the inner product in the extended space with double brackets and we have used

$$\langle q | e^{\pm i \delta \hat{t}} | q' \rangle = \int_{-T/2}^{T/2} \langle q | t \rangle e^{\pm i \delta t} \langle t | q' \rangle dt = \delta_{q-q',\pm 1} . \quad (1.33)$$

The central region of this matrix is shown in Figure 1.5, where it is seen to be block diagonal. Each 2×2 block governs the dynamics of a pair of Floquet eigenstates whose eigenvalues fall in a particular "zone" of width $\hbar \delta$. It will be shown in Chapter 3 that a physical state $|\psi\rangle$ can be described by the Floquet states in any single zone. Therefore, we may choose any block to understand the dynamics. Any block in Figure 1.5 is identical to the matrix in Eq. (1.28), up to an additive constant which will not affect the system dynamics.

It is interesting to note that the Hamiltonian in Eq. (1.22) is also time-periodic. Therefore Floquet theory could be applied before the rotating wave approximation is made. In that case, the system is not analytically solvable. However, if one applies perturbation theory to the resulting Floquet Hamiltonian, the simple model in Eq. (1.28) can be derived as a subsystem of the full dynamics in the limit that $d\mathcal{E}_0 \to 0$. This is precisely the method used in Chapter 5 when deriving a STIRAP model for atoms in a harmonically modulated optical lattice.

		$q' = -1$		$q' = 0$		$q' = 1$	
		$n' = +1$	-1	$n' = +1$	-1	$n' = +1$	-1
$q = -1$	$n = +1$	$-\hbar\delta$	0	0	0	0	
	$n = -1$	0	$-\hbar\delta$	$-d\mathcal{E}_0$	0		
$q = 0$	$n = +1$	0	$-d\mathcal{E}_0$	0	0	0	0
	$n = -1$	0	0	0	0	$-d\mathcal{E}_0$	0
$q = 1$	$n = +1$	0		0	$-d\mathcal{E}_0$	$\hbar\delta$	0
	$n = -1$			0	0	0	$\hbar\delta$

Figure 1.5: The central section of the infinite-dimensional Floquet Hamiltonian $\hat{H}_{F,R}$ of the Rabi two-level system in the basis $|n, q\rangle$. The matrix is block-diagonal, where each 2×2 block (for example the region outlined in bold) corresponds to a "zone" of Floquet eigenvalues and is dynamically equivalent to the system in Eq. 1.28.

Chapter 2

Effective Hamiltonians for ultracold atoms

The object of analysis for the work presented in this dissertation is the effective Hamiltonian describing the interaction of alkali atoms with a pair (or multiple pairs) of counter-propagating lasers. These lasers are assumed to be strongly detuned from a particular electronic transition, which allows for the adiabatic elimination of the internal energy structure, resulting in the effective Hamiltonian for the center of mass dynamics of atoms in the ground state of that transition [27]. This Hamiltonian, for the one-dimensional case of lasers propagating in the x-direction, has the following form,

$$\hat{H}_{eff}(x,t) = \frac{\hat{p}_x^2}{2m} + V_{eff}(x,t)\,, \tag{2.1}$$

where the effective potential V_{eff} depends on the particular choice of laser frequencies and describes a space and time-dependent "light shift" of the ground state energy. Because of the harmonic nature of the laser fields, the effective potential will be periodic in both space and time and we can therefore describe this type of system as an "optical lattice." In this chapter we will present a derivation of the

effective Hamiltonian and provide a few examples of the types of effective potentials which are achievable.

Although our primary purpose in this dissertation is to analyze quantum dynamics in systems of the simple form shown in Eq. (2.1), it must be noted that such systems would not be possible to study without the myriad developments of modern laser-cooling techniques over the past 20 years. As is noted by Chu in his review of the subject, the dipole force responsible for the coherent interaction of atoms and light is "too feeble even to overcome random thermal motions at room temperature" [14]. Moreover, the dynamics we hope to describe using the effective Hamiltonian involve atomic motions on the order of the recoil momentum of the atom. Therefore, the preparation of an experimental system which is accurately described by such a Hamiltonian requires cooling atoms below this limit. A description of these cooling techniques is beyond the scope of this work, though an overview of some key developments and the theoretical underpinnings are given in Appendix C. The interested reader is directed to the following references [6; 14; 35; 40; 79].

2.1 Derivation of the effective Hamiltonian

In this section, we show how the effective Hamiltonian can be used to describe an experimental system of lasers impinging on non-interacting alkali atoms. This analysis involves the consideration of a two-level subsystem of the atom's electronic levels, application of the rotating-wave approximation, and adiabatic elimination of the excited level, to obtain a spatially and temporally-periodic potential for atoms in the ground state.

We begin by considering the Hamiltonian of this two level system, in dipole interaction with a z-polarized classical electric field:

$$H = H_{atom} + H_{int} \,, \tag{2.2}$$

with

$$H_{atom} = \hbar\omega_{at}|e\rangle\langle e| + \frac{p_x^2}{2m}\left(|e\rangle\langle e| + |g\rangle\langle g|\right) , \tag{2.3}$$

and

$$H_{int} = -dE_z(x,t)\left(|e\rangle\langle g| + |g\rangle\langle e|\right) , \tag{2.4}$$

where $\hbar\omega_{at}$ is the energy spacing of the two levels, p_x is the atomic momentum operator in the x-direction, and $d \equiv \langle e|\hat{d}_z|g\rangle = \langle g|\hat{d}_z|e\rangle$ is the dipole matrix element coupling the ground state $|g\rangle$ to the excited state $|e\rangle$. The total electric field amplitude $E_z(x,t)$ is assumed to be the superposition of the electric fields due to N lasers, all polarized along the z direction, so that

$$E_z(x,t) = \sum_{j=1}^{N} E^{(j)} \cos\left[(k_L + \frac{\delta k_j}{2})x + \sigma_j(\omega_L + \frac{\delta\omega_j}{2})t + \phi_j\right] \tag{2.5}$$

where $E^{(j)}$ is the amplitude of the jth laser, ω_L is a positive reference frequency and k_L its corresponding wavenumber, σ_j can be ± 1, and $\delta k_j = \delta\omega_j/c$ (the usefulness of this form will be evident below). We can then write

$$E_z(x,t) = A(x,t)\,\mathrm{e}^{-i\omega_L t} + A^{\star}(x,t)\,\mathrm{e}^{i\omega_L t} , \tag{2.6}$$

with

$$A(x,t) = \sum_{j} \frac{E^{(j)}}{2} \exp\left\{-i\sigma_j\left[(k_L + \frac{\delta k_j}{2})x + \sigma_j\frac{\delta\omega_j}{2}t + \phi_j\right]\right\} . \tag{2.7}$$

Under a time-dependent unitary transformation of the Schrödinger equation, the Hamiltonian transforms like

$$H \to U\,H\,U^{\dagger} + i\hbar\frac{\partial U}{\partial t}\,U^{\dagger} . \tag{2.8}$$

Using the unitary matrix

$$U = \exp\left[i\omega_L \left|e\right\rangle\left\langle e\right| t\right] , \qquad (2.9)$$

to transform to the rotating frame of the laser leaves the Hamiltonian as

$$H = \hbar\Delta\left|e\right\rangle\left\langle e\right| + \frac{p_x^2}{2m}(\left|e\right\rangle\left\langle e\right| + \left|g\right\rangle\left\langle g\right|)$$
$$- d\, E_z(x,t)\left(\left|e\right\rangle\left\langle g\right|e^{i\omega_L t} + \left|g\right\rangle\left\langle e\right|e^{-i\omega_L t}\right) , \quad (2.10)$$

where $\Delta = \omega_{at} - \omega_L$ is the detuning of the reference laser frequency from the atomic transition.

Let us now insert E_z from Eq. (2.6) and make the rotating wave approximation by neglecting terms with high-frequency exponential dependence (i.e. $e^{\pm i2\omega_L t}$). The Hamiltonian then takes the form

$$H = \hbar\Delta\left|e\right\rangle\left\langle e\right| + \frac{p_x^2}{2m}(\left|e\right\rangle\left\langle e\right| + \left|g\right\rangle\left\langle g\right|) - d\left(A(x,t)\left|e\right\rangle\left\langle g\right| + A^\star(x,t)\left|g\right\rangle\left\langle e\right|\right) . \quad (2.11)$$

Writing an arbitrary state $\left|\psi\right\rangle = \psi_g(x,t)\left|g\right\rangle + \psi_e(x,t)\left|e\right\rangle$, the Schrödinger equation can be written

$$i\hbar\frac{\partial\psi_g}{\partial t} = -\frac{\hbar^2}{2m}\frac{\partial^2}{\partial x^2}\psi_g - dA^\star(x,t)\psi_e \qquad (2.12)$$

$$i\hbar\frac{\partial\psi_e}{\partial t} = -dA(x,t)\psi_g + \left(\hbar\Delta - \frac{\hbar^2}{2m}\frac{\partial^2}{\partial x^2}\right)\psi_e . \qquad (2.13)$$

Adiabatic elimination of the excited state is performed by assuming that the detuning of the laser Δ is large enough to allow us to neglect the time and space derivatives of the excited state. Thus, atoms prepared in the ground state will remain there and we are left with an *effective Hamiltonian* for their evolution:

$$i\hbar\frac{\partial\psi_g}{\partial t} = H_{eff}\,\psi_g \quad ; \quad H_{eff} = \frac{p_x^2}{2m} - \frac{d^2|A(x,t)|^2}{\hbar\Delta} . \qquad (2.14)$$

Although we have treated the electric field classically so far, it is interesting to point out that the effective potential here, commonly called the "light shift," can be considered a two photon transition from the ground state to the ground state. The interaction is treated more rigorously in Appendix C where it can be seen that the potential results from the absorption of a photon from one laser and the stimulated emission of a photon due to interaction with the other laser. Because the lasers are counter-propagating, the atom acquires a two photon momentum "kick."

2.2 Effective potentials and their experimental achievement

The particular form of $A(x, t)$, and therefore the effective potential, will depend on the choice of lasers. In the case of two counter-propagating lasers with equal frequencies, the electric field can be written $E_z(x, t) = E_0 \left[\cos(k_L x - \omega_L t) + \cos(k_L x + \omega_L t) \right]$, and $A(x) = (E_0/2) \cos(k_L x)$. Therefore the effective Hamiltonian will have the form of a stationary standing wave

$$H_{eff} = \frac{p_x^2}{2m} - \frac{d^2 E_0^2}{4\hbar\Delta} \cos(2k_L x) , \qquad (2.15)$$

where we have neglected a constant offset of the energy. We will call this simplest type of optical lattice system the *quantum pendulum*. It should be noted here that, as long as all pairs of lasers are tuned to approximately the same carrier frequency ω_L, the effective potential will always have periodic spatial dependence with period $2\pi/(2k_L)$. This is equivalent to saying that momentum transfer between the lattice lasers and the atoms occurs in discrete units of $2\hbar k_L$ and is a consequence of the two photon transition described above.

Two counter-propagating lasers with slightly offset frequencies ($E^{(1)} = E^{(2)} \equiv E$; $\delta\omega_1 = -\delta\omega_2 \equiv \delta\omega$; $\sigma_1 = -\sigma_2$; $\phi_1 = \phi_2 = 0$) will produce a traveling periodic

potential:

$$A_{trav}(x,t) = \frac{E}{2}\left\{ e^{i\left[(k_L + \frac{\delta k}{2})x - \frac{\delta \omega}{2}t\right]} + e^{-i\left[(k_L - \frac{\delta k}{2})x - \frac{\delta \omega}{2}t\right]} \right\}$$

$$\rightarrow \quad |A_{trav}(x,t)|^2 \sim \frac{E^2}{2}\cos(2k_L x - \delta \omega t). \quad (2.16)$$

If we combine these two pairs of lasers, we create an effective potential with two resonances (a system required for the STIRAP analysis in Chapter 5):

$$H = \frac{p_x^2}{2m} - \frac{d^2 E^2}{2\hbar\Delta}\left[\cos(2k_L x) + \cos(2k_L x - \delta \omega \, t)\right]. \quad (2.17)$$

It is clear, however, that the $|A(x,t)|^2$ for such a system will also contain unwanted cross-terms, which we have neglected in writing Eq. (2.17). In order to minimize the effect of these cross terms, we offset the carrier frequency of the second pair of lasers by some amount $\Delta\omega$ ($E^{(1)} = E^{(2)} = E^{(3)} = E^{(4)} \equiv E$; $\delta\omega_1 = \delta\omega_2 = 0$; $\delta\omega_3 = \Delta\omega + \delta\omega$; $\delta\omega_4 = \Delta\omega - \delta\omega$; $\sigma_1 = \sigma_3 = -\sigma_2 = -\sigma_4$; and $\phi_i = 0 \,\forall\, i$), where $\omega_L \gg \Delta\omega \gg \delta\omega$. This yields,

$$|A_{two-res}(x,t)|^2 \sim \frac{E^2}{2}\left[\cos(2k_L x) + \cos(2k_L x - \delta \omega t)\right.$$

$$\left. + \cos(\Delta k x)\cos(\Delta\omega t) + \cos(2k_L x)\cos(\Delta\omega t)\right], \quad (2.18)$$

where $\Delta k = \Delta\omega/c$ and we have retained only the highest-order terms in the frequencies and wavenumbers (e.g. $\delta\omega$ is neglected in the presence of $\Delta\omega$). The last two terms in this equation present high-frequency oscillations, depending on the particular value of $\Delta\omega$.

As a concrete example, we can consider a system of cesium atoms whose energy level structure is shown in Figure 2.1. In references [78; 80], the laser light was detuned by $\Delta \sim 10^{11}$Hz from the D_2 line ($\omega_L \sim 10^{15}$Hz) and a modulation of $\delta\omega \sim 10^5$Hz was applied to the standing lattice to affect travelling terms in the
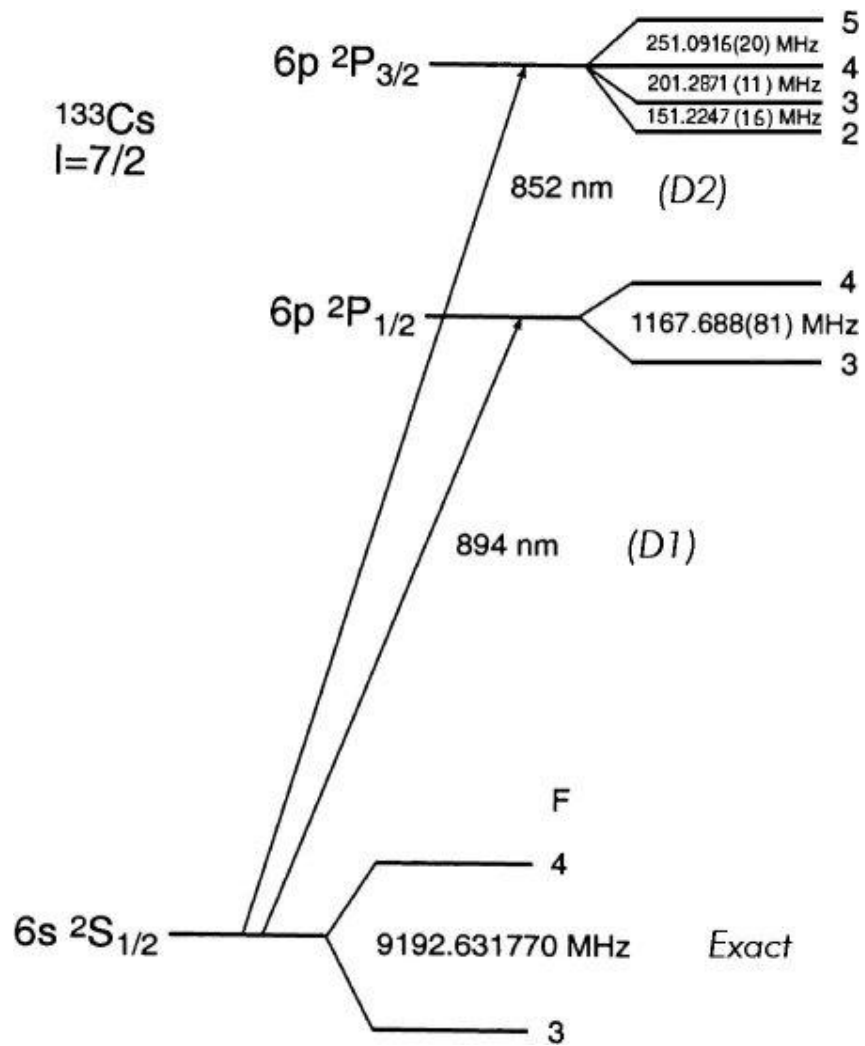
Figure 2.1: The energy structure for cesium atoms. (Reproduced from [10])

effective potential. Therefore, an offset of the carrier frequency for the second pair of lasers in the hundreds of MHz will satisfy $\Delta >> \Delta\omega >> \delta\omega$, and allow one to safely neglect the last two terms in the square brackets of Eq. (2.18) [73].

2.3 Dimensionless form of the effective Hamiltonian and spatially periodic solutions

In Chapters 4 and 5, it will be useful to work with dimensionless units. We use this section to introduce our particular choice of non-dimensionalization and explain why this is a natural choice given the experimental setup.

As a concrete example system we consider the two-resonance system in Eq. (2.17) of the previous section. We change to dimensionless variables (p', x', H', t', ω') as follows. Let $p' = \frac{p_x}{2\hbar k_L}$, $x' = 2k_L x$, $H' = \frac{1}{4\hbar\omega_r}H$, $t' = 4\omega_r t$, and $\omega' = \frac{1}{4\omega_r}\delta\omega$ where the recoil frequency of an atom is $\omega_r = \frac{\hbar k_L^2}{2m}$. The Hamiltonian in Eq. (2.17) then takes the form

$$H' = \left(p'\right)^2 + \kappa \left[\cos\left(x'\right) + \cos\left(x' + \omega't\right)\right] \tag{2.19}$$

where $\kappa \equiv -\frac{d^2 E^2}{4\omega_r \hbar^2 \Delta}$. The effective Planck's constant in the associated Schrödinger equation is unity. It is important to note that in these dimensionless units, changes in momentum due to the interaction of an atom with the lasers are integer-valued. Moreover, experimental techniques allow for the preparation of atoms in a very narrow range of momentum values with $|\langle p_x \rangle| << 2\hbar k_L$ [40; 78; 80]. Therefore, the eigenvalues of the dimensionless momentum operator will take only integer values, i.e. $\hat{p}'|n\rangle = n|n\rangle$ with $n \in \mathbb{Z}$. This discretization of allowed momentum values implies that solutions of the associated Schrödinger equation are spatially periodic.

Chapter 3

Theoretical tools

In this chapter we discuss some of the theoretical tools for analysis of the effective Hamiltonian. The first section concerns Floquet analysis, i.e. the solution of the Schrödinger equation when the effective Hamiltonian is a periodic function of time. As we have already mentioned, all of the optical lattice systems we will study in this dissertation have this property and the tools of Floquet analysis will be vitally important for the work presented in the final two chapters. In the second section of this chapter we discuss some methods for comparing a particular quantum system to its classical analog. This will be important for two reasons. First, many of the phenomena we will consider in the following chapters are of interest because of their fundamental departure from classical behavior. The tunneling behavior observed in the experiment described in Chapter 4 is a purely quantum effect and it will be important to identify those quantum states which have some classical analog and those which do not. Similarly, the coherent acceleration of atoms described in Chapter 5 involves the transport of atoms through dynamical barriers in the classical phase space, but the initial and final states each have simple classical analogs. The second reason for developing methods to compare classical and quantum systems is to determine the influence of underlying classical phase space dynamics on the quantum

systems. In the limit of small effective Planck's constant and integrability of the classical Hamiltonian this influence is trivial: quantum states lie on the classical orbit structures. For departures from this limit, however, one can study the influence of underlying classical chaos on the corresponding quantum dynamics, i.e. "quantum chaos."

3.1 Periodic time dependence and Floquet Theory

Here, we present an overview of the techniques used to analyze time-periodic systems. The foundation of these methods is Floquet's theorem [22; 59; 77; 76]. Mathematically, in a very general sense, the theorem states that the problem of solving a system of linear, first-order, ordinary differential equations with time-periodic coefficients can be reduced to solving a system of linear equations with constant coefficients. For the case of the Schrödinger equation, the theorem can be stated as follows. Given a Hamiltonian periodic in time with period T, $\hat{H}(t+T) = \hat{H}(t)$, any solution to the corresponding Schrödinger equation can be written in the form

$$|\psi_\alpha(t)\rangle = \mathrm{e}^{-i\frac{\epsilon_\alpha t}{\hbar}}|\phi_\alpha(t)\rangle \quad \text{with} \quad |\phi_\alpha(t+T)\rangle = |\phi_\alpha(t)\rangle. \tag{3.1}$$

The time-periodic state $|\phi_\alpha(t)\rangle$ is called a Floquet eigenstate and the real number ϵ_α a Floquet eigenvalue (the latter is sometimes also referred to as a quasienergy or Floquet eigenphase).

In the following, we present a proof of Floquet theory for the Schrödinger equation and a description of an extended Hilbert space in which the Floquet states live. This extended space will allow us to apply all of the tools for studying time-independent systems to a time-periodic system. Most important for Chapters 4 and 5, we will be able to use the methods of time-independent perturbation theory. As a final subsection here we present the (t, t') method as a means of parameterizing

a Floquet Hamiltonian by time. This separation of time into two independent variables, which also involves the use of an extended Hilbert space, will allow us in Chapter 5 to determine "time-evolution" of a Floquet Hamiltonian.

3.1.1 A proof of Floquet theory for the time-dependent Schrödinger equation

We consider the time-dependent Schrödinger Equation for a system described by a Hamiltonian which is periodic in both space and time:

$$i\hbar\frac{\partial}{\partial t}|\psi(t)\rangle = \hat{H}|\psi(t)\rangle \quad ; \quad H(x,t) = H(x,t+T) = H(x+2\pi,t)\,. \tag{3.2}$$

Writing a solution of this equation in the form

$$|\psi(t)\rangle = \exp\left[-\frac{iat}{\hbar}\right]|\psi'(t)\rangle\,, \tag{3.3}$$

with $a \in \mathbb{R}$, we obtain an "eigenvalue equation" for $|\psi'\rangle$

$$\hat{H}'|\psi'(t)\rangle \equiv \left[\hat{H} - i\hbar\frac{\partial}{\partial t}\right]|\psi'(t)\rangle = a|\psi'(t)\rangle\,. \tag{3.4}$$

At this point we move from the interpretation of time as a parameter to time as a coordinate. We therefore work in a composite, or *extended* Hilbert space $\mathcal{R} \otimes \mathcal{T}'$ [76; 16], where $\mathcal{R}$ is the space of all square-integrable functions $f(x)$ on the configuration space and $\mathcal{T}'$ is the space of all functions $a(t)$ with finite $\int_{-\infty}^{\infty}|a(t)|^2dt$. The inner product of two vectors $|\phi_a\rangle$ and $|\phi_b\rangle$ in this space is then defined by

$$\langle\langle\phi_a|\phi_b\rangle\rangle \equiv \int_{-\infty}^{\infty}\langle\phi_a|t\rangle\langle t|\phi_b\rangle dt = \int_{-\infty}^{\infty}\langle\phi_a(t)|\phi_b(t)\rangle dt\,, \tag{3.5}$$

where $\langle\phi_a(t)|\phi_b(t)\rangle = \int_{-\infty}^{\infty}\langle\phi_a(t)|x\rangle\langle x|\phi_b(t)\rangle dx$ is the usual inner product in $\mathcal{R}$ at a fixed time. The primed Hamiltonian $\hat{H}'$ is a Hermitian operation in this space.

The time-periodicity of $\hat{H}(t)$ implies that it commutes with its corresponding time-evolution operator over a single period $\hat{U}_T \equiv \hat{U}_H(t + T, t)$. Moreover, in the composite space,

$$\left[\hat{H}', \hat{U}_T\right] = 0 \,. \tag{3.6}$$

A fundamental theorem of quantum mechanics tells us that two commuting operators can be simultaneously diagonalized in the same eigenbasis, i.e. there exists a basis of solutions to (3.4) such that

$$\hat{H}'|\psi'\rangle = a|\psi'\rangle \tag{3.7}$$

and

$$\hat{U}_T|\psi'\rangle = \exp\left[\frac{ibT}{\hbar}\right]|\psi'\rangle \,, \tag{3.8}$$

where the eigenvalue of the unitary time-evolution operator must have modulus one. We now define a Floquet eigenstate $|\phi(t)\rangle$ via

$$|\psi'(t)\rangle = \exp\left[\frac{ibt}{\hbar}\right]|\phi(t)\rangle \,. \tag{3.9}$$

Acting on this form of $|\psi'\rangle$ with the time evolution operator, and using Eq. (3.8), we find

$$\begin{aligned}
\hat{U}_T|\psi'\rangle &= \exp\left[\frac{ibT}{\hbar}\right]\exp\left[\frac{ibt}{\hbar}\right]|\phi(t+T)\rangle \\
&= \exp\left[\frac{ibT}{\hbar}\right]\exp\left[\frac{ibt}{\hbar}\right]|\phi(t)\rangle \\
&\rightarrow |\phi(t+T)\rangle = |\phi(t)\rangle \,.
\end{aligned} \tag{3.10}$$

Thus the Floquet state has the time-periodicity of $\hat{H}(t)$.

Finally, we can write any solution to the Schrödinger equation in the form

$$|\psi(t)\rangle = \exp\left[-\frac{i\epsilon t}{\hbar}\right]|\phi(t)\rangle \quad ; \quad |\phi(t+T)\rangle = |\phi(t)\rangle \tag{3.11}$$

where the Floquet eigenvalue (or quasienergy) associated to the eigenstate is defined as $\epsilon \equiv a - b$. This proves the claim of Floquet's Theorem.

3.1.2 The extended Hilbert space

Plugging the Floquet form of a solution into the Schrödinger equation, we obtain an eigenvalue equation

$$\hat{H}_F|\phi_\alpha(t)\rangle \equiv \left[\hat{H}(t) - i\hbar\frac{\partial}{\partial t}\right]|\phi_\alpha(t)\rangle = \epsilon_\alpha|\phi_\alpha(t)\rangle. \tag{3.12}$$

The Floquet Hamiltonian is a Hermitian operator in a *new* extended Hilbert space $\mathcal{R} \otimes \mathcal{T}$ [76; 16], where $\mathcal{R}$ is again the space of all square-integrable functions $f(x)$ on the configuration space and $\mathcal{T}$ is the space of all time-periodic functions $a(t)$ with period T and finite $\int_{-T/2}^{T/2}|a(t)|^2 dt$. The inner product of two vectors $|\phi_a\rangle$ and $|\phi_b\rangle$ in this space is then defined by

$$\langle\langle\phi_a|\phi_b\rangle\rangle \equiv \frac{1}{T}\int_{-T/2}^{T/2}\langle\phi_a|t\rangle\langle t|\phi_b\rangle dt = \frac{1}{T}\int_{-T/2}^{T/2}\langle\phi_a(t)|\phi_b(t)\rangle dt, \tag{3.13}$$

where $\langle\phi_a(t)|\phi_b(t)\rangle = \int_{-\infty}^{\infty}\langle\phi_a(t)|x\rangle\langle x|\phi_b(t)\rangle dx$ is the usual inner product in $\mathcal{R}$. The Hermiticity of $\hat{H}_F$ of course implies that its eigenvalues are real and two Floquet eigenvectors corresponding to different eigenvalues are orthogonal.

The construction of the extended Hilbert space shows that the label of the Floquet eigenstates α is shorthand for two quantum numbers. As has been mentioned previously, we will consider systems in which solutions are spatially periodic (see Section 2.3 and the Floquet-Bloch discussion below). This, together with the

fact that Floquet states are, by definition, periodic in time, implies that $\alpha \in \mathbb{Z}^2$. We can select a complete basis $\{|p, q\rangle \equiv |p\rangle \otimes |q\rangle\}$ in the composite space which, in the position-time representation, takes the form

$$\langle\langle x, t | p, q \rangle\rangle = \mathrm{e}^{ipx}\mathrm{e}^{iqt} \quad (p, q \in \mathbb{Z}), \tag{3.14}$$

where $\hat{p}|p\rangle = \hbar p |p\rangle$ and, as in the Introduction, the states $|q\rangle$ are the eigenvectors of $\hat{q}$ where

$$\langle t | \hat{q} | q \rangle = -i\hbar \frac{\partial}{\partial t} \langle t | q \rangle = q\hbar\omega \langle t | q \rangle. \tag{3.15}$$

These basis vectors satisfy $\langle\langle p, q | p', q' \rangle\rangle = \delta_{p,p'}\,\delta_{q,q'}$. The solution to the Schrödinger equation can therefore be reduced to the diagonalization of the Floquet Hamiltonian in the basis $\{|p, q\rangle\}$. The consideration of time as a coordinate has transformed the Schrödinger equation from time-dependent to time-independent.

The Floquet eigenstates have an infinite multiplicity with respect to the solutions of the Schrödinger equation in the sense that for any Floquet eigenstate $|\phi\rangle$ with eigenvalue ϵ, there exists another solution $|\tilde{\phi}\rangle = \mathrm{e}^{iQ\omega t}|\phi\rangle$ $(Q \in \mathbb{Z})$ with eigenvalue $\tilde{\epsilon} = \epsilon + Q\hbar\omega$. These two Floquet states are, however, associated to the same physical state, i.e. $|\psi\rangle \equiv \mathrm{e}^{-i\epsilon t}|\phi\rangle = \mathrm{e}^{-i\tilde{\epsilon}t}|\tilde{\phi}\rangle$. The implication of this fact is that the dynamics of the physical system can be understood by considering only those Floquet states whose eigenvalues appear in a single "zone" $\epsilon^\star \le \epsilon < \epsilon^\star + \hbar\omega$, labeled by the constant $\epsilon^\star$. The zone centered around zero will be called the *fundamental zone*.

Floquet-Bloch picture

The complete solution of the Schrödinger equation for a time and spatially periodic Hamiltonian requires the use of Bloch theory. In the present context, Bloch theorem states that any Floquet eigenstate $\phi(x, t)$ of a spatially periodic Floquet Hamiltonian

can be written in the form

$$\phi_k(x,t) = \exp\left[\frac{ikx}{\hbar}\right]\bar{\phi}^k(x,t) \quad ; \quad \bar{\phi}^k(x+2\pi,t) = \bar{\phi}^k(x,t), \qquad (3.16)$$

where the *Floquet-Bloch eigenstate* $|\bar{\phi}_\alpha^k\rangle$, parameterized by the Bloch vector $k \in \mathbb{R}$, has both the spatial and time periodicity of $H(x,t)$. The proof of this is mathematically identical to that of Floquet Theorem: the unitary space-translation operator, defined by $\hat{T}_{2\pi}|x\rangle = |x+2\pi\rangle$, commutes with the Floquet Hamiltonian and therefore shares an eigenbasis in the composite Hilbert space. Writing our Hamiltonian explicitly as the sum of a kinetic energy part $-\frac{\hbar^2}{2m}\frac{\partial^2}{\partial x^2}$ and a (time and space-periodic) potential $V(x,t)$, we can now write the Schrödinger equation in the form

$$\hat{K}^k(t)|\bar{\phi}_\alpha^k(t)\rangle \equiv \left[\frac{(k+\hat{p})^2}{2m} + \hat{V}(t) - i\hbar\frac{\partial}{\partial t}\right]|\bar{\phi}_\alpha^k(t)\rangle = \epsilon_\alpha^k|\bar{\phi}_\alpha^k(t)\rangle \qquad (3.17)$$

where we have defined the Floquet-Bloch Hamiltonian $\hat{K}^k$. This operator is Hermitian in the composite space $\Theta \otimes \mathcal{T}$, where Θ is the coordinate space of periodic functions $g(\theta + 2\pi) = g(\theta)$, with eigenvectors $|\bar{\phi}_\alpha^k\rangle$ and eigenvalues $\bar{\epsilon}_\alpha^k$. This space has a complete orthogonal basis

$$\langle\langle\theta,t|p,q\rangle\rangle = e^{ip\theta}e^{iqt} \quad (p,q \in Z). \qquad (3.18)$$

Thus we see that, for a particular value of k, the Floquet-Bloch eigenstates and eigenvalues will be labeled by a pair of integer quantum numbers and are determined by diagonalization of the $\hat{K}^k$ in some basis of $\Theta \otimes \mathcal{T}$.

As was mentioned above and in the previous chapter, the experimental systems which we will consider are prepared such that the atoms have a very narrow distribution of momentum expectation. This is equivalent to populating only the lowest energy Bloch band. Therefore, to a good approximation we can restrict our

consideration of the full Floquet-Bloch Hamiltonian to the Bloch vector $k = 0$ such that $\hat{K}^k \rightarrow \hat{H}_F$.

Parity considerations

If Hamiltonian for a particular time-periodic system commutes with a parity operator, which can be defined by its action on the momentum eigenket $\hat{\Pi}|p\rangle = |-p\rangle$, then the corresponding Floquet Hamiltonian will also commute with that operator. Therefore the two operators can be diagonalized simultaneously and the Floquet eigenstates have definite parity: $\hat{\Pi}|\phi_\alpha\rangle = \pm 1|\phi_\alpha\rangle$. Floquet states with parity eigenvalue $+1$ will be called even, and those with eigenvalue -1 odd.

3.1.3 "Floquet Matrix" formalism

An arbitrary dynamical state of the system can be expanded, with the use of equation (3.1), in the basis of Floquet eigenstates,

$$|\psi(t)\rangle = \sum_\alpha{}' A_\alpha e^{-i\frac{\epsilon_\alpha t}{\hbar}}|\phi_\alpha(t)\rangle \,, \tag{3.19}$$

where the "prime" indicates that the sum is restricted to those Floquet states with ϵ_α in a single zone. The expansion coefficients are independent of time and can be written $A_\alpha = \langle\phi_\alpha(0)|\psi(0)\rangle$. Using the time-periodicity of the Floquet eigenstates, we can then write

$$|\psi(T)\rangle = \sum_\alpha{}' e^{-i\frac{\epsilon_\alpha T}{\hbar}}|\phi_\alpha(0)\rangle\langle\phi_\alpha(0)|\psi(0)\rangle \equiv \hat{U}(T)|\psi(0)\rangle \,, \tag{3.20}$$

showing that the time-evolution operator over a single period T

$$\hat{U}(T) = \sum_\alpha{}' e^{-i\frac{\epsilon_\alpha T}{\hbar}}|\phi_\alpha(0)\rangle\langle\phi_\alpha(0)| \tag{3.21}$$

is diagonalized by the Floquet eigenstates at time $t = 0$. We can determine these *time-strobed Floquet states* by constructing the matrix $U_{mm'} \equiv \langle m | \hat{U}(T) | m' \rangle$ in some convenient basis $\{|m\rangle\}$ in Θ, truncating this matrix at some appropriate level $m = M$ where it becomes approximately diagonal (i.e. $U_{MM} >> U_{Mm}$ for $m \neq M$), and then performing a numerical diagonalization to obtain the $|\phi_\alpha(0)\rangle$ and ϵ_α (mod $\hbar\omega$). The mth column of U is obtained by evolving the basis vector $|m\rangle$ over one period T via numerical integration of the Schrödinger equation.

By giving up any knowledge of the time-dependence of a given Floquet state, using the Floquet matrix is numerically a much more efficient procedure than the diagonalization of the Floquet Hamiltonian matrix in the extended Hilbert space. The multiplicity of eigenstates and eigenvalues mentioned in the previous section makes the knowledge of eigenvalues in more than one zone (which diagonalization of the Floquet Hamiltonian provides) an unnecessary redundancy. Moreover, since much of the analysis presented in the following chapters will be focused on the adiabatic changes of Floquet states under the variation of a parameter, the loss of time information over a single period will not be vitally important. Therefore, we use this method of analysis as our primary way of determining the Floquet state structure of a particular system.

3.1.4 "Evolution" of a Floquet Hamiltonian

In this section, the (t, t') formalism due to Peskin and Moiseyev [69; 21] is used to justify the time-parametrization of the model Hamiltonians in Eqs. (5.24) and (5.51) of Chapter 5. These models are each subsystems of a *Floquet* Hamiltonian which are constructed under the assumption that the Schrödinger equation is time-periodic. The subsequent parametrization of such a system by non-periodic functions of time therefore requires a more rigorous explanation. Here, we show that a physical system represented by a Hamiltonian with both periodic and arbitrary dependence on time,

can be associated to Floquet-like Hamiltonian in an extended Hilbert space where the periodic time-dependence has been reduced to dependence on a coordinate. This Hamiltonian is termed "Floquet-like" because its dependence on the *coordinate* time is identical to a Floquet Hamiltonian's dependence on time. The remaining *arbitrary* time-dependence of the Floquet-like Hamiltonian determines, via the Schrödinger equation, a dynamics in the extended space from which the dynamics of the original system can be recovered.

Consider the Schrödinger equation for a time-dependent Hamiltonian

$$i\frac{\partial}{\partial t}\psi(x;t) = H(x;t)\psi(x;t)\,,\tag{3.22}$$

where x can be considered a single spatial coordinate or a set of coordinates and $\hbar$ has been set to unity by non-dimensionalization of the variables. We will associate to $H(x;t)$ a Hamiltonian of one more coordinate $H_F(x,t';t)$ which is a Hermitian operator in a larger Hilbert space, extended to include this new coordinate t'. The relationship between the two Hamiltonians is defined by

$$H_F(x,t';t) = \bar{H}(x,t';t) - i\frac{\partial}{\partial t'}\,,\tag{3.23}$$

with

$$\bar{H}(x,t';t)|_{t'=t} = H(x;t)\,.\tag{3.24}$$

Clearly, $H(x;t)$ does not uniquely determine $H_F(x,t';t)$. The time-evolution of a state $\bar{\psi}(x,t';t)$ in the extended space is governed by the Schrödinger equation

$$i\frac{\partial}{\partial t}\bar{\psi}(x,t';t) = H_F(x,t';t)\bar{\psi}(x,t';t)\,,\tag{3.25}$$

which can also be written

$$i\left[\left(\frac{\partial}{\partial t} + \frac{\partial}{\partial t'}\right)\bar\psi(x,t';t)\right] = \bar H(x,t';t)\bar\psi(x,t';t)\,. \tag{3.26}$$

If we take this equation at the cut $t' = t$, it becomes

$$i\frac{\partial}{\partial t}\left[\bar\psi(x,t';t)|_{t'=t}\right] = H(x;t)\left[\bar\psi(x,t';t)|_{t'=t}\right]\,, \tag{3.27}$$

where we have used the identity

$$\frac{\partial}{\partial t}\left[\bar\psi(x,t';t)|_{t'=t}\right] = \left[\left(\frac{\partial}{\partial t} + \frac{\partial}{\partial t'}\right)\bar\psi(x,t';t)\right]_{t'=t}\,. \tag{3.28}$$

Comparing Eqs. (3.27) and (3.22), we see that the evolution of a state in the original system can be determined by evolution in the extended system using

$$\psi(x;t) = \bar\psi(x,t';t)|_{t'=t}\,, \tag{3.29}$$

and provided the same initial condition

$$\bar\psi(x,t';t)|_{t'=t=0} = \psi(x,0) \tag{3.30}$$

is used in each space.

We now apply this formalism to STIRAP transitions in the two-resonance Hamiltonian (see Section 5.4). The evolution plotted in Figure 5.9b was performed by numerical integration of the Schrödinger equation, using the Hamiltonian

$$H(x;t) = -\frac{\partial^2}{\partial x^2} + \kappa_0\left[\cos x + \cos(x - \omega_0 t)\right]$$
$$+ \lambda\cos x\left[\kappa_1(t)\cos(\Omega_1 t) + \kappa_2(t)\cos(\Omega_2 t)\right]\,, \tag{3.31}$$

where κ_1 and κ_2 were given Gaussian time-dependence in order to affect a STIRAP-like transition. The solid lines plotted in Figure 5.9a, were determined by evolution of a Schrödinger equation using the time-parameterized three-level model in Eq. (5.51). Using the above analysis we can show that, modulo the perturbation theory approximations, these two methods of time-evolution are equivalent. We define a Hamiltonian in the extended space

$$
\begin{aligned}
\bar{H}(x,t';t) = -\frac{\partial^2}{\partial x^2} + \kappa_0 \left[\cos x + \cos(x - \omega_0 t')\right] \\
+ \lambda \cos x \left[\kappa_1(t)\cos(\Omega_1 t') + \kappa_2(t)\cos(\Omega_2 t')\right] , \quad (3.32)
\end{aligned}
$$

which satisfies Eq. (3.24) for the two-resonance Hamiltonian and has the property that functions periodic in time are now functions of the extra coordinate, while the amplitudes of the modulations are functions of the usual time parameter. The full Hamiltonian in the extended space $H_F(x,t';t)$, defined by Eq. (3.23), has the same dependence on t' that the Floquet Hamiltonian in Eq. (5.29) has on time t. Therefore, the entire perturbation analysis performed on the Floquet Hamiltonian in Chapter 5 would proceed in identical fashion on $H_F(x,t';t)$, yielding a time-parameterized three-level model. If Eqs. (3.29) and (3.30) are satisfied, the "time-parameterized" Floquet Hamiltonian can be used to determine the physical evolution.

3.2   Connections to classical dynamics

Thus far, we have not discussed an important application of systems of ultracold atoms in an optical lattice: investigations of "quantum chaos." This term demands a precise definition, since the linearity of the Schrödinger equation in fact forbids chaotic dynamics of the quantum wavefunction. Therefore, we define "quantum chaos" to be the study of quantum systems for which the classical analog (determined

by replacing the position and momentum operators in the Hamiltonian operator with the classical phase space coordinates) is chaotic.

The simplest type of classical system which can exhibit chaos is one for which the Hamiltonian is a function of position, momentum and time (so called "one and a half degree of freedom" systems). For this reason, the effective Hamiltonians which we consider in this dissertation are particularly suited for quantum chaos studies. Indeed, many of the archetypal chaotic Hamiltonian systems which have been the focus of intense study in the field of classical chaos over the past 30 years are easily obtainable in quantum systems of atoms in an optical lattice. Two notable examples are the kicked rotor model, which can be considered the continuous-time generator for the standard map [56] (this was realized experimentally in a system of ultracold sodium atoms by a group at the University of Texas for studying dynamical localization of a quantum wavefunction [60]); and the two-resonance Hamiltonian, studied by Chirikov, Escande and Doveil, and others [13; 19; 74] in their pioneering works on the approach to chaos (we consider the quantum analog as a basis for coherent acceleration in Chapter 5).

Our primary tool for comparing classical and quantum systems will be the Husimi distribution.

3.2.1 Husimi distributions

In subsequent chapters, we will compare the phase space distributions of the time-strobed Floquet eigenstates $|\phi_\alpha(0)\rangle$ to the classical system. We can do this by introducing the Husimi distribution $\rho(x_0, p_0)$ [39; 47] of a quantum state $|\phi\rangle$ on the classical phase space (x_0, p_0)

$$\rho(x_0, p_0) \equiv \frac{1}{2\pi} |\langle x_0, p_0 | \phi \rangle|^2 \,, \tag{3.33}$$

where the *coherent state* $|x_0, p_0\rangle$ is defined as an eigenstate of the annihilation operator $\hat{a} = \frac{1}{\sqrt{2}} (\hat{x}/\sigma + i\sigma\hat{p})$ with position and momentum expectation values of x_0 and p_0 respectively. The free parameter σ is set according to the physical system considered (see below). The representation of such a coherent state in the discrete (dimensionless) momentum basis $\{|p\rangle\}$ is given by

$$\langle p|x_0, p_0\rangle = A \exp\left[-\frac{\sigma^2}{2}(p - p_0)^2 - ix_0(p - p_0)\right] , \qquad (3.34)$$

where A is a normalization factor guaranteeing $\langle x_0, p_0|x_0, p_0\rangle = 1$. The action of the annihilation operator on the coherent state can be used to show that $\langle p \rangle \equiv \langle x_0, p_0|\hat{p}|x_0, p_0\rangle = p_0$, $\langle x \rangle = x_0$, $\Delta x = \sigma/\sqrt{2}$, and $\Delta p = (\sigma\sqrt{2})^{-1}$. Thus, the coherent state is a minimum-uncertainty wave packet, where the free parameter determines the ratio of its uncertainty in position and momentum, i.e. $\sigma^2 = \Delta x/\Delta p$. Reference [47] presents an in-depth discussion on the selection of the parameter σ. In all Husimi plots shown in subsequent sections, we will set $\sigma = 1.18\,\kappa^{-1/4}$, a choice which provides the best association between the quantum pendulum Floquet eigenstates with parameter κ and the corresponding classical orbits). As we will see, the Husimi distributions of the Floquet states lie directly on the orbit structures of the classical phase space.

3.2.2 The pendulum and "quantum pendulum": A model system

We will consider here the "perturbed pendulum" system described by the Hamiltonian

$$H(x, p, t) = H_{pend}(x, p) + \lambda V(x, t) \equiv p^2 + \kappa \cos(x) + \lambda\left[\cos(x - \omega t) + \cos(x + \omega t)\right] . \tag{3.35}$$

The classical phase space of a such a time-periodic one-and-a-half degree-of-freedom system can be visualized by a strobe plot of the trajectories at times $t = \nu\frac{2\pi}{\omega}$ $(\nu \in$
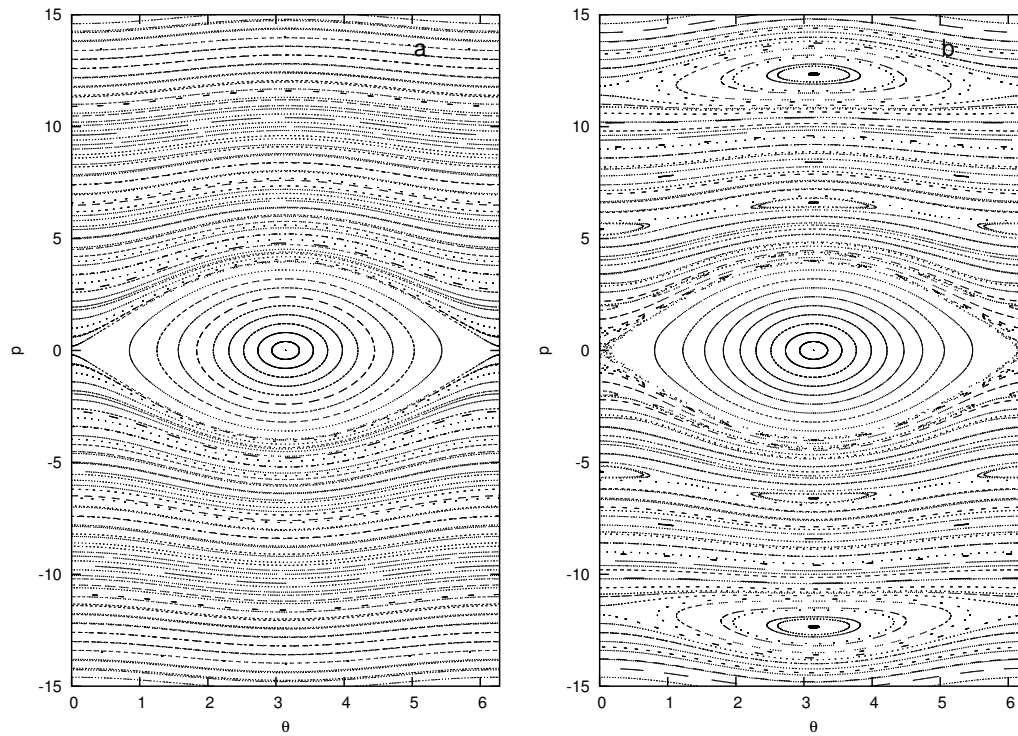
Figure 3.1: Strobe plots of the system in Eq. (3.35) with $\omega = 24$ and parameters: (a) $\kappa = 7.8$ and $\lambda = 0$; and (b) $\kappa = 7.8$ and $\lambda = 1.0$.

$\mathbb{Z}$). A strobe plot of phase space trajectories for the system governed by Hamiltonian $H(x,p,t)$ with $\omega = 24$ is shown in Figure 3.1a with parameters $\kappa = 7.8$ and $\lambda = 0$. (For the case of $\lambda = 0$, the system is independent of time and could be visualized with an ordinary parametric plot of phase space, however we plot the strobed phase space for convenience of comparison to the perturbed system). Because this system is integrable, all orbits lie on tori (in either the regions of the pendulum's libration or rotation) and the phase space is absent of chaos. Figure 3.1b shows a strobe plot of the phase space with parameters $\kappa = 7.8$, $\lambda = 0.5$, and $\omega = 24$. The traveling waves in the modulation term have phase velocities $v = \pm\omega$ and are seen as *primary resonance* structures at $p = \pm\frac{\omega}{2}$ where $\dot{x} = v$. Although much of the orbit structure of the integrable system is preserved, the tori with rational winding numbers have been destroyed, giving rise to a self-similar set of *daughter resonance* structures (see, for example, the two-island chains at $p = \pm\frac{\omega}{4}$). Regions of chaos surround these resonances, most visibly near the separatrix of the pendulum resonance. A more detailed description of the approach to chaos in classical Hamiltonian systems is given in Appendix E.

The corresponding quantum system can be obtained by replacing x and p in the above equation with their quantum mechanical operators. The position space solutions to the unperturbed eigenvalue equation $\hat{H}_{pend}|\chi_n\rangle = E_n|\chi_n\rangle$ are the Mathieu functions $\langle x|\chi_n\rangle$ ($n \in Z$) ([1], see also Appendix F), with n even labeling even-parity functions and n odd labeling odd-parity functions. The full system is time-periodic for any value of λ and therefore solutions of the Schrödinger equation will have the form given in Eq. (3.1). We will therefore define the unperturbed ($\lambda = 0$) Floquet Hamiltonian $\hat{H}_F^0 \equiv \hat{H}_{pend} - i\frac{\partial}{\partial t}$, which we will call the *Floquet pendulum*. The eigenstates of this unperturbed system have the simple form $\{|n,q\rangle = |n\rangle \otimes |q\rangle\}$ where $|q\rangle$ was defined in Section 3.1.2, and the eigenvalues are $\epsilon_{n,q} = E_n + q\omega$. Figure 3.2 shows the lowest nine energies of the even-parity eigenstates of the
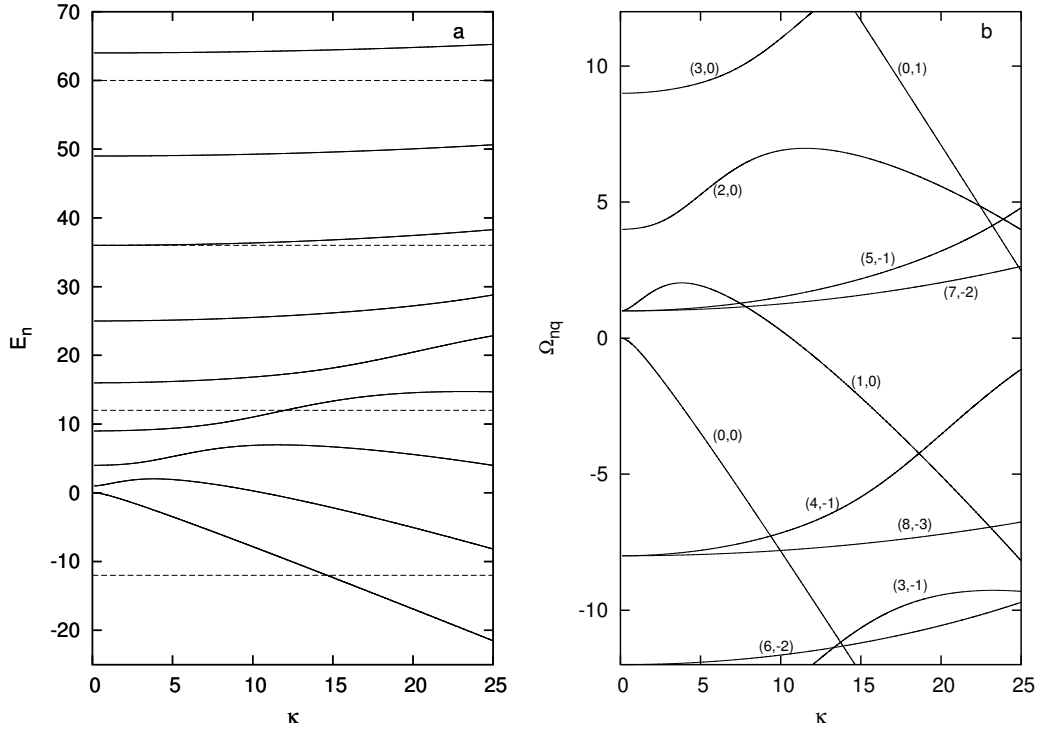
Figure 3.2: (a) Energy curves of the nine lowest-energy, even-parity eigenstates of the quantum pendulum. (b) The nine corresponding "Floquet pendulum" eigenvalues in the fundamental zone $-\frac{\omega}{2} < \epsilon \le +\frac{\omega}{2}$ with $\omega = 24$. The labels $(n/2, q)$ on each Floquet eigenvalue segment identify the corresponding Floquet eigenstate $|n, q\rangle$. The dashed lines in (a) indicate the Floquet eigenvalue zone boundaries.

quantum pendulum and the corresponding Floquet eigenvalues in the fundamental zone $-\omega/2 \le \epsilon < \omega/2$.

Chapter 4

"Chaos-assisted tunneling" and avoided crossings

The term "chaos-assisted tunneling" (CAT) was coined by Tomsovic and Ullmo in their 1994 theoretical investigations of a double well quantum system under the influence of a perturbation making the corresponding classical system non-integrable [82]. They observed that the two-state tunneling frequency of the unperturbed system (described in the Introduction to this dissertation) could be *enhanced* by many orders of magnitude in the presence of underlying classical chaos. Many other groups have studied this phenomenon and related processes in the 1990s, now known collectively as "chaotic tunneling," both theoretically and numerically [9; 28; 44; 51; 52; 53]. The experimental realization of the phenomenon was not achieved, however, until much more recently [78; 35; 80] when the techniques of cold atom optics made this process observable.

In this chapter we will first present an overview of the underlying mechanism for CAT, which can be described by a three level model of a relatively simple form. The tunneling rate enhancement will be shown to be the result of an avoided crossing between an isolated eigenvalue curve and one member of opposite parity doublet

undergoing normal two-state tunneling. Although non-integrability of an underlying classical system is required for an avoided crossing to occur, it will be shown that the basic mechanism for "chaos-assisted tunneling" in a quantum system does not necessarily require a fully chaotic classical analog.

In order to apply this model to the experimental optical lattice systems in which CAT has been observed, we develop a technique for characterizing avoided crossings in the eigenvalue spectrum of the effective Hamiltonian. The technique involves the application of a modified degenerate perturbation theory to the Floquet Hamiltonian. It will be seen that avoided crossings can be classified according to the properties of the unperturbed eigenstates involved in the crossing.

Finally, we apply these results to the particular experimental realization of CAT at the University of Texas at Austin. Although this system is not well described by the idealized avoided crossing model, we show that the observed tunneling frequency enhancements are very well predicted by the Floquet eigenvalue spectrum of three particular Floquet states involved in an avoided crossing.

Much of the work contained in this chapter has been published previously by the author [37].

4.1 The chaotic tunneling model system

The basic mechanism of chaos-assisted tunneling can be described by a three-state model Hamiltonian, which in some basis $\{|o_1\rangle, |e_1\rangle, |e_2\rangle\}$, has the following form [44]

$$H = \begin{pmatrix} a\delta\kappa & 0 & 0 \\ 0 & a\delta\kappa + \Delta & V \\ 0 & V & \Delta - a\delta\kappa \end{pmatrix}. \tag{4.1}$$

This system is nearly identical to the avoided crossing model presented in Section 1.1.2 (though the names of the matrix parameters have changed), with the addition
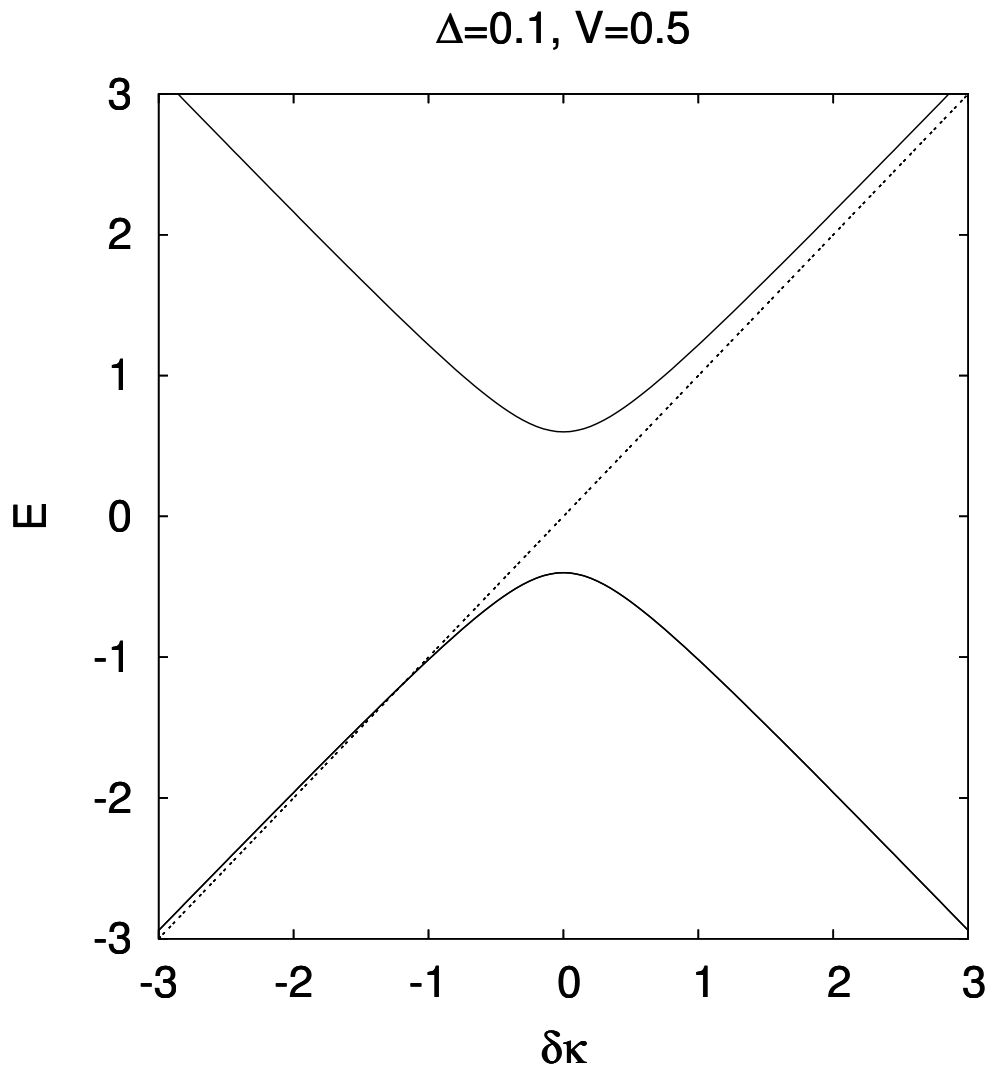
Figure 4.1: The chaotic tunneling model. A nearly-degenerate opposite parity doublet intersects with a third state of definite parity under the variation of a parameter $\delta\kappa$. The tunneling splitting (the spacing of the doublet eigenvalues) widens in the approach to the avoided crossing at $\delta\kappa = 0$. In the region of the avoided crossing itself, the splitting becomes double-valued due to the superposition of the two states involved.

of the third state $|o_1\rangle$ completely decoupled from the other two. In the case that $V = 0$, the energy eigenvalues of the two "even" parity states $|e_1\rangle$ and $|e_2\rangle$ with opposite slopes $\frac{dE}{d\delta\kappa} = \pm a$, respectively, will cross at $\delta\kappa = 0$ at an energy $E = \Delta$; the eigenvalue of the "odd" parity state has slope a and is at a constant offset Δ from the eigenvalue of state $|e_1\rangle$. For any nonzero V, the eigenvalues of the two even parity eigenstates $|e_1(\delta\kappa)\rangle$ and $|e_2(\delta\kappa)\rangle$ (not necessarily equal to the basis states $|e_1\rangle$ and $|e_2\rangle$) will *avoid* crossing at $\delta\kappa = 0$, while the odd eigenvalue and eigenstate is unchanged. An example of these adiabatic eigenvalues is shown in Figure 4.1.

The connection to tunneling is made by giving additional meaning to the parity assignments of the eigenstates. We define the asymptotic character of these states as $\delta\kappa \to -\infty$ to be

$$|o_1(\delta\kappa \to -\infty)\rangle = |o_1\rangle \equiv \frac{1}{\sqrt{2}}\left(|+\rangle - |-\rangle\right)$$

$$|e_1(\delta\kappa \to -\infty)\rangle \equiv \frac{1}{\sqrt{2}}\left(|+\rangle + |-\rangle\right) \tag{4.2}$$

$$|e_2(\delta\kappa \to -\infty)\rangle \equiv |c\rangle,$$

where we have identified two states as members of an opposite parity doublet in some basis $\{|+\rangle, |-\rangle\}$. If this basis can be associated to quantum states with classically explainable origins in dynamically separated regions of the classical phase space, then the time-evolution of a state prepared in either $|+\rangle$ or $|-\rangle$ will exhibit tunneling. Consideration of the model systems presented in Sections 1.1.1 and 1.1.2 of the Introduction allows for a full elucidation of the tunneling dynamics. Far from the avoided crossing a state prepared in $|+\rangle$ must be constructed as the sum of $|e_1\rangle$ and $|o_1\rangle$, and will exhibit tunneling oscillations with frequency $\omega_{tun} = \Delta/\hbar$. In the vicinity of the avoided crossing, however, the construction of $|+\rangle$ will necessarily involve the third state due to the superposition of the asymptotic character of the two even states. It can easily be seen that the dynamics in the region of the avoided

crossing will exhibit much higher tunneling frequencies, limited only by the minimum spacing of the even parity avoided crossing. Moreover, the tunneling dynamics at any value of $\delta\kappa$ can be decomposed into two frequencies determined by the eigenvalue difference between the odd parity state and the two even parity states.

4.2 Avoided crossings in the perturbed quantum pendulum

As was seen in the previous section, the essence of chaotic tunneling, or chaos-assisted tunneling, is the presence of avoided crossings in the eigenvalue spectrum. Before considering the system used in the experimental achievement of this process, we will consider a slightly simpler effective Hamiltonian: the quantum pendulum perturbed by two traveling resonances (introduced in Section 3.2.2):

$$\hat{H}(t) = \hat{H}_{pend} + \lambda\hat{V}(t) \equiv \hat{p}^2 + \kappa\cos(\hat{x}) + \lambda\left[\cos(\hat{x} - \omega t) + \cos(\hat{x} + \omega t)\right]. \quad (4.3)$$

This system, like the experimental system we will consider later, is a three-resonance type system, but unlike the experimental system, the limit of $\lambda \to 0$ allows for consideration of small perturbations of the, classically integrable, quantum pendulum system.

The Floquet pendulum is integrable and its eigenvalues $\epsilon_{n,q}(\kappa)$, shown in the previous section's Figure 3.2b, cross under the variation of κ. For any nonzero λ, however, the system represented by the Hamiltonian in Eq. 4.3 is non-integrable and the approach of any two (same parity) Floquet eigenvalues under variation of κ results in an avoided crossing. This well-known result, the *non-crossing theorem*, was first proven by von Neumann and Wigner for eigenvalues of generic Hermitian matrices ([84], see also Appendix B). They also showed that adiabatic passage of two quantum states through an avoided crossing leads to an exchange of character.

49

(In a two-parameter system, this exchange can be related to the partial circuit of a diabolical point [8; 4], while in single parameter systems it can be related to exceptional points in the complex parameter plane [32]). Avoided crossings of Floquet eigenvalues in the fundamental zone, which generally involve states localized in well-separated regions of the phase space, will therefore allow a wide variety of interesting quantum dynamical phenomena, including adiabatic transitions and tunneling.

In this section, we will consider the near-integrable regime $(0 < \lambda << \kappa)$, in which a clear association can be made between the Floquet eigenstates of the perturbed system $(\lambda \neq 0)$ and those of the Floquet pendulum $(\lambda = 0)$. In this regime, the Floquet eigenvalues will follow nearly the same dependence on κ as the unperturbed eigenvalues seen in Figure 3.2.b, except in the vicinity of an avoided crossing. For κ values sufficiently far from these avoided crossings, we can make a unique, though necessarily local, association $|\phi_\alpha\rangle \leftrightarrow |n_\alpha, q_\alpha\rangle$ of the Floquet eigenstate $|\phi_\alpha\rangle$ to the Floquet pendulum state with maximum overlap $|\langle n, q|\phi_\alpha\rangle|$. As $\lambda \to 0$, this association will become an equality. We will see that the fundamental characteristics of an avoided crossing between states $|\phi_\alpha\rangle$ and $|\phi_\beta\rangle$ will be determined by the difference

$$\Delta q_{\alpha\beta} \equiv |q_\alpha - q_\beta|. \tag{4.4}$$

In the subsections which follow, we first present a numerical analysis of some representative avoided crossings in the perturbed pendulum system with $\omega = 24$, and then use perturbation theory to show that the results are quite general.

4.2.1   Numerical Results

Three avoided crossings of Floquet eigenvalues in the fundamental zone with $\lambda = 5\times10^{-2}$ are shown in Figures 4.2, 4.3, and 4.4 with Husimi plots of the corresponding Floquet eigenstates overplotted on the figures. The dotted lines shown are the

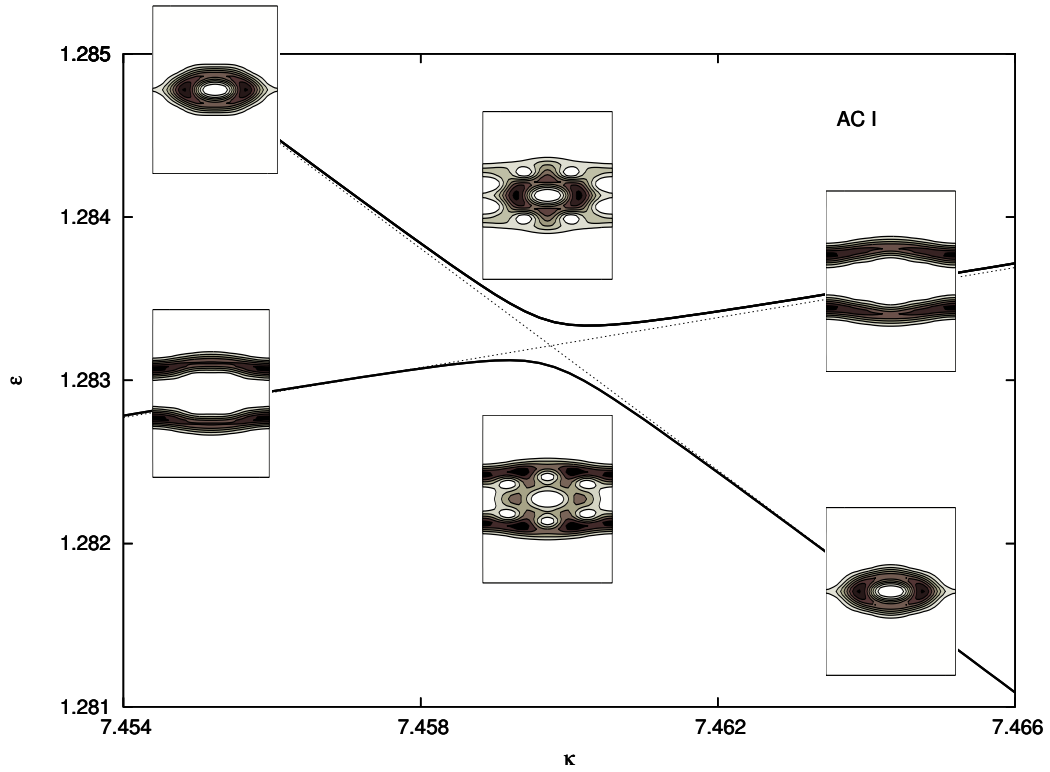Figure 4.2: A $\Delta q_{\alpha\beta} = 1$ avoided crossing of the system $\hat{H}_F$ with parameters $\omega = 24$ and $\lambda = 5 \times 10^{-2}$. The Husimi distributions of the corresponding Floquet eigenstates are shown at $\kappa = (7.455, 7.460, 7.465)$ (the horizontal axis is $x_0 \in [0, 2\pi)$, vertical is $p_0 \in [-15, 15]$). The dotted lines are the eigenvalue curves of the unperturbed Floquet pendulum.
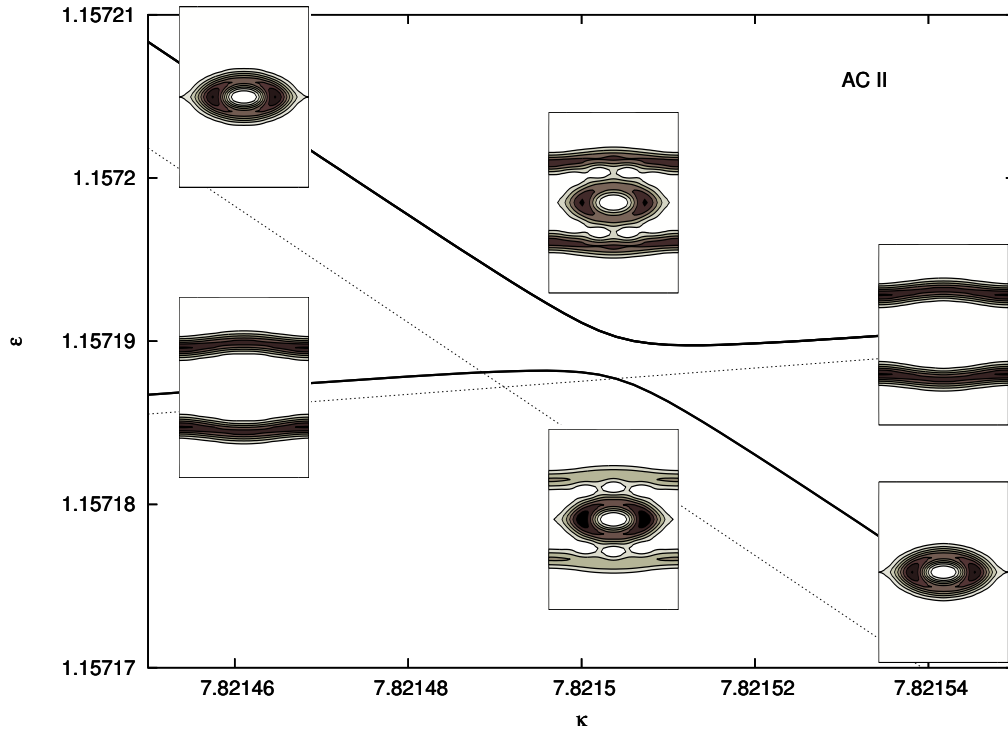
Figure 4.3: A $\Delta q_{\alpha\beta} = 2$ avoided crossing of the system $\hat{H}_F$ with the same λ and ω values as in Figure 4.2. The Husimi distributions shown are the two Floquet eigenstates at $\kappa = (7.82146, 7.82150, 7.82154)$ (axes are the same as Figure 4.2). The dotted lines are the eigencurves of the unperturbed Floquet pendulum.
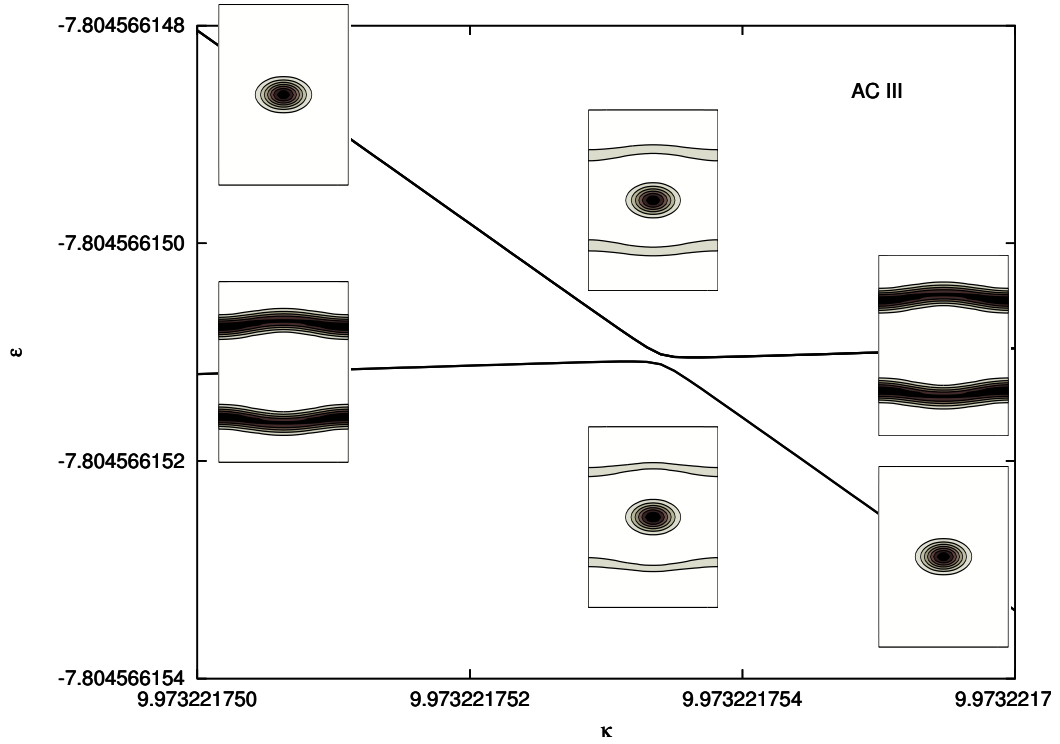
Figure 4.4: A $\Delta q_{\alpha\beta} = 3$ avoided crossing of the system $\hat{H}_F$ with the same λ and ω values as in Figure 4.2. The Husimi distributions shown are the two Floquet eigenstates at $\kappa = (9.973221751, 9.9732217534, 9.973221755)$ (axes are the same as Figure 4.2). The crossing of the corresponding eigencurves of the unperturbed Floquet pendulum falls outside of the plotted region at $\kappa_0 \approx 9.973242$.

eigenvalues of the unperturbed Floquet pendulum. These plots were created by numerically calculating the time-strobed Floquet states at a sequence of κ values. With each step forward in κ, the new states were associated to those of the previous step by calculating the maximum overlap and verifying continuity of the eigenvalues. In the case that two Floquet eigenvalues crossed between κ-steps, the size of the step was reduced and the process repeated until no crossing occurred.

Each of these three avoided crossings involves one Floquet eigenstate localized within the pendulum resonance at $p = 0$ and another localized outside of the pendulum resonance. The avoided crossing in Figure 4.2 involves the states $(n_\alpha, q_\alpha) = (2, 0)$ and $(n_\beta, q_\beta) = (10, -1)$; Figure 4.3 involves the states $(n_\alpha, q_\alpha) = (2, 0)$ and $(n_\beta, q_\beta) = (14, -2)$; and Figure 4.4 involves states $(n_\alpha, q_\alpha) = (0, 0)$ and $(n_\beta, q_\beta) = (16, -3)$ (recall that the even n-labels correspond to the $(n/2)^{\text{th}}$ even-parity Mathieu state). The associated crossings can be found in Figure 3.2.b. These particular avoided crossings were chosen as representative examples with $\Delta q_{\alpha\beta} = 1$, 2, and 3, respectively.

Some general characteristics of these avoided crossings deserve attention. First, the "exchange of character" between the two states is evident in the evolution of the Husimi distributions with κ. The associations $|\phi_\alpha\rangle \leftrightarrow |n_\alpha, q_\alpha\rangle$ and $|\phi_\beta\rangle \leftrightarrow |n_\beta, q_\beta\rangle$ well *before* the avoided crossing become $|\phi_\alpha\rangle \leftrightarrow |n_\beta, q_\beta\rangle$ and $|\phi_\beta\rangle \leftrightarrow |n_\alpha, q_\alpha\rangle$ well *after*. For κ values at the avoided crossing, the two Floquet states are superpositions of the asymptotic states. Second, there is quite a disparity of scale among the three avoided crossings. In particular, the minimum eigenvalue spacing $\Delta_{\alpha\beta}$, defined by

$$\Delta_{\alpha\beta} \equiv \min\left(|\epsilon_\alpha - \epsilon_\beta|\right), \tag{4.5}$$

is relatively large for the first and relatively small for the third. Finally, the position κ_{ac} of the minimum spacing (which we will henceforth call the "position of the avoided crossing"), is not necessarily equal to the position κ_0 of the unperturbed
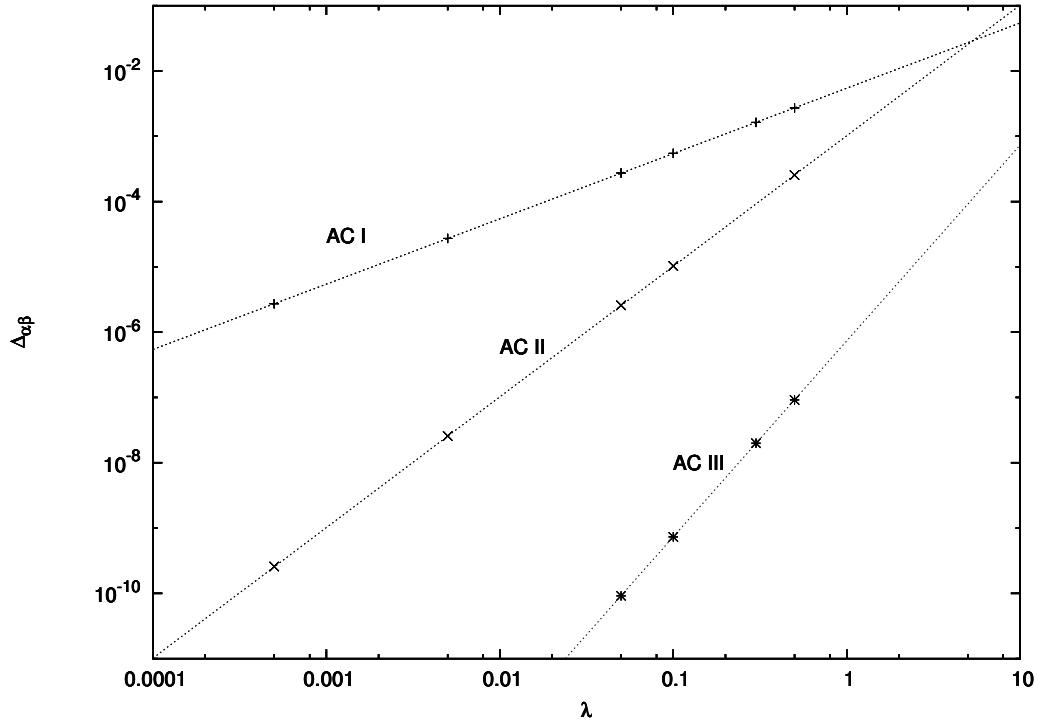
Figure 4.5: The minimum spacing $\Delta_{\alpha\beta}$ as a function of λ of the three avoided crossings shown in Figures 4.2, 4.3, and 4.4. The functions $\Delta_{\alpha\beta} = 5.44 \times 10^{-3}\lambda$, $\Delta_{\alpha\beta} = 1.02 \times 10^{-3}\lambda^2$, $\Delta_{\alpha\beta} = 7.35 \times 10^{-7}\lambda^3$ are overplotted.

crossing. Indeed, it seems that for $\Delta q_{\alpha\beta} \neq 1$, the avoided crossing is significantly offset in both κ and ϵ.

To make these last two observations more quantitative, we have computed dependence of $\Delta_{\alpha\beta}$ and $\Delta\kappa_{ac} \equiv |\kappa_0 - \kappa_{ac}|$ on the parameter λ. The results for the three example avoided crossings are shown in Figures 4.5 and 4.6. We see that, for small values of λ, the dependences are all well approximated by power laws with integer exponents. The minimum spacing of the avoided crossings is given by

$$\Delta_{\alpha\beta} = A\,\lambda^{\Delta q_{\alpha\beta}}\,, \tag{4.6}$$

where the coefficients are $A \approx \{5.44 \times 10^{-3}, 1.02 \times 10^{-3}, 7.35 \times 10^{-7}\}$ for avoided
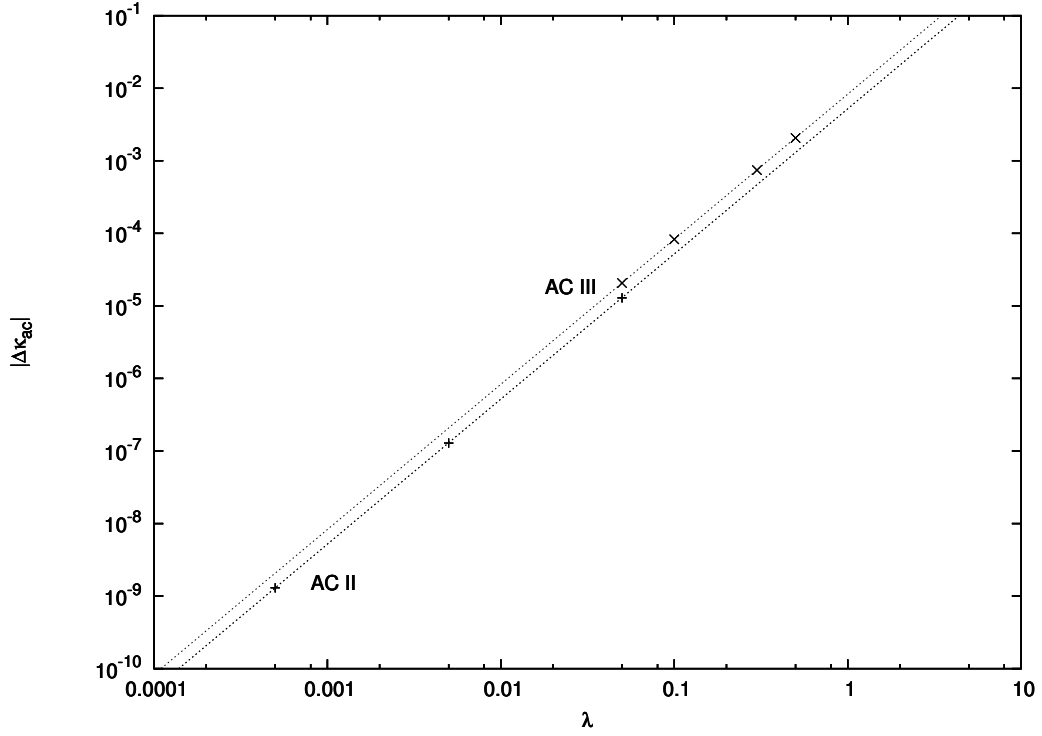
Figure 4.6: The κ-offset $\Delta\kappa_{ac}$ as a function of λ for the avoided crossings shown in Figures 4.3 and 4.4. The functions $|\Delta\kappa_{ac}| = 5.2 \times 10^{-3}\ \lambda^2$ and $|\Delta\kappa_{ac}| = 8.3 \times 10^{-3}\ \lambda^2$ are overplotted.

crossings I,II, and III, respectively. The κ-offset of the avoided crossings are given by

$$\Delta\kappa_{ac} = B\ \lambda^2\,, \tag{4.7}$$

where $B \approx \{5.2 \times 10^{-3}, -8.3 \times 10^{-3}\}$ for avoided crossings II and III ($\Delta\kappa_{ac} = 0$ for avoided crossing I).

4.2.2 Perturbation theory results

We now use perturbation theory to determine the behavior of the Floquet eigenvalues and eigenstates in the neighborhood of avoided crossings. We will obtain

approximate solutions $(|\phi_\alpha\rangle, \epsilon_\alpha)$ to the Floquet eigenvalue equation

$$\hat{H}_F(\kappa, \lambda)|\phi_\alpha(\kappa, \lambda)\rangle = \left(\hat{H}_F^0(\kappa) + \lambda\hat{V}\right)|\phi_\alpha(\kappa, \lambda)\rangle = \epsilon_\alpha(\kappa, \lambda)|\phi_\alpha(\kappa, \lambda)\rangle, \qquad (4.8)$$

where $\hat{H}_F^0(\kappa)$ is the Floquet pendulum Hamiltonian, $\hat{V} = 2\cos\hat{x}\,\cos(\omega t)$, and λ is considered a small parameter. Our unperturbed system is the two-fold degenerate system $\hat{H}_F^0(\kappa_0)$, where κ_0 is the parameter value at which the eigenvalue curves of two Floquet pendulum states $|\alpha^0(\kappa)\rangle \equiv |n_\alpha, q_\alpha\rangle$ and $|\beta^0(\kappa)\rangle \equiv |n_\beta, q_\beta\rangle$ cross. We have seen in Section 4.2.1 that, for $\lambda \neq 0$, the closest approach of the eigenvalues ϵ_α and ϵ_β involved in an avoided crossing may not occur at $\kappa = \kappa_0$, so an offset must be allowed for. We therefore introduce into (4.8) an arbitrary function $\kappa(\lambda) = \kappa_0 + \Delta\kappa(\lambda)$ and expand $\Delta\kappa(\lambda)$ as a power series in λ. The particular value $\kappa_{ac}(\lambda)$ at which the eigenvalues make their closest approach can then be determined by solving the extremal condition for $\Delta\epsilon_{\alpha\beta} \equiv |\epsilon_\alpha(\kappa, \lambda) - \epsilon_\beta(\kappa, \lambda)|$,

$$\left.\frac{\partial\Delta\epsilon_{\alpha\beta}}{\partial\kappa}\right|_{\kappa=\kappa_{ac}} = 0\,, \qquad (4.9)$$

at each order to fix the expansion coefficients of $\Delta\kappa(\lambda)$. In this manner, we find the perturbed eigenstates and eigenvalues at $\kappa = \kappa_{ac}$.

The details of the perturbation analysis are given in Appendix A. The results may be summarized as follows. The breaking of the degeneracy between states $|\alpha^0\rangle$ and $|\beta^0\rangle$ occurs at the lowest order λ^N for which the coupling between these states, $v_{\alpha\beta}^{(N)}$ (defined below), is nonzero. At this order, the two Floquet eigenvalues in the region of the avoided crossing are determined by the eigenproblem of a 2×2 matrix in the basis of the unperturbed states $|\alpha^0(\kappa_0)\rangle$ and $|\beta^0(\kappa_0)\rangle$:

$$\begin{pmatrix} \Delta\kappa^{(N)}\delta E_\alpha + v_{\alpha\alpha}^{(N)} & v_{\alpha\beta}^{(N)} \\ v_{\beta\alpha}^{(N)} & \Delta\kappa^{(N)}\delta E_\beta + v_{\beta\beta}^{(N)} \end{pmatrix} \begin{pmatrix} C_\alpha^\pm \\ C_\beta^\pm \end{pmatrix} = \epsilon_\pm^{(N)} \begin{pmatrix} C_\alpha^\pm \\ C_\beta^\pm \end{pmatrix}. \qquad (4.10)$$

The coefficients $C_\alpha^\pm$ and $C_\beta^\mp$ determine the zeroth-order near-degenerate eigenstates in the region of the avoided crossing; $\Delta\kappa^{(N)}$ and $\epsilon_\pm^{(N)}$ are the coefficients of λ^N in the expansions of the arbitrary κ-offset and the near-degenerate Floquet eigenvalues $\epsilon_\pm$, respectively; $\delta E_i = \langle n_i(\kappa_0)|\cos\hat{x}|n_i(\kappa_0)\rangle$ are the slopes of the unperturbed eigencurves; and $v_{ij}^{(N)}$ depends on the matrix elements of the perturbation operator:

$$V_{lm} \equiv \langle\langle n_l, q_l|\hat{V}|n_m, q_m\rangle\rangle = \langle n_l(\kappa_0)|\cos\hat{x}|n_m(\kappa_0)\rangle\left(\delta_{q_l,q_m+1} + \delta_{q_l,q_m-1}\right) . \quad (4.11)$$

For the first three orders in λ, these couplings are

$$v_{ij}^{(1)} = V_{ij} \quad (4.12)$$

$$v_{ij}^{(2)} = \sum_{\gamma\notin\{\alpha,\beta\}} \frac{V_{i\gamma}V_{\gamma j}}{\epsilon^{(0)} - \epsilon_\gamma^{(0)}} \quad (4.13)$$

$$v_{ij}^{(3)} = \sum_{\gamma\notin\{\alpha,\beta\}} \left\{ \sum_{\sigma\notin\{\alpha,\beta\}} \frac{V_{i\gamma}V_{\gamma\sigma}V_{\sigma j}}{\left(\epsilon^{(0)} - \epsilon_\gamma^{(0)}\right)\left(\epsilon^{(0)} - \epsilon_\sigma^{(0)}\right)} \right.$$

$$\left. +\delta_{ij}\frac{V_{i\gamma}V_{\gamma i}\left[V_{\alpha\alpha}(\delta E_\alpha - \delta E_\gamma) + V_{\beta\beta}\left(\delta E_\gamma - \delta E_\beta\right)\right]}{\left(\epsilon^{(0)} - \epsilon_\gamma^{(0)}\right)^2} \right\} , \quad (4.14)$$

where $i,j \in \{\alpha,\beta\}$, the zeroth-order eigenvalues $\epsilon_l^{(0)}$ are taken at κ_0, and we write $\epsilon^{(0)} = \epsilon_\pm^{(0)}$. Using Eqs. (4.10) and (4.9) we find that the Nth-order corrections to the eigenvalues, at the position of the avoided crossing, are given by

$$\epsilon_\pm^{(N)}(\kappa_{ac}) = \frac{1}{2}\left[v_{\alpha\alpha}^{(N)} + v_{\beta\beta}^{(N)} + \Delta\kappa_{ac}^{(N)}\left(\delta E_\alpha + \delta E_\beta\right)\right]$$

$$\pm \frac{1}{2}\sqrt{\left[v_{\alpha\alpha}^{(N)} - v_{\beta\beta}^{(N)} + \Delta\kappa_{ac}^{(N)}\left(\delta E_\alpha - \delta E_\beta\right)\right]^2 + 4|v_{\alpha\beta}^{(N)}|^2} \quad (4.15)$$

$$= \frac{v_{\beta\beta}^{(N)} - v_{\alpha\alpha}^{(N)}}{\delta E_\alpha - \delta E_\beta} \pm |v_{\alpha\beta}^{(N)}| .$$

κ_{ac}	(n_α, q_α)	(n_β, q_β)	$\Delta q_{\alpha\beta}$	A_{num}	A_{pt}	B_{num}	B_{pt}
7.46	$(1,0)$	$(5,-1)$	1	5.44×10^{-3}	5.5×10^{-3}	$---$	$---$
7.83	$(1,0)$	$(7,-2)$	2	1.02×10^{-3}	1.0×10^{-3}	5.2×10^{-3}	5.2×10^{-3}
9.97	$(0,0)$	$(8,-3)$	3	7.35×10^{-7}	7.3×10^{-7}	-8.3×10^{-3}	-8.3×10^{-3}

Table 4.1: Comparison of numerical results to those of perturbation theory. The quantities A_{num} and B_{num} are obtained from numerical simulation and A_{pt} and B_{pt} are obtained from perturbation theory.

At orders $0 < M < N$, the two eigenvalues $\epsilon_\pm$ are degenerate at an offset from $(\kappa_0, \epsilon^{(0)})$ specified by the coefficients

$$\Delta\kappa^{(M)} = \frac{v_{\beta\beta}^{(M)} - v_{\alpha\alpha}^{(M)}}{\delta E_\alpha - \delta E_\beta} , \tag{4.16}$$

and

$$\Omega^{(M)} = \frac{v_{\beta\beta}^{(M)} \delta E_\alpha - v_{\alpha\alpha}^{(M)} \delta E_\beta}{\delta E_\alpha - \delta E_\beta} . \tag{4.17}$$

The origin of the numerical results presented in section 4.2.1 is now clear. The matrix elements of the perturbation V_{ij} are non-zero only when $\Delta q_{ij} = 1$. Therefore, for an avoided crossing between states $|\phi_\alpha\rangle$ and $|\phi_\beta\rangle$, we must have $\Delta q_{\alpha\beta} = N$. Using Eq. (4.15) and the fact that $\epsilon^{(M<N)}$ is the same for $|\phi_\alpha\rangle$ and $|\phi_\beta\rangle$, we find that, to lowest order in λ, the minimum spacing is given by

$$\Delta_{\alpha\beta} = 2 \left| v_{\alpha\beta}^{(\Delta q_{\alpha\beta})} \right| \lambda^{\Delta q_{\alpha\beta}} . \tag{4.18}$$

Its interesting to note that the κ-offset of an avoided crossing in this system is dependent on λ^2, because $v_{\alpha\alpha}^{(2)}$ and $v_{\beta\beta}^{(2)}$ are non-zero, even when $\Delta q_{\alpha\beta} > 2$.

Table 4.1 shows a quantitative comparison of the numerical results presented in the previous section (in terms of the coefficients A and B of Eqs. (4.6) and (4.7)) to those obtained by the perturbation analysis. For all three examples of

avoided crossings, we see excellent agreement. We have also verified the predictions of perturbation theory for a number of other avoided crossings in this system (as well as those in systems with different values of ω), finding similar agreement.

A number of other characteristics of the avoided crossings can be determined from our perturbation analysis. Substituting $\epsilon_\pm^{(N)}(\kappa_{ac})$ and $\Delta\kappa_{ac}^{(N)}$ into Eq. (4.10), we find that at the position of the avoided crossing, the two perturbed Floquet eigenstates (to lowest order in λ) become an equal superposition of the two associated Floquet pendulum states, i.e.

$$|C_\alpha^\pm(\Delta\kappa_{ac})| = |C_\beta^\pm(\Delta\kappa_{ac})|. \tag{4.19}$$

We may also determine the relative magnitudes of these coefficients at some κ value near the avoided crossing. If, instead of calculating $\Delta\kappa^{(N)}$ by the extremal condition, we instead determine the κ-offset where the eigenvalue separation is a times the minimum value, we find

$$\Delta\kappa^{(N)}\Big|_{\Delta\epsilon_{\alpha\beta}=a\Delta_{\alpha\beta}} = \frac{v_{\alpha\alpha}^{(N)} - v_{\beta\beta}^{(N)}}{\delta E_{\alpha\alpha} - \delta E_{\beta\beta}} \pm \frac{2\sqrt{a^2 - 1}\,|v_{\alpha\beta}^{(N)}|}{|\delta E_{\alpha\alpha} - \delta E_{\beta\beta}|}. \tag{4.20}$$

A simple calculation then shows that the coefficients obey

$$\left[\frac{|C_\alpha^\pm|}{|C_\beta^\pm|}\right]_{\Delta\epsilon_{\alpha\beta}=a\Delta_{\alpha\beta}} = \frac{1}{|a \pm \sqrt{a^2 - 1}|}, \tag{4.21}$$

where we have assumed that $(\delta E_\alpha - \delta E_\beta) > 0$. As $a \to (0, \infty)$, we see that, for example, $\frac{|C_\alpha^+|}{|C_\beta^+|} \to (1, 0)$, as expected. This verifies the qualitative behavior seen in the Husimi distributions plotted in Figures 4.2-4.4.

4.3 Tunneling in perturbed quantum pendulum

Under the evolution of the system given in Eq. 4.3, an initial state $|\psi_+(0)\rangle$ which is localized in classical phase space (in the sense of its Husimi distribution) in a region of positive momentum at $p \approx p_0$ may undergo time-periodic dynamical tunneling [15], across the central resonance (and all intervening KAM tori) to the opposite momentum region at $p \approx -p_0$. The mechanism for this behavior is the existence of a near-degenerate and opposite parity pair of Floquet eigenstates which each have localization near p_0 and $-p_0$. If the Floquet eigenvalues of these two states are far from any avoided crossings, the tunneling dynamics are well described by a two-state process exactly analogous to the tunneling through a potential barrier in the time-independent double well system ([75], see also Section 1.1.1). In the vicinity of an avoided crossing, however, the dynamics are influenced by a third state with partial localization in the regions of $\pm p_0$ and the time-evolution takes on a more complicated beating behavior. In this section we analyze this tunneling behavior in the perturbative regime (λ small) and then apply the results to tunneling oscillations observed in the Texas experiment. Although the experimental system cannot be considered to be in a perturbative regime, we identify the diabolical point associated to the relevant avoided crossing and show that an approximate result can be obtained numerically which characterizes this avoided crossing quite well.

To analyze the tunneling induced by the Hamiltonian in the perturbed quantum pendulum Eq. 4.3, we consider again the one-period time-evolution operator $\hat{U}(T)$ defined in Section 3.1.3 and its eigenvectors, the time-strobed Floquet eigenstates $|\phi_\alpha(T)\rangle = |\phi_\alpha(0)\rangle$ (we will drop the explicit reference to "time-strobed" in this section). As a particular example, consider the avoided crossing shown in Figure 4.7 (the same as that shown in Figure 4.2, but with the odd-parity state now included, shown as a dotted line). At $\kappa = 7.456$, a value far from the avoided crossing, the opposite-parity pair of states $|\phi_\alpha\rangle$ and $|\phi_\gamma\rangle$ are near-degenerate
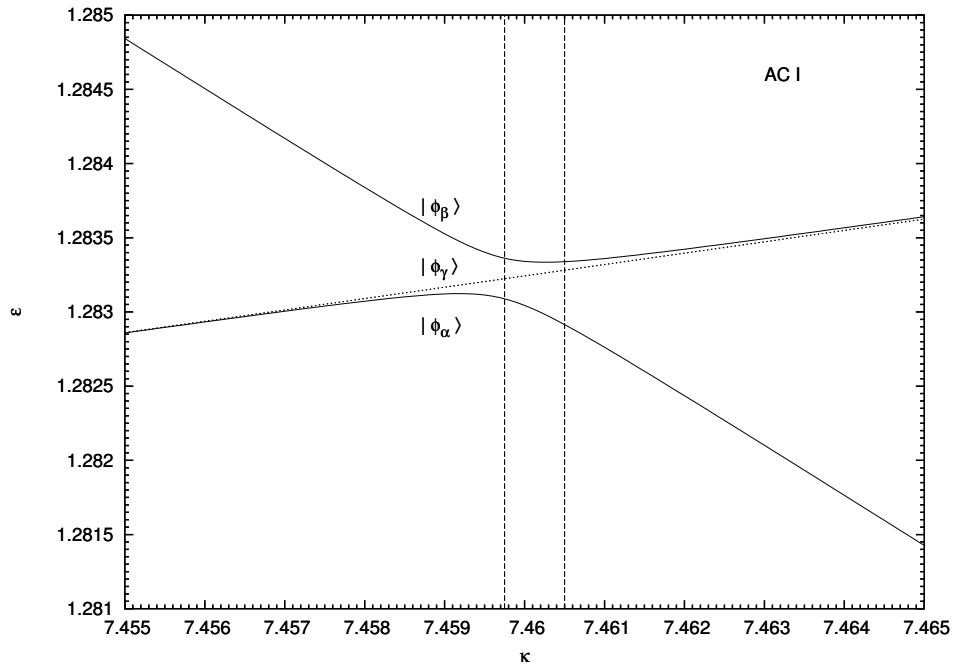
Figure 4.7: The avoided crossing from Figure 4.2 (a), now with the relevant odd-parity state included (dotted line). The vertical lines are the κ values at which the time-evolution in Figure 4.8 was obtained.

$(|\epsilon_\gamma - \epsilon_\alpha| \approx 4.5 \times 10^{-6})$ and have localization at $p \approx \pm 5$. The phase space localization of state $|\phi_\beta\rangle$ is completely within the central resonance and does not overlap significantly with this pair. We can construct an initial state, localized at either $p \approx 5$ or -5, as an equal superposition of the two near-degenerate Floquet states, i.e. $|\psi_\pm(0)\rangle = \frac{1}{\sqrt{2}}(|\phi_\alpha\rangle \pm |\phi_\gamma\rangle)$. When either is acted on by $\hat{U}(nT)$, the evolution is periodic, oscillating between $p \approx \pm 5$ with a tunneling frequency $\omega_{tun} = |\epsilon_\alpha - \epsilon_\gamma|$. The corresponding number of modulation periods for complete oscillation is then $n_{tun} = \omega/\omega_{tun} \approx 5.3 \times 10^6$.

In the region of the avoided crossing, the odd-parity state $|\phi_\gamma\rangle$ will be approximately unchanged, while states $|\phi_\alpha\rangle$ and $|\phi_\beta\rangle$ become, to lowest order in λ, superpositions of their unperturbed, Floquet pendulum, counterparts. Therefore, in the neighborhood of the avoided crossing, both $|\phi_\alpha\rangle$ and $|\phi_\beta\rangle$ will have significant support in the same region of phase space as $|\phi_\gamma\rangle$. At the exact position κ_{ac} of the avoided crossing, where $|\phi_\alpha\rangle$ and $|\phi_\beta\rangle$ are an equal superposition of the unperturbed states, the initial conditions localized at either $p \approx 5$ or -5 can then be written

$$|\psi_\pm(0)\rangle = \frac{1}{2}|\phi_\alpha\rangle + \frac{1}{2}|\phi_\beta\rangle \pm \frac{1}{\sqrt{2}}|\phi_\gamma\rangle \,, \tag{4.22}$$

where all three eigenstates are evaluated at $\kappa = \kappa_{ac}$. Applying the time-evolution matrix to $|\psi_+(0)\rangle$ we find, after n applications,

$$\begin{aligned}|\psi_+(nT)\rangle &= \hat{U}(nT)|\psi_+(0)\rangle \tag{4.23}\\ &= e^{-inT\epsilon_\beta}\left(\frac{e^{-inT\Delta\epsilon_{\alpha\beta}}}{2}|\phi_\alpha\rangle + \frac{1}{2}|\phi_\beta\rangle + \frac{e^{-inT\Delta\epsilon_{\gamma\beta}}}{\sqrt{2}}|\phi_\gamma\rangle\right) \,,\end{aligned}$$

where $\Delta\epsilon_{ij} \equiv \epsilon_i - \epsilon_j$, here. If we make the assumption that $|\Delta\epsilon_{\beta\gamma}| = |\Delta\epsilon_{\alpha\gamma}| \equiv \Delta$ at $\kappa = \kappa_{ac}$, we see that $|\psi_+(\frac{\pi}{\Delta})\rangle \sim |\psi_-(0)\rangle$. This three-state process therefore generates a new, larger, tunneling frequency $\omega_{tun} = \Delta$. The time-evolution of $|\psi_+(0)\rangle$ at $\kappa \approx \kappa_{ac}$ is shown in Figure 4.8.a. Notice that the theoretical tunneling
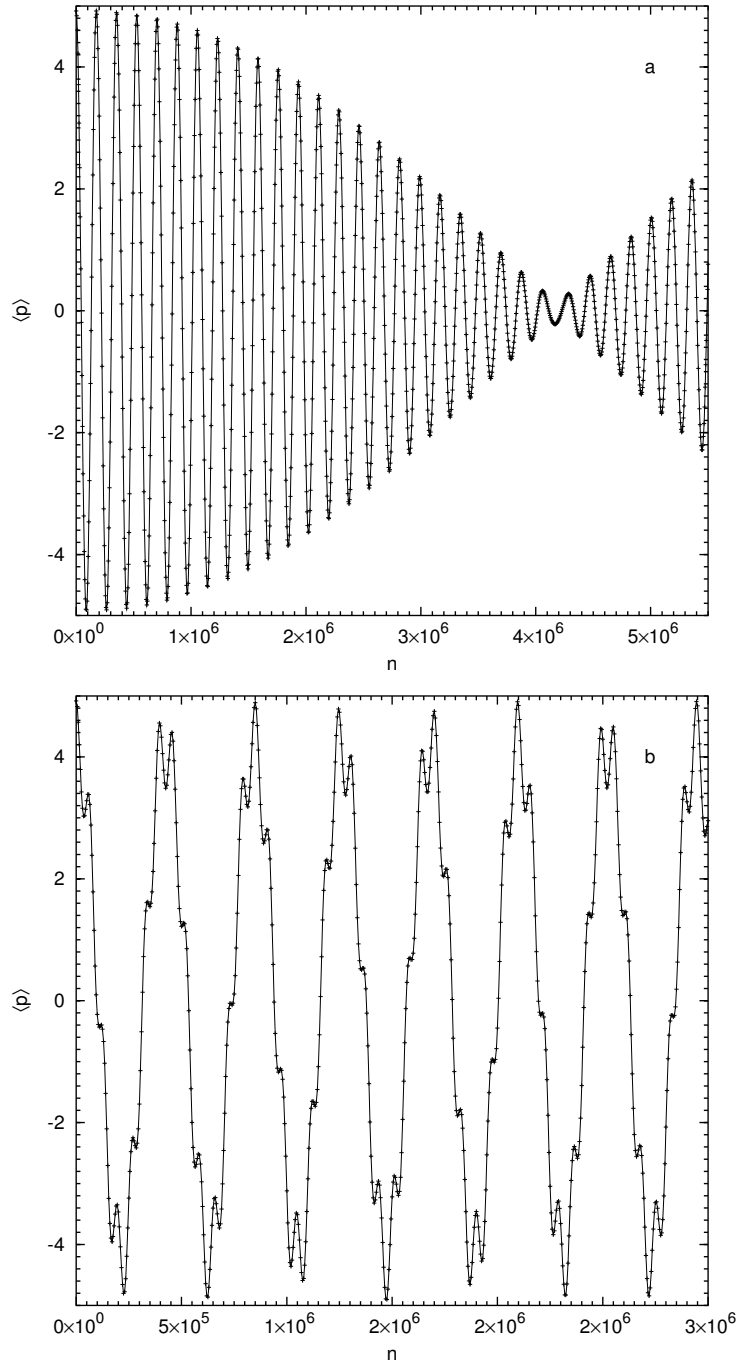
Figure 4.8: The evolution of state $|\psi_+(0)\rangle$ (created by the superposition of the near-degenerate states at $\kappa = 7.456$) under the action of $\hat{U}(T)$ at $\kappa \approx \kappa_{ac}$ (a) and $\kappa = 7.4605$ (b).

period $n_{tun} = \frac{\omega}{\Delta} \approx 1.8 \times 10^5$ is modulated by a beat period resulting from the small difference $\Delta\epsilon_{\beta\gamma} - \Delta\epsilon_{\gamma\alpha}$. As the position of the avoided crossing is chosen more precisely, and $\epsilon_\gamma \to \frac{\epsilon_\alpha + \epsilon_\beta}{2}$, the period of beating goes to infinity.

Between these two extremes of regular two-state and three-state tunneling, at other values of the parameter κ along the avoided crossing, the tunneling takes on a beating behavior due to the two eigenvalue differences between the odd-parity state and each even-parity state. An example of this (the evolution of $|\psi_+(0)\rangle$ under $\hat{U}(T)$ at $\kappa = 7.4605$) is shown in Figure 4.8.b. For this and all values of the parameter κ, the evolution of the momentum expectation of $|\psi_+(0)\rangle$ is well fit by the simple function

$$\langle p \rangle(nT) = A_\alpha \cos\left(\Delta\epsilon_{\gamma\alpha} nT\right) + A_\beta \cos\left(\Delta\epsilon_{\beta\gamma} nT\right) , \qquad (4.24)$$

where A_α and A_β can be related to the overlap of $|\psi_+(0)\rangle$ with $|\phi_\alpha\rangle$ and $|\phi_\beta\rangle$, respectively.

The variation of two-state tunneling frequencies in the vicinity of avoided crossings has been remarked on by many authors [51; 52; 53; 28; 85; 82; 9; 63] in many different systems, and is often attributed to the influence of underlying classical chaos. Classical chaos in a non-perturbative regime will certainly introduce additional complications to the quantum dynamical tunneling process which we have not investigated here (notably the interaction between tunneling through dynamical barriers and free evolution in a region dominated by chaos [71]); and avoided crossings will become larger, more numerous, and may overlap, leading to interaction of more than three relevant states. However, as we have seen in this and previous sections, the basic mechanism for "tunneling enhancement" does not necessarily require global chaos but only the non-integrability which leads to avoided crossings. Indeed, for the non-integrability parameter used in this section ($\lambda = 5 \times 10^{-2}$), the classical phase space has only small regions of chaos.
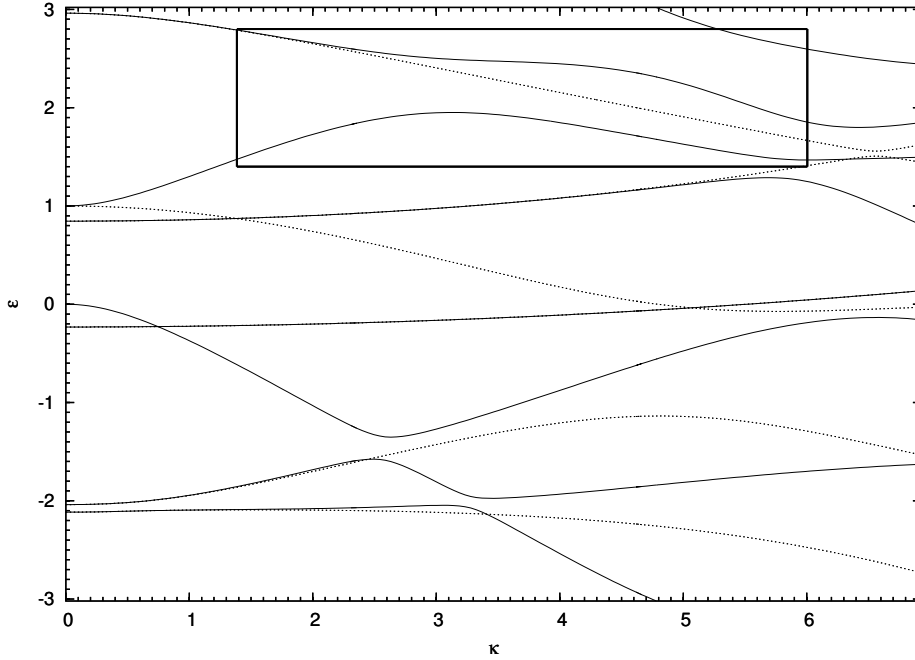
Figure 4.9: Floquet eigenvalue curves for the system considered in [80] ($\lambda = \kappa/2$, $\omega \approx 6.04$).

4.4   Analysis of tunneling in the Texas experiment

As an application of the tunneling results of the previous section, we consider the experiment of Steck, Oskay and Raizen [78; 80]. The effective Hamiltonian which describes this optical lattice experiment depends on a single parameter, α, and can be considered a special case of the perturbed quantum pendulum by setting $\kappa \approx \alpha/2.17$ (up to a sign difference which can be removed by a π-translation of the angle variable), $\lambda = \kappa/2$, and $\omega \approx 6.04$. It should be noted that this system is not connected to the Floquet pendulum system since λ is not an independent parameter. Instead, in the limit $\lambda, \kappa \to 0$, the free particle Hamiltonian is obtained.

The primary result of the experiments detailed in [80] is the observation of dynamical tunneling between two resonance islands in the classical phase space (located at $p \approx \pm 3$), which exhibits oscillation frequencies dependent on the parameter

66

value considered and independent of the modulation frequency. In particular, for a range of parameter values, the observed tunneling oscillations were dominated by two primary frequencies. The Floquet eigenvalue curves for the experimental system are shown in Figure 4.9, and the experimentally observed tunneling frequencies are shown in Figure 4.10.b, overplotted on the differences of eigenvalues between three particular Floquet eigenstates. These three states exhibit significant localization in the region of the classical resonance islands at some values of the parameter κ [54]. The experimental frequencies are well predicted by only two of these differences, namely $\Delta\epsilon_{\alpha\gamma}$ and $\Delta\epsilon_{\beta\gamma}$.

The oscillations seen in the parameter region $\kappa \in [3, 4.75]$ are due to the existence of an avoided crossing between the eigenvalues of the even-parity states labeled $|\phi_\alpha\rangle$ and $|\phi_\beta\rangle$. As can be seen in the overplotted Husimi distributions, these two even-parity states originate at small κ values from two disconnected regions of the phase space, the first residing at $p \approx 0$, and the other at the positions of the classical resonance islands where the odd parity state $|\phi_\gamma\rangle$ also has its primary support. In passing through this avoided crossing, the odd-parity state retains its original character, while the two even-parity states become mutual superpositions of their small κ character. It is clear that this avoided crossing is not of the ideal form considered in the perturbative regime. The superposing effects of this avoided crossing extend well beyond the minimum eigenvalue separation at $\kappa \approx 3.0$ (see Figure 4.10.a), due to the natural eigenvalue curvature of a state with the low κ character of $|\phi_\beta\rangle$ (a simpler example of this is the eigenvalue labeled $(2, 0)$ in Figure 3.2.b). Just past this minimum spacing, the eigenvalue of state $|\phi_\alpha\rangle$ curves back downward toward that of $|\phi_\beta\rangle$, immediately beginning a second avoided crossing and thus preserving the composite nature of these two even-parity states through $\kappa \approx 6$. As a further complication, in the parameter region $\kappa \in [5, 7]$, states $|\phi_\alpha\rangle$ and $|\phi_\beta\rangle$ are joined by two other even-parity states in a complex and overlapping set of

67

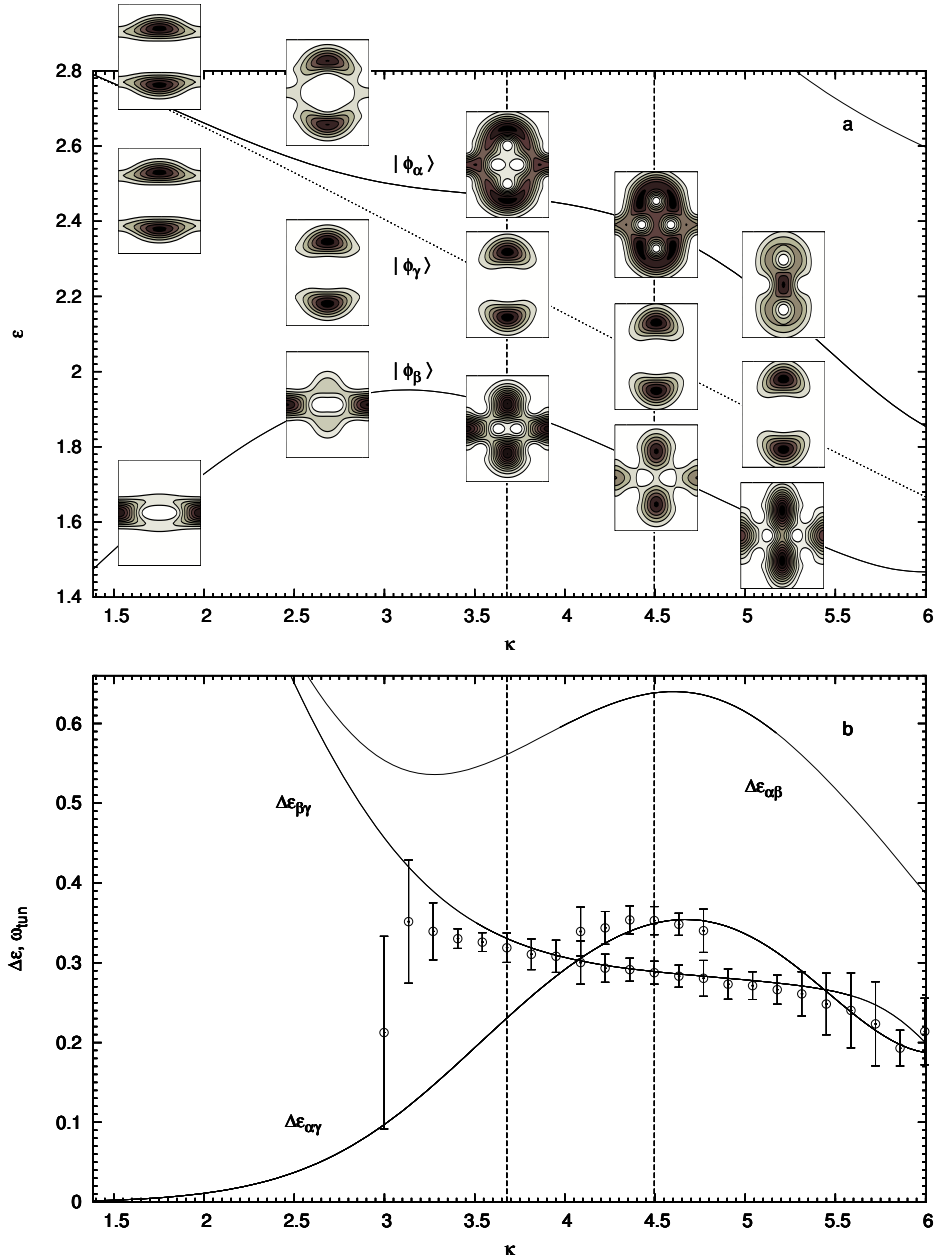Figure 4.10: The boxed region of Figure 4.9 where an avoided crossing occurs between two even parity states (a). The Husimi distributions of these and a third, odd-parity, state are overplotted, with axes of $x_0 \in (0, 2\pi)$ and $p_0 \in (-6, 6)$. The differences of these three eigenvalues are shown in (c), with experimental tunneling frequencies overplotted (circles, reprinted with permission from Steck, *et. al.* [80], Fig. 1).

avoided crossings.

Despite these complications, we can identify the dynamical tunneling in the parameter region $\kappa \in [2.5, 4.75]$ to be a three-state process involving those states shown in Figure 4.10.a. As predicted by the results of the previous section, the observed tunneling frequencies involve only differences in Floquet eigenvalue between the odd parity state and the two even parity states. A direct comparison of the oscillations from [80] with the numerically calculated evolution of an initially localized state $|\psi_+(0)\rangle$ under $\hat{U}(T)$ is shown in Figure 4.11 for the values $\kappa = 3.68$ and 4.50. Neglecting dissipation and a momentum offset of the experimental values (due to the fact that not all atoms contributing to the average are participating in the dynamics), there is good agreement in the second case. In the first case, and for all parameter values between $\kappa = 3$ and 4, the experiment seems to pick up only one of the underlying frequencies ($\Delta\epsilon_{\gamma\beta}$, while the numerics predict nearly equal contributions from $\Delta\epsilon_{\gamma\beta}$ and $\Delta\epsilon_{\alpha\gamma}$. It was noted in Reference [55] that the detection of fewer than the predicted number of frequency contributions to the tunneling behavior was also found in another experimental system [35].

Finally, we would like to consider the origin of the avoided crossing involved in the dynamical tunneling observed in [80]. Figure 4.12 shows the avoided crossing of Figure 4.10.a lying on the eigenvalue surfaces ϵ_α and ϵ_β in $\kappa - \lambda$ space. One can see that these two surfaces meet at a diabolical point on the $\kappa = 0$ axis, where $\lambda \approx 2.8$. Numerical analysis shows that, *in the neighborhood of the diabolical point,* the minimum spacing between the two eigenvalue surfaces is linearly dependent on κ, with

$$\Delta_{\alpha\beta} = 9.22 \times 10^{-2}\kappa\,. \tag{4.25}$$

This result is in good agreement with a perturbation analysis similar to that of Appendix A, but with κ as the small expansion parameter. The predicted minimum
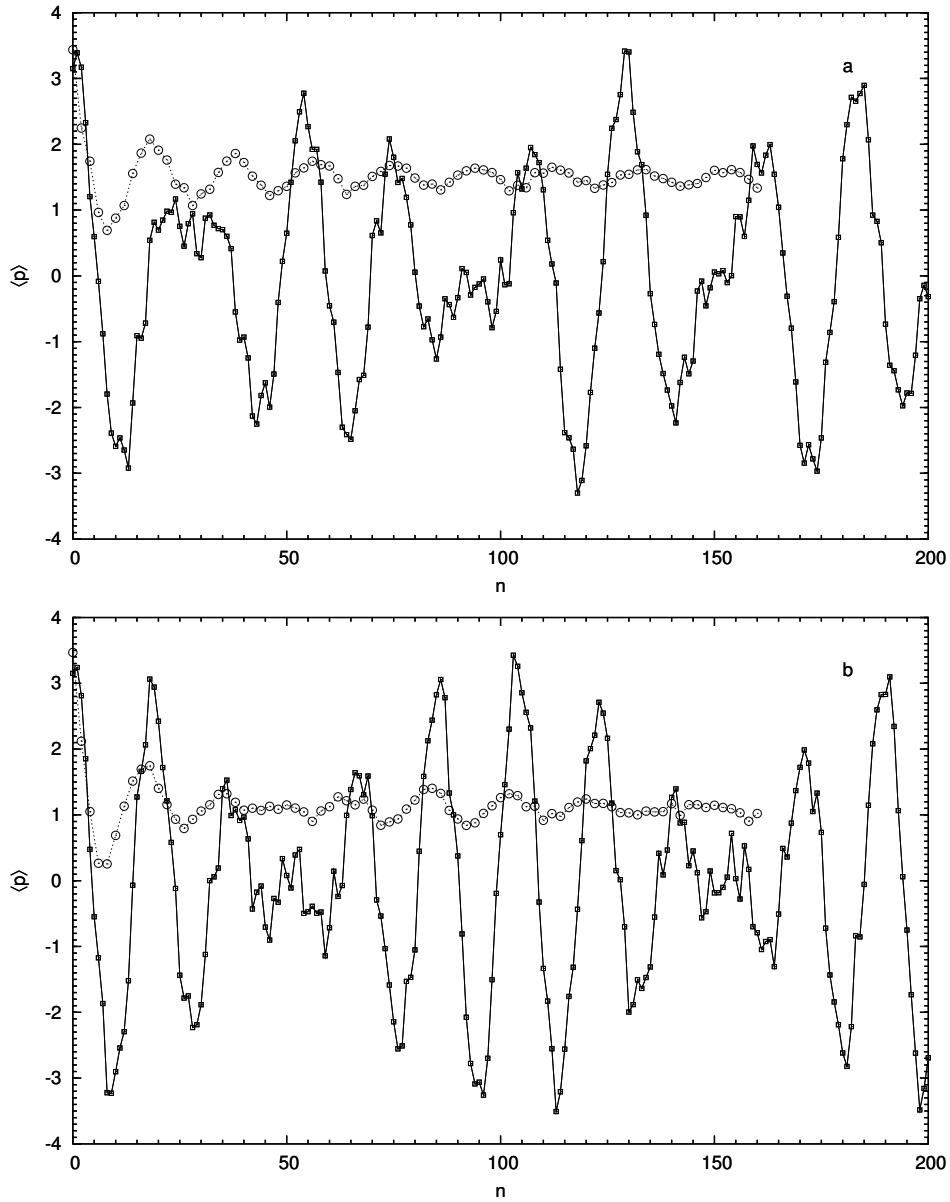
Figure 4.11: Numerical evolution (squares) of a positive momentum centered initial state under the time-evolution operator at $\kappa = 3.68$ (a) and 4.50 (b), with experimental values overplotted (circles, reprinted with permission from Steck, *et. al.* [80], Fig. 2).

Figure 4.12: Eigenvalue surfaces, over $\kappa - \lambda$ space, of the even parity Floquet eigenstates involved in the avoided crossing of Figure 4.10.a. The eigenvalues on the particular curve investigated in reference [80] are overplotted in bold. A dashed line traces the minimum separation of the two surfaces from the diabolical point at $\kappa = 0$, $\lambda \approx 2.8$ to the avoided crossing seen in the experiment.

spacing from such an analysis yields

$$\Delta_{\alpha\beta,\text{pt}} = 2|V'_{\alpha\beta}|\kappa \approx 9.2 \times 10^{-2}\kappa\,, \tag{4.26}$$

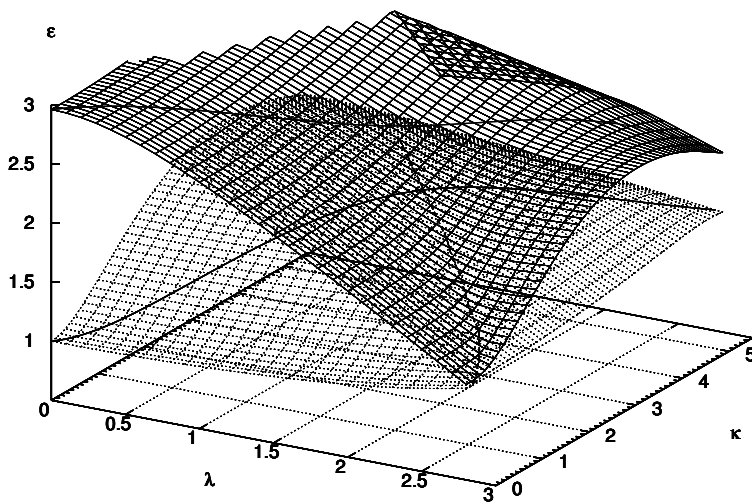where the matrix element must be numerically calculated as the coupling of the two degenerate Floquet eigenstates of the ($\kappa = 0.0, \lambda = 2.8$) system through $\hat{V}' = \cos\hat{x}$, the coefficient of κ. Although the avoided crossing in the experiment (Figure 4.10.a) appears at a parameter value outside the range of validity of perturbation theory, the observed minimum spacing between $\Delta\epsilon_\alpha$ and $\Delta\epsilon_\beta$ agrees with Eq. 4.26 to within a factor of two.

Chapter 5

STIRAP-like transitions in an optical lattice

In this chapter, we introduce a method for the coherent acceleration of atoms trapped in an optical lattice, using the well-known model for stimulated Raman adiabatic passage (STIRAP). Specifically, we show that small harmonic modulations of the optical lattice amplitude, with frequencies tuned to the eigenvalue spacings of three "unperturbed" eigenstates, reveals a three-state STIRAP subsystem. We use this model to realize an experimentally achievable method for transferring trapped atoms from stationary to motional eigenstates. The work detailed in this chapter has been accepted for publication and will appear later this year [38].

5.1 Coherent acceleration of atoms

In this chapter we present a method for coherently accelerating atoms by affecting a transition between the ground states of a stationary and traveling optical lattice. The analysis is performed on the eigenstates of the effective Hamiltonian for a system of two optical lattices and can be interpreted as a transition between

motional eigenstates for atoms in a time and spatially periodic potential. The resulting momentum transfer for the particular system we study is approximately six recoil momenta, but could be applied to obtain an acceleration of larger momentum change by the choice of different values of the parameters in the effective Hamiltonian. Although this work is unique in the sense that the analysis is performed solely on the dynamical eigenstates of the effective "two-resonance" Hamiltonian, a number of other methods for atomic acceleration have been presented and implemented. Here, we review a few of these techniques.

We described in Chapter 2 how an effective Hamiltonian is derived for a two-level atom in the presence of far-detuned counter-propagating lasers. The detuning of these lasers allows for the elimination of the excited level and analysis in terms the dynamical eigenstates of atoms in the ground state. A number of authors have used the *resonant* coupling by lasers of the internal electronic energy levels to produce momentum transfer. The STIRAP model, which we describe in the next section, was utilized by Chu and co-workers [90; 91] to affect transitions between the two ground states of ultracold cesium atoms. The two levels were each resonantly coupled to an excited level with lasers. A STIRAP transition from an occupied ground state to the target ground state was achieved by applying the laser pulses in a "non-intuitive" sequence where the target (unpopulated) ground state was coupled to the excited level before the populated state. When the lasers are counter-propagating, this results in a two photon momentum kick. In Reference [91] the authors describe how a sequence of these transitions can be used to accelerate atoms by 140 recoil momenta.

Another method for atom acceleration has been proposed and implemented by two groups, one at the University of Texas at Austin [89] and another at Ecole Normale Supérieure (ENS) in Paris [7] (see also [72]). In these experiments, a standing wave of light was accelerated by a linear change in the frequency difference

of two counter-propagating lasers (see Section 2.1). In the frame of the accelerating lattice, atoms trapped in the ground state (lowest Bloch band) experience an inertial force which induces Bloch oscillations. In the laboratory frame these oscillations are superposed on a linear increase in atomic velocity, where in each Bloch oscillation period atoms obtain a two photon increase in momentum. Under the influence of such an accelerating lattice, atoms were accelerated from far below the recoil momentum to approximately 120 recoil momenta.

A third method for atom acceleration was implemented by a group at Oxford [67; 25]. In this experiment, a standing wave of light was pulsed at a particular frequency (yielding an effective Hamiltonian for the δ-kicked rotor) leading to a momentum change with each pulse. At certain values of the pulse frequency an "accelerator mode" is obtained in which the momentum of the atoms increases linearly with the number of kicks. This behavior is exactly analogous to the acceleration of a child on a swing by adjusting the time between applied pushes. In this manner the authors were able to obtain atomic velocities corresponding to $\sim$100 photon recoil momenta.

5.2   STIRAP Introduction

Stimulated Raman adiabatic passage (STIRAP) is a method for achieving coherent transitions between quantum states by applying two coupling fields in a non-intuitive pulse sequence. The frequencies of these fields are tuned to the eigenvalue spacings between the "initial" and "target" states and a third "intermediate" state. When the coupling of the target and intermediate states precedes that of the initial and intermediate states in time, population transfer from the initial to target state is achieved. In the adiabatic limit, the transition is 100% efficient and involves no occupation of the intermediate state. The use of STIRAP for atomic and molecular systems was first demonstrated experimentally by Gaubatz and coworkers [23; 24],

who achieved population transfer between vibrational levels in a beam of sodium molecules. Further references on the STIRAP transitions in atoms and molecules can be found in the review by Vitanov *et al* [83]. In atom optics experiments, STIRAP has been used for coherent momentum transfer [58; 26; 90; 91], and velocity-selective coherent population trapping for laser cooling of trapped atoms [20; 49; 46]. Extensions of STIRAP, with a particular focus on the influence of quantum chaos, have been studied by Na and Reichl [64; 65]. Na *et al* [66] have also use STIRAP to control the isomerization transition of HOCl.

As a theoretical model, STIRAP can be defined by the adiabatic behavior of a three-level system, which in some basis $(|a\rangle, |b\rangle, |c\rangle)$ is represented by the Hamiltonian

$$H(t') = -\frac{\hbar}{2} \begin{pmatrix} 0 & W_1(t') & 0 \\ W_1(t') & -2\Delta & W_2(t') \\ 0 & W_2(t') & 0 \end{pmatrix}, \tag{5.1}$$

under the variation of the parameters W_1 and W_2, with Δ a constant. This model, which we refer to as the "STIRAP model" hereafter, was first introduced by Kuklinski *et al* [48], following significant work by Hioe *et al* [36; 68; 11], to succinctly describe the experimental results of Gaubatz *et al* [23]. Starting from a system in which the pairs of states $(|a\rangle, |b\rangle)$ and $(|b\rangle, |c\rangle)$ are each dipole-coupled by monochromatic electric fields, the STIRAP model is derived by applying the rotating-wave approximation and assuming an equal detuning of the coupling frequencies Δ (see Figure 5.1). In that particular system the $W_i(t')$ are the Rabi oscillation frequencies corresponding to the two couplings. The STIRAP transition, however, does not depend on the physical system from which Eq. (5.1) is derived. In a novel application of this model by Eckert *et al* [17], for example, the functions W_i were related to the spatial separations of three optical microtraps in order to induce coherent transport of atoms between the ground states of the two farthest separated traps.
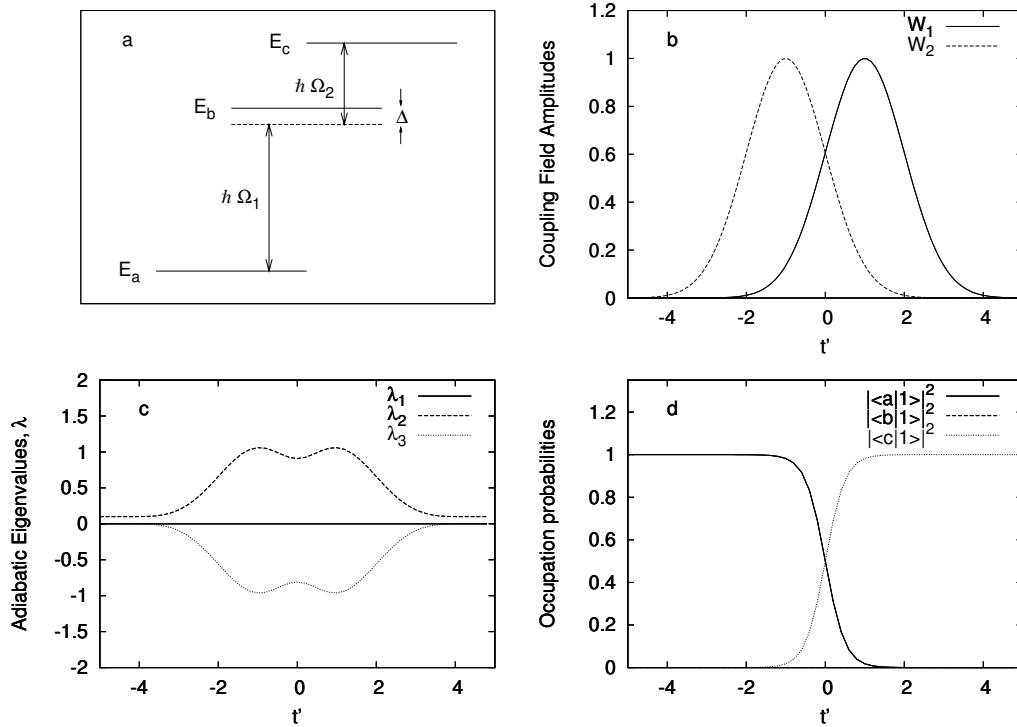
Figure 5.1: The 3-level "ladder" STIRAP system (Eq. 5.1) with parameters $\Delta = 0.05$, $W_1 = W_2 = 1$ and $\hbar = 2$. Coupling fields are applied with frequencies equally detuned from the spacings of the unperturbed energy levels by Δ (a). Adiabatic variation of amplitudes of the coupling fields (b) in the manner described by Eq. (5.3) affects a transition of the $|1\rangle$ eigenvector between basis states $|a\rangle$ and $|b\rangle$ (d). The eigenvalue corresponding to this state remains unchanged at zero throughout the transition (c)

The matrix in Eq. (5.1) allows for a transition of the type described above because of the existence of the eigenvector

$$|1(t')\rangle = \cos\theta(t')|a\rangle - \sin\theta(t')|c\rangle \,, \tag{5.2}$$

where $\tan\theta(t') \equiv \frac{W_1(t')}{W_2(t')}$. Under the conditions

$$\lim_{t'\to-\infty} \frac{W_1(t')}{W_2(t')} \to 0 \quad\text{and}\quad \lim_{t'\to+\infty} \frac{W_2(t')}{W_1(t')} \to 0 \,, \tag{5.3}$$

the adiabatic evolution of state $|1\rangle$ is from $|a\rangle$ to $|c\rangle$. Thus, the transition is achieved by first coupling the upper two levels and then coupling the lower two (in some continuous, e.g. Gaussian, manner). Moreover, because of the form of the eigenstate $|1\rangle$, the state $|b\rangle$ remains unoccupied throughout the transition.

In this chapter, we apply the method of STIRAP to the motional states of atoms in an optical lattice. As was first shown by Graham, Schlautmann and Zoller [27], the interaction of a single transition in an alkali atom with a pair of counter-propagating lasers can be reduced to an effective Hamiltonian for the center-of-mass motion of the atom in a cosine potential. Modulation of the laser amplitudes and/or the introduction of laser pairs with offset frequencies introduces a periodic time-dependence (see Chapter 2). Here we will analyze the "two-resonance" system described by the effective Hamiltonian

$$\hat{H}_0(t) = \hat{p}^2 + \kappa_0 \left[\cos\hat{x} + \cos(\hat{x} - \omega_0 t)\right] \,, \tag{5.4}$$

where each of the two cosine terms are produced by a pair of counter-propagating lasers with κ_0 proportional to the square of the laser amplitudes. We show, using perturbation analysis of an associated Floquet Hamiltonian, that small harmonic modulations of the laser amplitudes can be used to affect a STIRAP-like transition

from a state localized in the stationary cosine well into a state localized in the traveling cosine well.

In Section 5.3 we present an analysis of the time-independent "quantum pendulum" system which reveals a three-level STIRAP model in the regime of small perturbation. Section 5.4 contains a slightly modified method in order to obtain a STIRAP-like model for the time-dependent "two-resonance" system. In each case, adiabatic results are compared to numerical evolution of the Schrödinger equation and transitions of nearly 100% efficiency are observed.

5.3   STIRAP transitions in the Quantum Pendulum

Before analyzing the two-resonance effective Hamiltonian presented in the introduction, we will consider STIRAP-like transitions within the quantum pendulum system:

$$\hat{H}_{pend} = \hat{p}^2 + \kappa_0 \cos \hat{x} \,. \tag{5.5}$$

This is the simplest type of effective Hamiltonian for optical lattice experiments, achieved with a single pair of counter-propagating lasers with equal frequencies. The parameter κ_0 is proportional to the square of the electric field amplitude. Because of experimental techniques which can limit momentum values to the integers (see Chapter 2), the eigenstates can be considered considered spatially periodic with period 2π. The position space solutions to the eigenvalue equation $\hat{H}_{pend}|\chi_n\rangle = E_n|\chi_n\rangle$ are the Mathieu functions $\langle x|\chi_n\rangle$ ($n \in Z$) [1], with n even labeling even-parity functions and n odd labeling odd-parity functions.

To affect a transition in this system using STIRAP, we add a time-periodic modulation of the lattice amplitude of the form

$$\lambda\hat{V}(t) = \lambda \cos \hat{x} \left[\kappa_1 \cos(\Omega_1 t) + \kappa_2 \cos(\Omega_2 t) \right] \,, \tag{5.6}$$

where λ is small, and Ω_1 and Ω_2 are commensurate with $\frac{\Omega_1}{\Omega_2} = \frac{m_1}{m_2}$ $(m_i \in Z)$. It is useful to write Ω_1 and Ω_2 in terms of a common frequency ω such that $\Omega_1 = m_1\,\omega$ and $\Omega_2 = m_2\,\omega$, where $\omega = \frac{2\pi}{T}$ and T is the periodicity of the perturbation. This perturbation is achieved experimentally by modulating the intensity of the counter-propagating laser radiation about the κ_0 value, meaning that the lasers' electric field amplitude $E(t)$ should take the form

$$|E(t)|^2 \sim \kappa_0 + \lambda\left[\kappa_1 \cos(m_1 \omega t) + \kappa_2 \cos(m_2 \omega t)\right] . \tag{5.7}$$

For now, we will consider the coefficients κ_1 and κ_2 to have constant values. Perturbation analysis will reveal that, for small values of λ, there exists a 3-state subsystem identical to the STIRAP model, parameterized by these coefficients. A STIRAP-type transition can then be affected by adiabatic variation of κ_1 and κ_2 in the manner described in Eq. (5.3). The justification of this time-parameterization of the κ_i, following a Floquet analysis of the system where they are considered constant, is provided by the (t, t') method described in Section 3.1.4.

Having required that the frequencies Ω_1 and Ω_2 are commensurate, we can analyze the dynamics of the full system

$$i\frac{\partial}{\partial t}|\psi(t)\rangle = \left[\hat{H}_{pend} + \lambda\hat{V}(t)\right]|\psi(t)\rangle \tag{5.8}$$

using Floquet theory (see Section 3.1). This states that any solution of Eq. (5.8) can be written in the form

$$|\psi_\alpha(t)\rangle = \mathrm{e}^{-i\epsilon_\alpha t}|\phi_\alpha(t)\rangle , \tag{5.9}$$

where the *Floquet eigenstate* $|\phi_\alpha(t)\rangle$ is periodic in time with period T, and ϵ_α is called the *Floquet eigenvalue*. Plugging this solution into the Schrödinger equation

we arrive at the eigenvalue equation

$$\hat{H}_F|\phi_\alpha\rangle \equiv \left[\hat{H}_{pend} + \lambda\hat{V}(t) - i\frac{\partial}{\partial t}\right]|\phi_\alpha\rangle = \epsilon_\alpha|\phi_\alpha\rangle\,, \tag{5.10}$$

where the *Floquet Hamiltonian* $\hat{H}_F$ is a Hermitian operator in an extended Hilbert space which has time as a periodic *coordinate* [37; 76; 16].

The STIRAP model system is derived by applying perturbation theory to Eq. (5.10), where the two frequencies in $\hat{V}(t)$ are chosen to "couple" three pendulum eigenvalues, at a particular value of κ_0, in the manner shown in Figure 5.1a. Although, in general, the ratio of these eigenvalue spacings is not rational, the equal detuning Δ allows for Ω_1 and Ω_2 to be chosen as commensurate. More precisely, given three eigenvalues of the quantum pendulum $E_a < E_b < E_c$, any pair of integers (m_1, m_2) uniquely determines Δ and ω via the coupled equations

$$m_1\,\omega = E_b - E_a - \Delta$$
$$m_2\,\omega = E_c - E_b + \Delta\,. \tag{5.11}$$

Eliminating ω we obtain an expression for Δ

$$\Delta = \frac{m_2\,\omega_1 - m_1\,\omega_2}{m_1 + m_2}\,, \tag{5.12}$$

where we have defined $\omega_1 = E_b - E_a$ and $\omega_2 = E_c - E_b$. We can see that the integer vectors $\vec{m} \equiv (m_1, m_2)^{\mathrm{T}}$ which minimize Δ are those which satisfy

$$\vec{m}\cdot\vec{\nu} \approx 0 \quad \text{with} \quad \vec{\nu} \equiv (-\omega_2, \omega_1)^{\mathrm{T}} \tag{5.13}$$

Therefore, the best choices for $\vec{m}$ are those for which m_1/m_2 are the best rational approximants of the ratio $w \equiv \omega_1/\omega_2$.
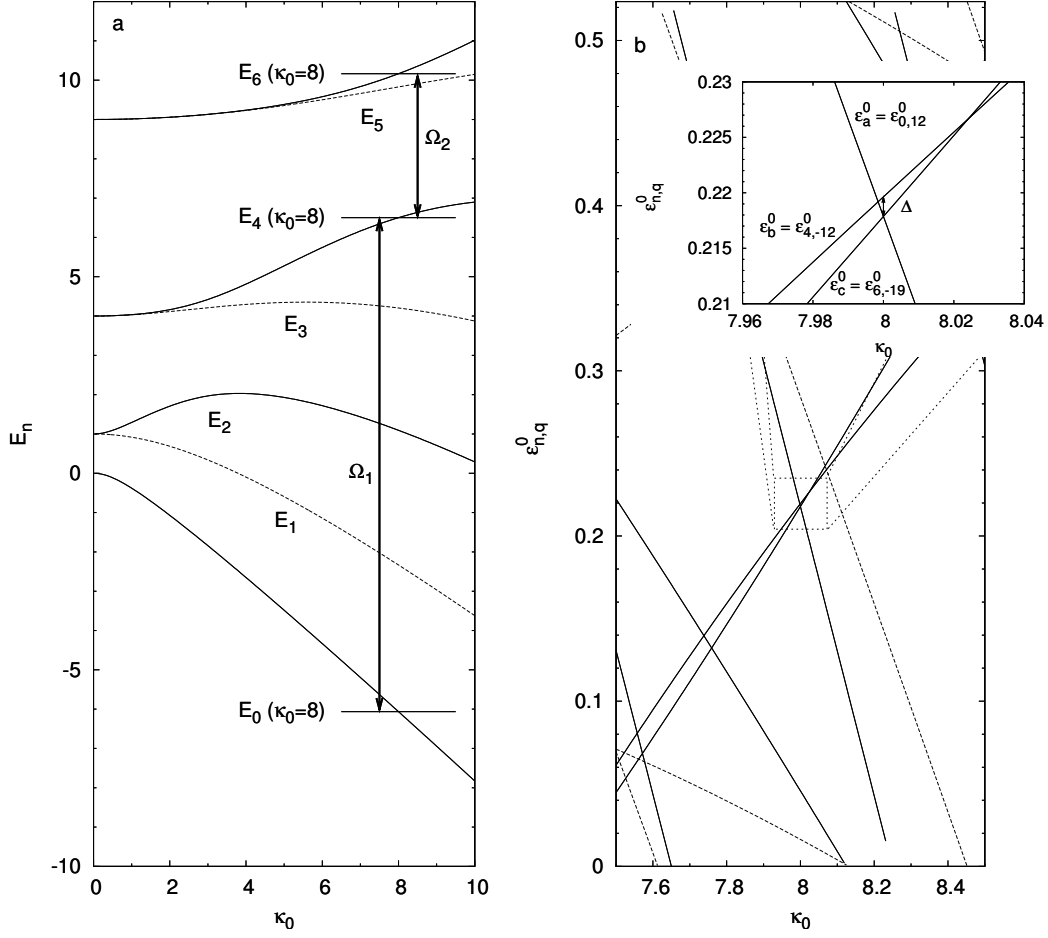
Figure 5.2: The lowest seven eigenvalues of the quantum pendulum (a) as a function of the parameter κ_0 (solid lines are the eigenvalues of even-parity states, dashed odd). The coupling of levels E_0-E_4 and E_4-E_6 at $\kappa_0 = 8$ via the perturbation $\hat{V}(t)$ requires a Floquet treatment of the pendulum system. The corresponding Floquet eigenvalues (for $\omega = 0.5235$) are shown in (b). The degeneracy and near-degeneracy of the the three coupled eigenvalues can be seen in the enlarged (inset) view.

Let us denote the unperturbed Floquet Hamiltonian ($\hat{H}_F$ when $\lambda = 0$) as

$$\hat{H}_F^0 \equiv \hat{H}_{pend} - i\frac{\partial}{\partial t}. \tag{5.14}$$

In the extended Hilbert space, $\hat{H}_F^0$ has normalized eigenvectors of the form

$$\langle t|\chi_n, q\rangle = \langle t|q\rangle|\chi_n\rangle = \frac{1}{\sqrt{T}}\, e^{iq\omega t}|\chi_n\rangle \quad , \quad q \in \mathbb{Z}. \tag{5.15}$$

The corresponding eigenvalues are $\epsilon_{n,q}^0 = E_n + q\omega$. We are interested in the dynamics of an initial population of atoms localized in the pendulum state $|\chi_a\rangle$. With $\lambda = 0$, state $|\chi_a\rangle$ is represented in a particular zone of Floquet eigenvalues of $\hat{H}_F^0$ by a Floquet eigenstate $|\chi_a, q_a\rangle$ with eigenvalue ϵ_{a,q_a} in that zone. The coupling frequencies Ω_1 and Ω_2 have been chosen in Eq. (5.11) such that ϵ_{c,q_c}^0, the Floquet eigenvalue in that zone corresponding to the physical state $|\chi_c\rangle$, is equal to ϵ_{a,q_a}^0 and the eigenvalue ϵ_{b,q_b}^0 is offset from this value by Δ. The degeneracy of these two eigenvalues and the near-degeneracy of the third requires that any perturbation analysis must be performed in the degenerate form [37]. Therefore, we expand the extended Hilbert space state $|\phi\rangle$ in powers of the small parameter λ

$$|\phi\rangle = |\phi^{(0)}\rangle + \lambda|\phi^{(1)}\rangle + \lambda^2|\phi^{(2)}\rangle + \dots \tag{5.16}$$

and take the zeroth-order state to be a superposition of the three degenerate or near-degenerate eigenstates of $\hat{H}_F^0$:

$$|\phi^{(0)}\rangle = C_a|\chi_a, q_a\rangle + C_b|\chi_b, q_b\rangle + C_c|\chi_c, q_c\rangle. \tag{5.17}$$

The eigenvalue is likewise expanded in orders of the small parameter

$$\epsilon = \epsilon^{(0)} + \lambda\epsilon^{(1)} + \lambda^2\epsilon^{(2)} + \dots. \tag{5.18}$$

For brevity of notation, we write the unperturbed eigenstates $|a\rangle \equiv |\chi_a, q_a\rangle$, $|b\rangle \equiv |\chi_b, q_b\rangle$ and $|c\rangle \equiv |\chi_c, q_c\rangle$, with associated eigenvalues $\epsilon_a^0 \equiv \epsilon_{a,q_a}^0$, $\epsilon_b^0 \equiv \epsilon_{b,q_b}^0$ and $\epsilon_c^0 \equiv \epsilon_{c,q_c}^0$, respectively.

Retaining terms up to first-order in λ, we obtain an isolated subsystem of Equation (5.10):

$$
\begin{pmatrix} \epsilon_a^0 + \lambda V_{a,a} & \lambda V_{a,b} & \lambda V_{a,c} \\ \lambda V_{b,a} & \epsilon_b^0 + \lambda V_{b,b} & \lambda V_{b,c} \\ \lambda V_{c,a} & \lambda V_{c,b} & \epsilon_c^0 + \lambda V_{c,c} \end{pmatrix} \begin{pmatrix} C_a \\ C_b \\ C_c \end{pmatrix} = \epsilon' \begin{pmatrix} C_a \\ C_b \\ C_c \end{pmatrix} , \tag{5.19}
$$

where $\epsilon' \equiv \epsilon_a^0 + \lambda \epsilon^{(1)}$ and we have assumed that Δ is of order λ. The matrix elements of the perturbation are determined in the following way:

$$
V_{i,j} = \langle\langle \chi_i, q_i | \hat{V} | \chi_j, q_j \rangle\rangle \equiv \int_{-\pi/\omega}^{\pi/\omega} \langle q_i | t \rangle \langle t | q_j \rangle \langle \chi_i | \cos \hat{x} | \chi_j \rangle
$$

$$
\times \left[\kappa_1 \cos(m_1 \omega t) + \kappa_2 \cos(m_2 \omega t) \right] dt
$$

$$
= \frac{\langle \chi_i | \cos \hat{x} | \chi_j \rangle}{2} \tag{5.20}
$$

$$
\times \left[\kappa_1 \delta_{q_j, q_i + m_1} + \kappa_1 \delta_{q_j, q_i - m_1} + \kappa_2 \delta_{q_j, q_i + m_2} + \kappa_2 \delta_{q_j, q_i - m_2} \right] .
$$

The selection of Ω_1 and Ω_2 guarantees that the q indices for these states satisfy

$$
q_b - q_a = m_1 \quad \text{and} \quad q_c - q_b = m_2 . \tag{5.21}
$$

Therefore, the only non-zero matrix elements of the perturbation are $V_{a,b} = V_{b,a}$ and $V_{b,c} = V_{c,b}$. Further, we can write

$$
V_{a,b} = V_{b,a} = \kappa_1 v_{a,b} \quad \text{and} \quad V_{b,c} = V_{c,b} = \kappa_2 v_{b,c} \tag{5.22}
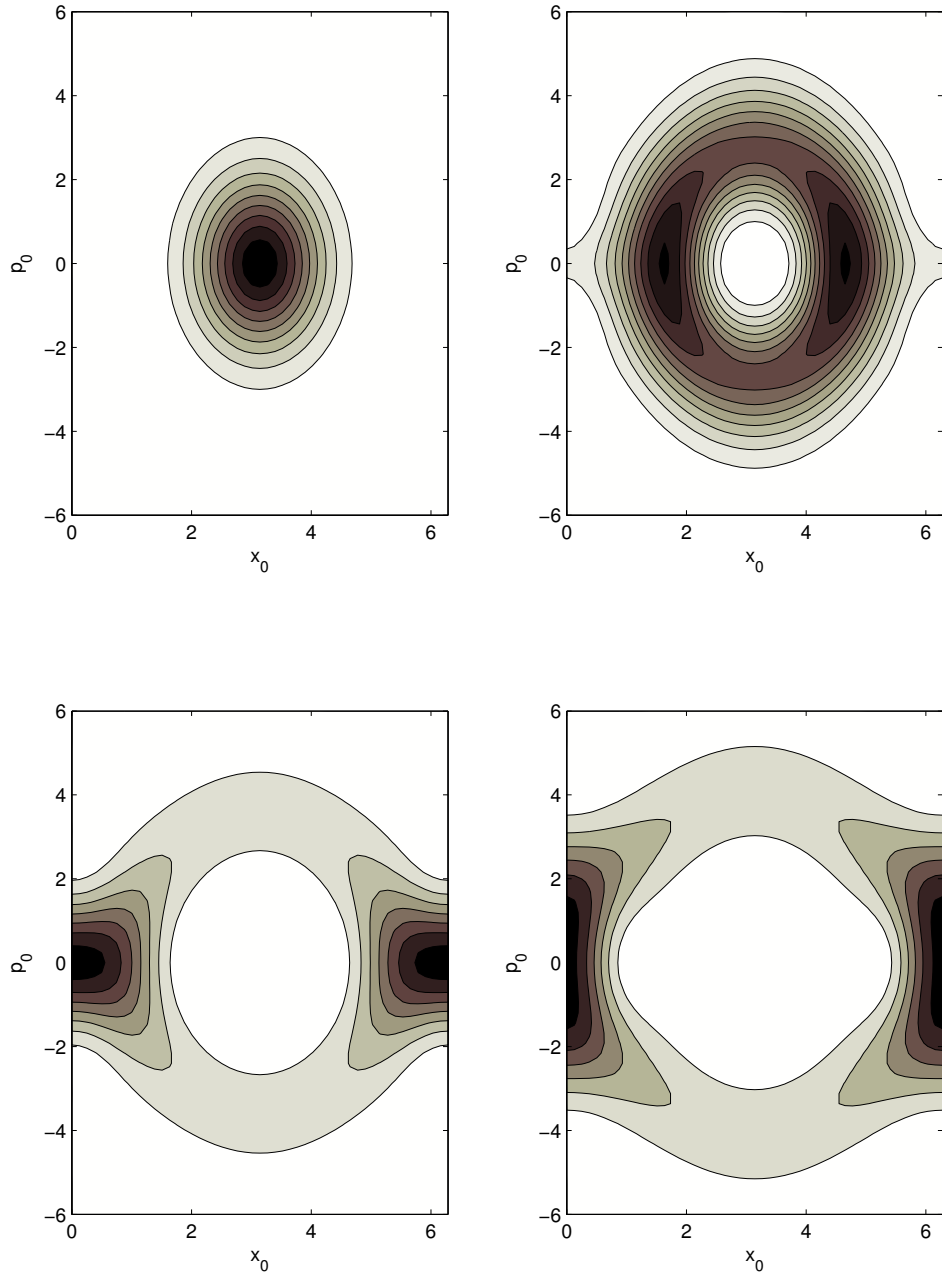$$

Figure 5.3: The Husimi functions of the first four even-parity eigenstates of the quantum pendulum on classical phase space (x_0, p_0). The states are, clockwise from top left: $|\chi_0\rangle, |\chi_2\rangle, |\chi_6\rangle, |\chi_4\rangle$.

where the numerical values of

$$v_{i,j} = \frac{\langle \chi_i | \cos \hat{x} | \chi_j \rangle}{2} \tag{5.23}$$

are calculated using the Mathieu functions. Subtracting $\epsilon_a^0 (C_a, C_b, C_c)^{\mathrm{T}}$ from both sides of Eq. (5.19) and redefining $\epsilon' - \epsilon_a^0 \to \epsilon'$, we arrive at

$$\begin{pmatrix} 0 & \lambda \kappa_1 v_{a,b} & 0 \\ \lambda \kappa_1 v_{b,a} & \Delta & \lambda \kappa_2 v_{b,c} \\ 0 & \lambda \kappa_2 v_{b,c} & 0 \end{pmatrix} \begin{pmatrix} C_a \\ C_b \\ C_c \end{pmatrix} = \epsilon' \begin{pmatrix} C_a \\ C_b \\ C_c \end{pmatrix}, \tag{5.24}$$

which is equivalent to the STIRAP model system. Thus, in the limit of small λ (and Δ), the parameters κ_1 and κ_2 can be adiabatically varied in the manner described in the introduction to affect a transition between the unperturbed states $|a\rangle$ and $|c\rangle$.

We now provide a concrete example on which to demonstrate the analysis. Figure 5.2a shows the energies of the first few eigenstates of $\hat{H}_{pend}$ as a function of κ_0. Husimi representations [39; 37] of the even eigenstates, at $\kappa_0 = 8$, are shown in Figure 5.3. At this value of κ_0, we choose energies $E_a = E_0$, $E_b = E_4$ and $E_c = E_6$ for coupling. These energy levels have spacings $\omega_1 = E_b - E_a = 12.5668395$ and $\omega_2 = E_c - E_b = 3.6630472$ with ratio

$$w = 3.43070639... = [3, 2, 3, 9, ...] = 3 + \cfrac{1}{2 + \cfrac{1}{3 + \cfrac{1}{9 + \cdots}}} . \tag{5.25}$$

Thus, the best rational approximates of w, found by truncating the continued fraction, are $\{\frac{3}{1}, \frac{7}{2}, \frac{24}{7}, \frac{223}{65}, ...\}$. Using the third approximation, the modulation frequencies shown in the example have been chosen to be $\Omega_1 = 24\omega$ and $\Omega_2 = 7\omega$, giving $\omega = 0.5235$ and $\Delta = 1.766 \times 10^{-3}$.

In Figure 5.2b, the Floquet eigenvalues of H_F^0 are shown in the zone $\epsilon^\star = 0$. In the inset figure, one can see that $\epsilon_a^0 = \epsilon_{0,12}^0$ and $\epsilon_c^0 = \epsilon_{6,-19}^0$ are equal at $\kappa_0 = 8$

86

and $\epsilon_b^0 = \epsilon_{4,-12}^0$ is offset by Δ. Using the Mathieu functions, the perturbation matrix elements are calculated to be

$$V_{a,b} = V_{b,a} = \kappa_1 \, v_{a,b} = -1.16 \times 10^{-2} \kappa_1 \tag{5.26}$$

$$V_{b,c} = V_{c,b} = \kappa_2 \, v_{b,c} = 2.50 \times 10^{-1} \kappa_2 \,. \tag{5.27}$$

To accomplish a STIRAP transition from $|a\rangle$ to $|c\rangle$, we give κ_1 and κ_2 Gaussian dependence on an adiabatic time parameter t' (see Figure 5.4a):

$$\kappa_i(t') = \exp\left[-\frac{(t' - t_i)^2}{2\sigma_i^2}\right] \,. \tag{5.28}$$

The conditions of Eq. (5.3) are satisfied by setting $t_1 = -t_2 = 1.0$ and $\sigma_1 = \sigma_2 = 1.0$. Figure 5.4 shows good agreement between the adiabatic dynamics of the model system in Eq. (5.24) (5.4b and d), and that of the full Floquet Hamiltonian (5.4c and e).

The implementation of this transition in an experimental system (or the numerical evolution of the Schrödinger equation) is not dependent on the time-periodicity which we have required thus far. Floquet analysis has proven an essential theoretical tool for revealing the existence of the STIRAP model, but the method has introduced no upper limit on the integers m_1 and m_2 whose ratio approximates ω_1/ω_2. Therefore we may choose the coupling frequencies to be resonant ($\Omega_1 = \omega_1$ and $\Omega_2 = \omega_2$) to any desired accuracy. The results for the numerical evolution of the effective Schrödinger equation (5.8) are shown in Figure 5.5a, for the case of both resonant and near-resonant coupling ($\Delta = 1.77 \times 10^{-3}$) with $\lambda = 0.1$. The evolution was performed over a set time period $[0, t_{tot}]$ with initial condition $|\langle \chi_a | \psi \rangle|^2 = 1$, and Gaussian parameters for the coupling amplitudes κ_1 and κ_2 of $\sigma_1 = \sigma_2 = 0.1 t_{tot}$, $t_1 = 0.6 t_{tot}$ and $t_2 = 0.4 t_{tot}$. It is seen that resonant coupling provides a more rapid approach to the adiabatic behavior. In Figure 5.5b, good agreement is seen between
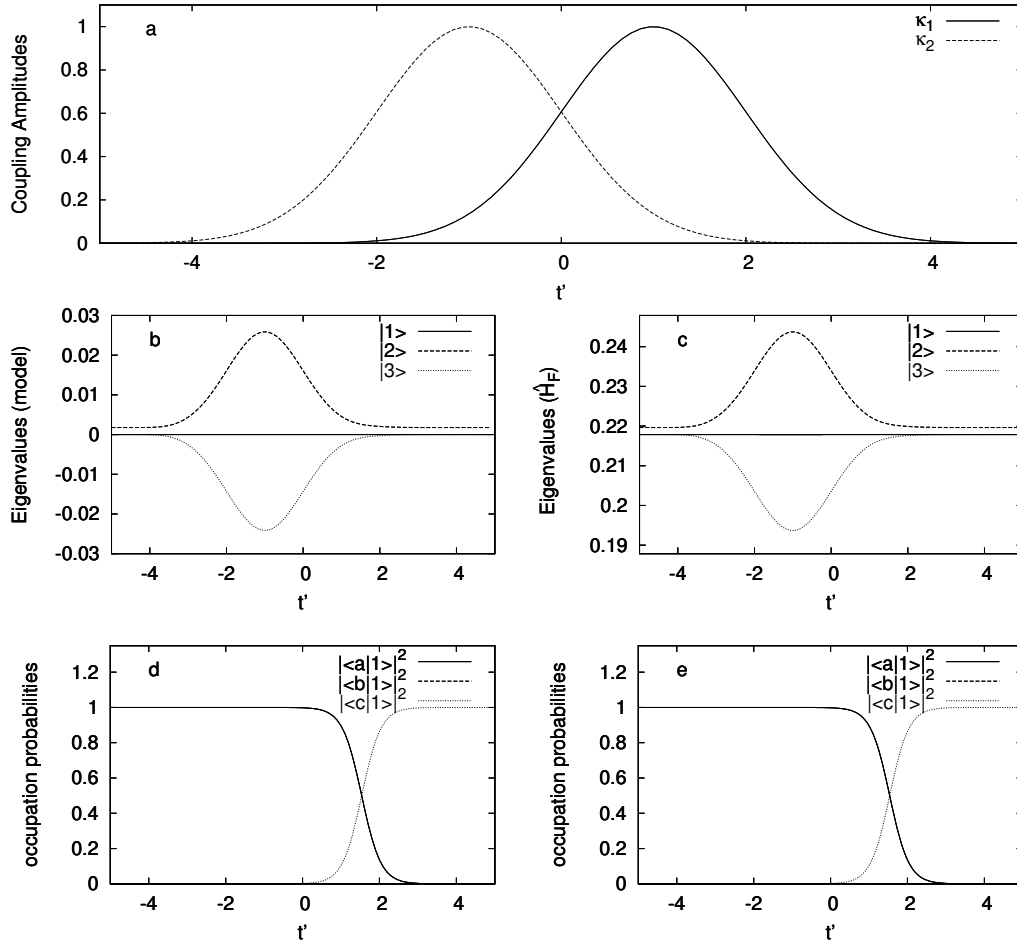
Figure 5.4: Adiabatic evolution of the pendulum system under STIRAP coupling, comparing the dynamics of the model in Eq. (5.24) (b and d) to that of the full Floquet Hamiltonian in Eq. (5.8) (c and e) for $\lambda = 0.1$. The coupling field κ_2 is seen to have a greater effect on the eigenvalues at $t' = -1$ than that of κ_1 at $t' = 1$, since $v_{b,c} \gg v_{a,b}$. This asymmetry also shifts the transition of the $|1\rangle$ eigenstate from pendulum states $|a\rangle$ to $|c\rangle$ to a later time (d and e).

the resonant evolution of the full effective Schrödinger equation and the adiabatic predictions of Figure 5.4.

5.4 STIRAP transitions from stationary to moving atoms

We now consider the case in which the "unperturbed" Hamiltonian has the form of Eq. (5.4), which consists classically of a stationary cosine wave and a cosine wave that travels through phase space with a speed ω_0. Our goal is to cause a coherent transition of an entire cloud of trapped atoms from a state localized in the stationary wave (in the sense of its Husimi distribution) into a state localized in the traveling wave, so that the entire collection of atoms changes velocity from $v = 0$ to $v = \omega_0$.

Our approach is analogous to that of the previous section. We apply perturbation theory to a Floquet eigensystem of the form

$$\hat{H}_F(t)|\phi(t)\rangle = \left[\hat{H}_F^0(t) + \lambda\hat{V}(t)\right]|\phi(t)\rangle = \epsilon|\phi(t)\rangle\,, \tag{5.29}$$

where $\hat{H}_F$ is periodic in time with period $T = 2\pi/\omega$ and the perturbation operator $\hat{V}$ has the same form as in Eq. (5.6). Again we find that, in the limit of small λ, there exists an isolated three-level subsystem in which a STIRAP-type transition between eigenstates of $\hat{H}_F^0$ can be induced. The construction of $\hat{H}_F$, however, differs significantly from the previous section because of the explicit time-dependence of the two-resonance Hamiltonian. In the pendulum analysis the frequencies Ω_1 and Ω_2 were chosen to couple the energies of pendulum eigenstates. Here, these frequencies are chosen to couple the eigenvalues of the two-resonance Floquet Hamiltonian,

$$\hat{H}_F^0(t) = \hat{p}^2 + \kappa_0\left[\cos\hat{x} + \cos(\hat{x} - \omega_0 t)\right] - i\frac{\partial}{\partial t}\,, \tag{5.30}$$

within a particular zone. Selection of coupling frequencies such that they and ω_0 are commensurate allows for Floquet analysis of the full system, but requires that the
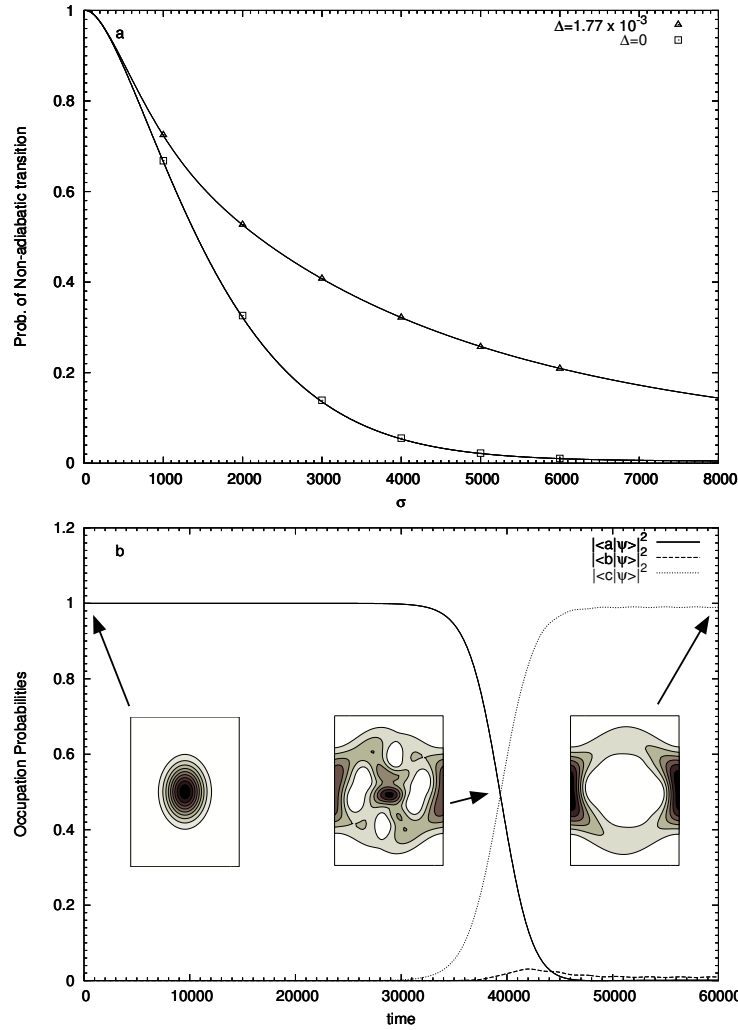
Figure 5.5: The numerical evolution of a state initially localized in the $|\chi_a\rangle$ pendulum state, under STIRAP coupling of the energies. The probability of a non-adiabatic transition (transition to any state other than $|c\rangle$) is plotted versus the width of the gaussian field $\sigma = \sigma_1 = \sigma_2$ (a), for resonant (triangles) and near-resonant coupling (squares) with $\lambda = 0.1$. The solid lines are the values predicted by evolution of the three-state model (see Section 3.1.4 for a justification of this use of the model). Figure (b) shows the numerical evolution, under the effective Schrödinger equation, of a state classically localized within the pendulum well to one localized on the separatrix (axes on inset Husimi functions are the same as in Fig. 5.3). This evolution corresponds to the point at $\sigma = 6000$ with resonant ($\Delta = 0$) coupling in (a).

eigenvectors of $\hat{H}_F^0$ be translated from their natural Hilbert space, containing functions periodic in time with period $\bar{T} \equiv 2\pi/\omega_0$, into the space containing T-periodic functions of time. The relevant Floquet eigenvalues associated to the eigenvectors in this latter space take near-degenerate values and perturbation analysis leads to similar results as the previous section. [It should also be noted that although we call the two-resonance system in Eq. (5.30) an "unperturbed" Hamiltonian, it is not analytically solvable. Perturbation theory will be a useful tool to demonstrate the existence of a STIRAP-like model for this system, but the eigenvectors of $\hat{H}_F^0$ and all related quantities (e.g. the matrix elements of the three-level system) must be determined numerically.]

We begin by constructing Floquet eigenvectors $|\bar{\phi}_\alpha^0\rangle$ of $\hat{H}_F^0$ (the "overbar" will be used to indicate that these vectors belong to the Hilbert space $\bar{\mathcal{H}}$, defined below). We will assume that the parameters κ_0 and ω_0 have constant values, which may be set arbitrarily. The only limitation on this choice is that, given ω_0, κ_0 should be chosen such that the set of eigenvectors with eigenvalues in a particular zone contains one state localized purely in the stationary cosine wave and one state localized in the traveling wave (i.e. a κ_0 value far from avoided crossings involving the eigenvalues of these states). The eigenvectors $|\bar{\phi}_\alpha^0\rangle$ lie in the extended Hilbert space $\bar{\mathcal{H}} \equiv \Theta \otimes \bar{\mathcal{T}}$, where Θ is the space of all 2π-periodic, square-normalizable position-space functions and $\bar{\mathcal{T}}$ is the space of all $\bar{T}$-periodic, square-normalizable functions of time. We select the complete set of momentum eigenstates $|n\rangle$ (see Section 2.3) as a basis in Θ and the analogous eigenstates $|q\rangle$ as a basis in $\bar{\mathcal{T}}$, yielding normalized basis vectors in the extended space which can be written

$$\langle x, t | n, q \rangle = \langle x | n \rangle \langle t | q \rangle = \frac{1}{\sqrt{2\pi\bar{T}}} \mathrm{e}^{inx} \mathrm{e}^{iq\omega_0 t} , \tag{5.31}$$

91

with $n, q \in \mathbb{Z}$. The eigenstates $|\bar{\phi}_\alpha^0\rangle$ can then be written

$$|\bar{\phi}_\alpha^0(t)\rangle = \sum_{n,q} \frac{1}{\sqrt{\bar{T}}} e^{iq\omega_0 t} \langle n, q | \bar{\phi}_\alpha^0 \rangle |n\rangle, \tag{5.32}$$

where $|\bar{\phi}_\alpha^0(t)\rangle = \langle t | \bar{\phi}_\alpha^0 \rangle$ and the coefficients $\langle n, q | \bar{\phi}_\alpha^0 \rangle$ are determined by diagonalization of $\hat{H}_F^0$ in $\bar{\mathcal{H}}$.

We select a zone $\epsilon^\star \le \bar{\epsilon}_\alpha^0 < \epsilon^\star + \omega_0$ within which to perform a coupling of the eigenvalues $\bar{\epsilon}_\alpha^0$ of $\hat{H}_F^0$. Two of these eigenvalues, denoted $\bar{\epsilon}_a^0$ and $\bar{\epsilon}_c^0$, are those of the states localized in the stationary and traveling waves, respectively. A third eigenvalue $\bar{\epsilon}_b^0$ is chosen with the restriction that the corresponding eigenvector is localized "nearby" in phase space (the matrix element of $\cos \hat{x}$ between this and the other two vectors should not be vanishingly small). As before, the coupling frequencies Ω_1 and Ω_2 must be chosen to be commensurate. In this case, however, analogous equations to Eqs. (5.11) cannot be solved simultaneously with the requirement that ω_0 is likewise commensurate:

$$\omega_0 = m_0 \, \omega \quad (m_0 \in \mathbb{Z}). \tag{5.33}$$

Therefore, in the following, we will relax the constant detuning requirement and allow for two independent detunings defined by the equations

$$\begin{aligned} \Omega_1 &= m_1 \, \omega = \left(\bar{\epsilon}_b^0 - \bar{\epsilon}_a^0 \right) - \Delta_1 \\ \Omega_2 &= m_2 \, \omega = \left(\bar{\epsilon}_c^0 - \bar{\epsilon}_b^0 \right) + \Delta_2 \, . \end{aligned} \tag{5.34}$$

Given any integer vector $\vec{m} \equiv (m_0, m_1, m_2)^{\mathrm{T}}$, Eqs. (5.33) and (5.34) can be solved for $(\Delta_1, \Delta_2, \omega)$. Eliminating ω and defining $\omega_1 \equiv \bar{\epsilon}_b^0 - \bar{\epsilon}_a^0$ and $\omega_2 \equiv \bar{\epsilon}_c^0 - \bar{\epsilon}_b^0$, we

obtain

$$\Delta_1 = \frac{m_0\,\omega_1\ -m_1\,\omega_0}{m_0}$$
$$\Delta_2 = \frac{m_2\,\omega_0 - m_0\,\omega_2}{m_0}\,.$$

(5.35)

Thus, we see that the integer vectors $\vec{m}$ which simultaneously minimize the two detunings will be those closest to the vector perpendicular to the plane defined by $\vec{\nu}^{(1)} \equiv (\omega_1, -\omega_0, 0)^{\mathrm{T}}$ and $\vec{\nu}^{(2)} \equiv (-\omega_2, 0, \omega_0)^{\mathrm{T}}$. This perpendicular vector is of course $\vec{n} = (\omega_0, \omega_1, \omega_2)^{\mathrm{T}}$, and the problem of minimizing the detunings is reduced to finding the best integer approximate of $\vec{n}$ or, equivalently, finding the simultaneous pair of rational approximants for $(\omega_1/\omega_0, \omega_2/\omega_0)$.

In the context of the three-level model system presented in the introduction, non-equal detuning of the coupling frequencies leads to a Hamiltonian of the form

$$H = -\frac{\hbar}{2} \begin{pmatrix} 0 & W_1 & 0 \\ W_1 & -2\Delta_1 & W_2 \\ 0 & W_2 & \Delta_2 - \Delta_1 \end{pmatrix}.$$

(5.36)

It was recognized by Kuklinski *et al* [48] that this system could allow for a STIRAP transition, despite the absence of an analytical result analogous to Eqs. (5.2) and (5.3), as long as the condition $\sqrt{W_1^2 + W_2^2} >> |\Delta_2 - \Delta_1|$ is satisfied. In order to satisfy this requirement, and that of small perturbations, we will seek integer vectors $\vec{m}$ which provide detunings $|\Delta_2 - \Delta_1| << \Delta_1 << 1$.

Since the full, perturbed system $\hat{H}_F(t)$ is periodic in time with period $T \equiv 2\pi/\omega$, we must determine the eigenstates of the unperturbed Floquet Hamiltonian in the extended Hilbert space $\mathcal{H} \equiv \Theta \otimes \mathcal{T}$, where $\mathcal{T}$ is the Hilbert space of T-periodic

functions. These eigenstates $|\phi_\alpha^0\rangle$ can be expanded in $\mathcal{H}$ as

$$|\phi_\alpha^0(t)\rangle = \sum_{n,q} \frac{1}{\sqrt{T}} \, e^{iq\omega t} \langle n, q|\phi_\alpha^0\rangle \, |n\rangle \,, \qquad (5.37)$$

where the q-eigenvectors now have the time-periodicity of $\mathcal{T}$. Since the Schrödinger equation for the unperturbed system

$$i\frac{\partial}{\partial t}|\psi(t)\rangle = \left\{ \hat{p}^2 + \kappa_0 \left[\cos\hat{x} + \cos(\hat{x} - \omega_0 t) \right] \right\} |\psi(t)\rangle \qquad (5.38)$$

can be viewed as time-periodic with either period $\bar{T}$ or $T = m_0\bar{T}$, a physical solution $|\psi_\alpha(t)\rangle$ can be written, using Eq. (5.9), in terms of a Floquet state with either periodicity. Equating these two representations, we obtain a relationship between the Floquet eigenstates of $\hat{H}_F^0$ in spaces $\bar{\mathcal{H}}$ and $\mathcal{H}$:

$$\exp\left[-i\bar{\epsilon}_\alpha^0 t\right] |\bar{\phi}_\alpha^0(t)\rangle = A \, \exp\left[-i\epsilon_\alpha^0 t\right] |\phi_\alpha^0(t)\rangle \,, \qquad (5.39)$$

where ϵ_α^0 is the eigenvalue associated to $|\phi_\alpha^0(t)\rangle$ and A is a proportionality constant. Equating coefficients of the momentum eigenstate $|n\rangle$ in Eqs. (5.32) and (5.37), we find

$$\sum_q \exp[iqm_0\omega t]\langle n, q|\bar{\phi}_\alpha^0\rangle = \sum_{q'} A' \, \exp\left[i\left(q'\omega - \epsilon_\alpha^0 + \bar{\epsilon}_\alpha^0\right) t\right] \langle n, q'|\phi_\alpha^0\rangle \,, \qquad (5.40)$$

where A' is again a constant. A non-trivial solution to this equation requires that the eigenvalues satisfy $\epsilon_\alpha^0 - \bar{\epsilon}_\alpha^0 = Q\,\omega$, where Q is an integer. We see, then, that associated to each Floquet eigenstate in $\hat{\mathcal{H}}$ is a family of eigenstates in $\mathcal{H}$:

$$\left\{ |\phi_{\alpha,Q}^0\rangle, \epsilon_{\alpha,Q}^0 \right\} \quad Q \in \mathbb{Z} \,, \qquad (5.41)$$

94

with $\epsilon_{\alpha,Q}^0 = \bar{\epsilon}_\alpha^0 + Q\omega$. Selecting a particular value of Q, Equation (5.40) becomes

$$\sum_q \exp\left[iqm_0\omega t\right] \langle n, q | \bar{\phi}_\alpha^0 \rangle = \sum_{q'} A' \exp\left[i(q' - Q)\omega t\right] \langle n, q' | \phi_{\alpha,Q}^0 \rangle . \qquad (5.42)$$

Equating coefficients of the exponentials, we find

$$\langle n, q | \phi_{\alpha,Q}^0 \rangle = \begin{cases} \langle n, \frac{q-Q}{m_0} | \bar{\phi}_\alpha^0 \rangle & \text{when } \frac{q-Q}{m_0} \in Z \\[2em] 0 & \text{otherwise} , \end{cases} \qquad (5.43)$$

where we have set $A' = 1$ under normalization. Therefore we see that the unperturbed eigenstates in the space $\mathcal{H}$ have non-zero coefficients $\langle n, q | \phi_{\alpha,Q}^0 \rangle$ only at m_0-separated values of q, with an offset of Q from $q = 0$.

Within a particular zone, we denote the unbarred eigenvalues corresponding to $\{\bar{\epsilon}_a^0, \bar{\epsilon}_b^0, \bar{\epsilon}_c^0\}$ as $\left\{\epsilon_{a,Q_a}^0, \epsilon_{b,Q_b}^0, \epsilon_{c,Q_c}^0\right\}$, with values related by

$$\begin{aligned} \epsilon_{b,Q_b}^0 - \epsilon_{a,Q_a}^0 &= \Delta_1 \\ \epsilon_{b,Q_b}^0 - \epsilon_{c,Q_c}^0 &= \Delta_2 \end{aligned} \qquad (5.44)$$

and corresponding eigenstates $\left\{|\phi_{a,Q_a}^0\rangle, |\phi_{b,Q_b}^0\rangle, |\phi_{c,Q_c}^0\rangle\right\}$. The Q-indices of these states are related by $Q_a - Q_b = m_1$ and $Q_b - Q_c = m_2$.

Perturbation analysis of Eq. (5.29) is now performed by expanding the eigenstate $|\phi\rangle$ and eigenvalue ϵ in powers of λ. Assuming that $|\phi_{a,Q_a}^0\rangle$ is initially occupied with probability one, and taking into account the near-degeneracies of Eq. (5.44), the zeroth-order term in the expansion of the perturbed eigenstate is chosen to be of the form

$$|\phi^{(0)}\rangle = C_a|\phi_{a,Q_a}^0\rangle + C_b|\phi_{b,Q_b}^0\rangle + C_c|\phi_{c,Q_c}^0\rangle . \qquad (5.45)$$

Retaining terms up to first order in λ and making the assumption that Δ_1 and Δ_2

95

are of order λ, we obtain

$$
\begin{pmatrix} \epsilon_a^0 + \lambda V_{a,a} & \lambda V_{a,b} & \lambda V_{a,c} \\ \lambda V_{b,a} & \epsilon_b^0 + \lambda V_{b,b} & \lambda V_{b,c} \\ \lambda V_{c,a} & \lambda V_{c,b} & \epsilon_c^0 + \lambda V_{c,c} \end{pmatrix} \begin{pmatrix} C_a \\ C_b \\ C_c \end{pmatrix} = \epsilon' \begin{pmatrix} C_a \\ C_b \\ C_c \end{pmatrix} ,
\tag{5.46}
$$

where $\epsilon' \equiv \epsilon_a^0 + \lambda \epsilon^{(1)}$ and the matrix elements are calculated, defining $|i\rangle \equiv |\phi_{i,Q_i}\rangle$, as follows

$$
V_{i,j} \equiv \langle\langle i|\hat{V}|j\rangle\rangle = \sum_{n,q,n',q'} \left[\langle i|n,q\rangle \langle n|\cos\hat{x}|n'\rangle \langle n',q'|j\rangle \right]
\tag{5.47}
$$

$$
\times \left[\kappa_1 \langle q|\cos(m_1\omega\hat{t})|q'\rangle + \kappa_2 \langle q|\cos(m_2\omega\hat{t})|q'\rangle \right]
$$

$$
= \frac{1}{2} \sum_{n,q,n'} \kappa_1 \langle n|\cos\hat{x}|n'\rangle \left[\langle i|n,q\rangle\langle n',q+m_1|j\rangle + \langle i|n,q\rangle\langle n'q-m_1|j\rangle \right]
$$

$$
+ \kappa_2 \langle n|\cos\hat{x}|n'\rangle \left[\langle i|n,q\rangle\langle n',q+m_2|j\rangle + \langle i|n,q\rangle\langle n',q-m_2|j\rangle \right] .
$$

Recalling the structure of the states $|\phi_{i,Q_i}^0\rangle$ given in Eq. (5.43), we see that the sum

$$
\sum_q \langle i|n,q\rangle\langle n',q+m|j\rangle = \sum_q \langle\phi_{i,Q_i}^0|n,q\rangle\langle n',q+m|\phi_{j,Q_j}^0\rangle ,
\tag{5.48}
$$

can be non-zero only when $Q_j+m = Q_i+k\,m_0$ with $k \in Z$. Thus, the only non-zero matrix elements of $\hat{V}$ in Eq. (5.46) are

$$
V_{a,b} = \frac{\kappa_1}{4} \sum_{n,q} \left(\langle a|n,q\rangle\langle n+1,q-m_1|b\rangle + \langle a|n,q\rangle\langle n-1,q-m_1|b\rangle \right)
$$

$$
= \frac{\kappa_1}{4} \sum_{n,q} \left(\langle\bar{\phi}_a^0|n,q\rangle\langle n+1,q|\bar{\phi}_b^0\rangle + \langle\bar{\phi}_a^0|n,q\rangle\langle n-1,q|\bar{\phi}_b^0\rangle \right)
$$

$$
= \kappa_1 \frac{\langle\langle\bar{\phi}_a^0|(\cos\hat{x}\otimes\mathbb{I})|\bar{\phi}_b^0\rangle\rangle}{2}
\tag{5.49}
$$

and

$$V_{b,c} = \frac{\kappa_2}{4} \sum_{n,q} \left(\langle b|n,q \rangle \langle n+1, q-m_2|c \rangle + \langle b|n,q \rangle \langle n-1, q-m_2|c \rangle \right)$$

$$= \frac{\kappa_2}{4} \sum_{n,q} \left(\langle \bar{\phi}_b^0|n,q \rangle \langle n+1, q|\bar{\phi}_c^0 \rangle + \langle \bar{\phi}_b^0|n,q \rangle \langle n-1, q|\bar{\phi}_c^0 \rangle \right)$$

$$= \kappa_2 \frac{\langle\langle \bar{\phi}_b^0|(\cos \hat{x} \otimes \mathbb{I})|\bar{\phi}_c^0 \rangle\rangle}{2} \tag{5.50}$$

where the second and third equalities for each matrix element have been written in terms of the Floquet states in $\bar{\mathcal{H}}$, using Eq. (5.43). Subtracting $\epsilon_a^0 (C_a, C_b, C_c)^T$ from both sides, redefining $\epsilon' - \epsilon_a^0 \to \epsilon'$, and defining $v_{a,b} = V_{a,b}/\kappa_1$ and $v_{b,c} = V_{b,c}/\kappa_2$, Eq. (5.46) becomes

$$\begin{pmatrix} 0 & \lambda\kappa_1 \, v_{a,b} & 0 \\ \lambda\kappa_1 \, v_{b,a} & \Delta_1 & \lambda\kappa_2 \, v_{b,c} \\ 0 & \lambda\kappa_2 \, v_{c,b} & \Delta_1 - \Delta_2 \end{pmatrix} \begin{pmatrix} C_a \\ C_b \\ C_c \end{pmatrix} = \epsilon' \begin{pmatrix} C_a \\ C_b \\ C_c \end{pmatrix}, \tag{5.51}$$

which is equivalent to the desired model system in Eq. (5.36).

Again, we provide a example system on which to demonstrate the analysis. Figure 5.6a shows some eigenvalues $\bar{\epsilon}_\alpha^0$ of the two-resonance Floquet Hamiltonian, in the zone labeled by $\epsilon^\star = -\omega_0/2$ with $\omega_0 = 6.180339887$, plotted as functions of κ_0. A triplet of eigenvalues $\bar{\epsilon}_a^0 < \bar{\epsilon}_b^0 < \bar{\epsilon}_c^0$ has been chosen at $\kappa_0 = 1$ for STIRAP coupling. The Husimi functions of the three corresponding eigenstates are shown in Figure 5.7. The values of these eigenvalues satisfy $\omega_1 = \bar{\epsilon}_b^0 - \bar{\epsilon}_a^0 = 1.67227495$ and $\omega_2 = \bar{\epsilon}_c^0 - \bar{\epsilon}_b^0 = 1.14207065$. Therefore we seek simultaneous rational approximates $(m_1/m_0, m_2/m_0)$ to the pair $(0.270579771, 0.184790913)$. Performing a numerical exhaustive search, we find that the integer vector $\vec{m} = (325, 88, 60)$ provides detunings $\Delta_1 = -1.17 \times 10^{-3}$ and $\Delta_2 = -1.08 \times 10^{-3}$, which satisfy the required conditions of $\Delta_1 \sim O(\lambda) <<$ 1 and $|\Delta_1 - \Delta_2| << \lambda$. The unbarred eigenvalues in the zone $\epsilon^\star = -\omega/2 = -\omega_0/(2\times$
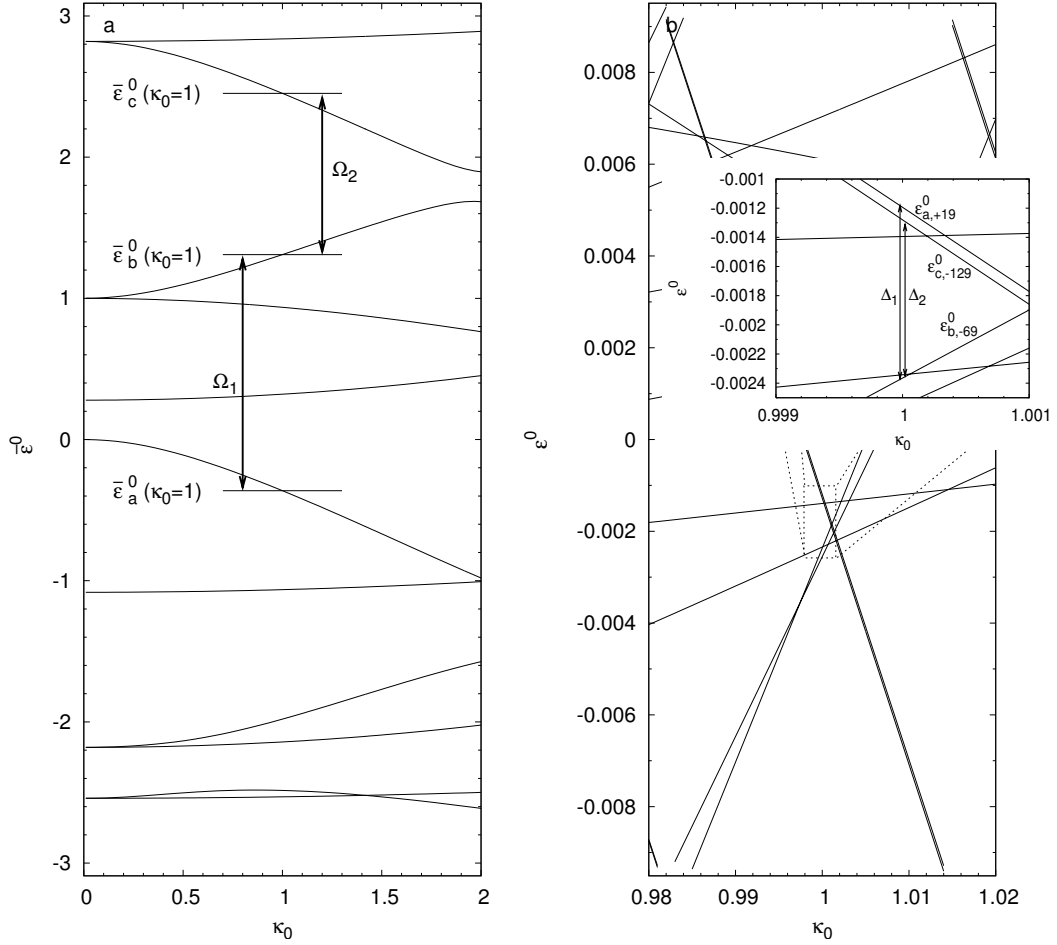
Figure 5.6: Eleven eigenvalues of the two-resonance Floquet Hamiltonian with $\omega_0 \approx$ 6.18, viewed as an operator in $\bar{\mathcal{H}}$, plotted as a function of κ_0 (a). The corresponding "unbarred" Floquet eigenvalues of the same Hamiltonian, viewed as an operator in the space $\mathcal{H}$ with $\omega = \omega_0/325$, are shown in the zone labeled by $\epsilon^\star = -\omega/2$ (b). The near-degeneracy of three eigenvalues ϵ^0_{a,Q_a}, ϵ^0_{b,Q_b} and ϵ^0_{c,Q_c} at $\kappa_0 = 1$ can be seen in the inset. It is evident that there are other eigenvalues nearly degenerate with these three, however these need not be considered in Eq. (5.45) since their respective Q-values will yield zero-valued matrix elements.
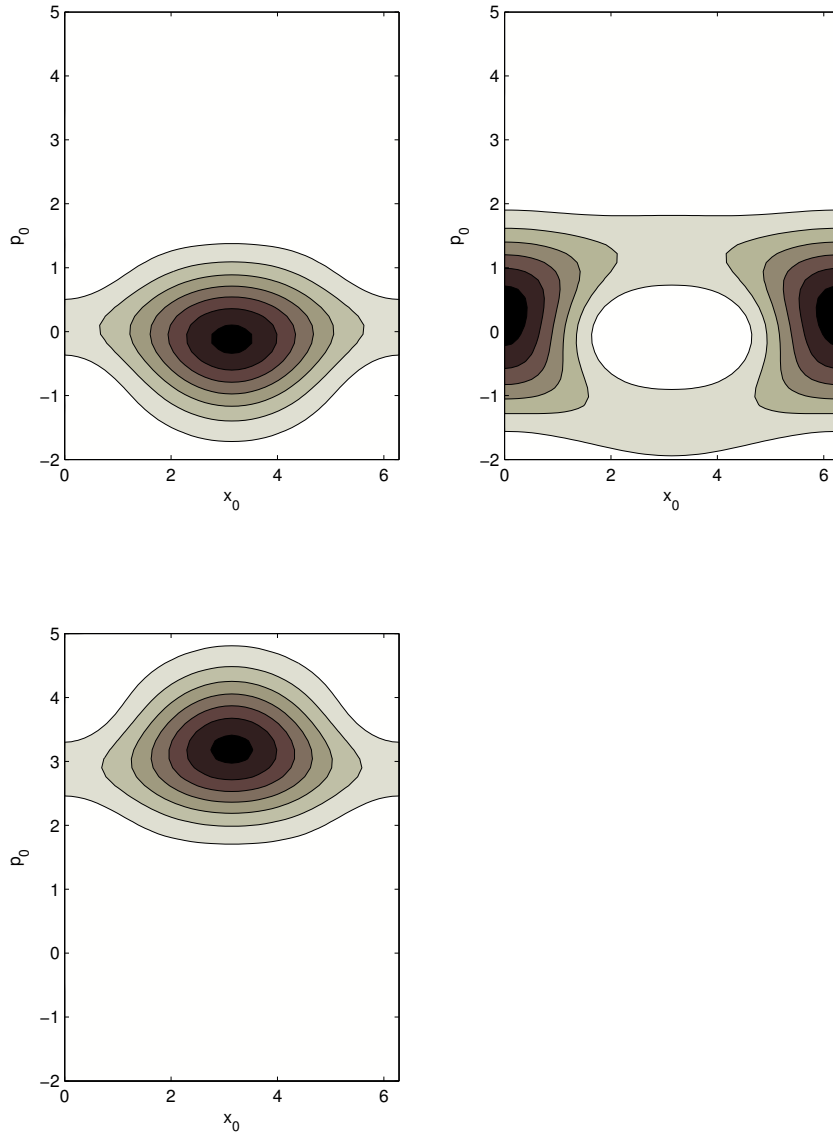
98

Figure 5.7: The Husimi representations of three Floquet states of the two-resonance Hamiltonian $\left(|\bar\phi_a^0(t)\rangle, \; |\bar\phi_b^0(t)\rangle \text{ and } |\bar\phi_c^0(t)\rangle, \; \text{clockwise from top left} \right)$ viewed at time $t = 0$. The parameter values are $\kappa_0 = 1$ and $\omega_0 \approx 6.18$.

325) are shown in Figure 5.6b. The detunings Δ_1 and Δ_2 can be seen in the enlarged section of the graph (inset), separating $\epsilon^0_{b,-69}$ from $\epsilon^0_{a,19}$ and $\epsilon^0_{c,-129}$, respectively. The coefficients

$$v_{a,b} = \frac{0.4442}{2} \tag{5.52}$$

$$v_{b,c} = \frac{-0.0673}{2} \tag{5.53}$$

are calculated using Eqs. (5.49) and (5.50) after numerical diagonalization of $\hat{H}^0_F$ in $\bar{\mathcal{H}}$.

The adiabatic dynamics of the model system in Eq. (5.51) and the full system in Eq. (5.29) are shown in Figure 5.8, using the same parametrization of the κ_i as in Eq. (5.28) and $\lambda = 0.02$. Although good agreement is seen between the two, it is evident that the STIRAP transition between eigenstates $|a\rangle$ and $|c\rangle$ is not achieved in either case. The reason for this failure is a narrow avoided crossing at $t' \approx -2.5$ between the eigenvalues of adiabatic states $|1\rangle$ and $|3\rangle$ (see inset of Figure 5.8a), which affects a transition between unperturbed states $|a\rangle$ and $|c\rangle$ *before* the STIRAP transition. This type of avoided crossing, reversing the effects of the desired transition, will always exist in the adiabatic limit when a matrix of the type given in Eq. (5.36) is used for STIRAP evolution because of the non-degeneracy of the eigenvalues of $|a\rangle$ and $|c\rangle$. Although this model does allow for a broad STIRAP-type transition, the resulting change in character of the adiabatic state $|1\rangle$ as t' passes from $-\infty$ to ∞ requires that its eigenvalue change from 0 to $\Delta_1 - \Delta_2$.

The problem with the adiabatic model can be avoided in the numerical or experimental achievement of a STIRAP transition in one of two ways. First, it is possible to achieve a non-adiabatic evolution of the system which is slow enough to guarantee a STIRAP transition, but too rapid to "see" the problematic sharp avoided crossing (via Landau-Zener tunneling [50; 92; 88]). Second, one can abandon time-periodicity and apply resonant coupling fields, reducing the model to the
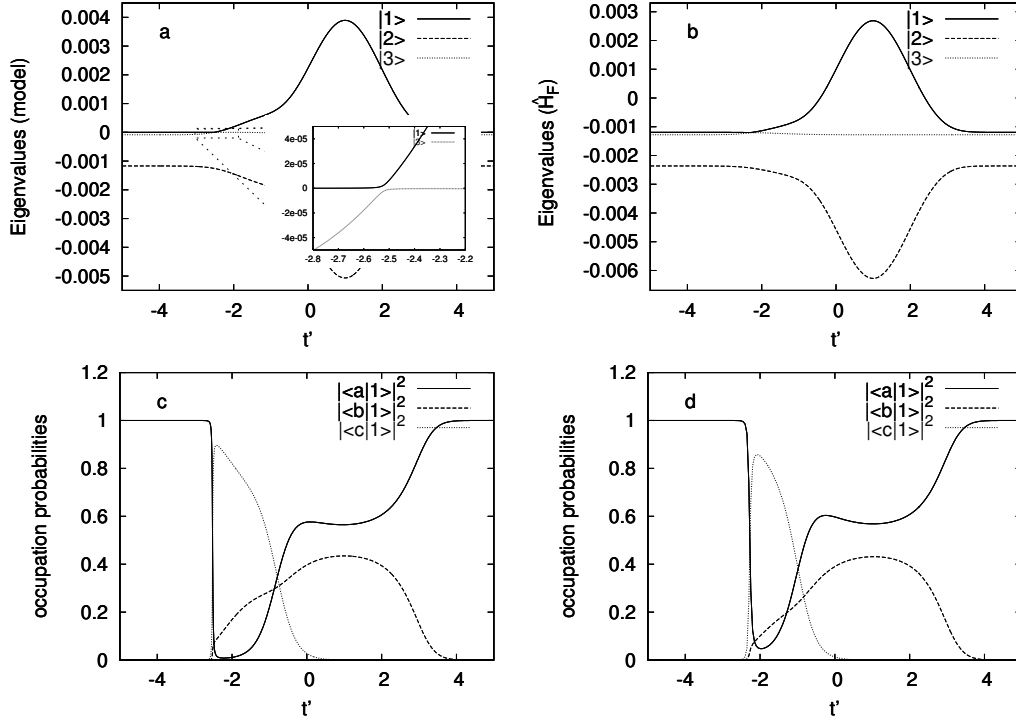
Figure 5.8: The adiabatic dynamics of the 3-level model in Eq. (5.51) (a and c) and the three relevant states of the corresponding full two-resonance Floquet system with $\omega_0 \approx 6.18$ (b and d) for the example at $\kappa_0 = 1$. The perturbation amplitude functions $\kappa_1(t')$ and $\kappa_2(t')$ are the same as in Figure 5.4a, and $\lambda = 0.02$; model parameters are as determined in the text. The eigenvalues under the application of the perturbation are show in (a) & (b). The influence of $\kappa_1(t')$ on the adiabatic eigenvalues is stronger than that of $\kappa_2(t')$ because $|v_{a,b}| > |v_{b,c}|$. Overlaps of the $|1\rangle$ adiabatic eigenvector with the unperturbed states are shown in (c) and (d). The inset in (a) shows a sharp avoided crossing which prohibits the STIRAP-like transition in the adiabatic limit.

classic form in Eq. (5.1). The efficacy of both methods can be seen in Figure 5.9a, where long-time evolution of both the model (see Section 3.1.4) and the full Schrödinger equation yields a STIRAP-like transition in the case of resonant and detuned coupling fields. As in the pendulum case, the resonant coupling provides a faster approach to the transition. The evolution of a state initially prepared in the stationary wave eigenstate $|a\rangle$ is shown to pass into the traveling wave state $|c\rangle$ under resonant coupling in Figure 5.9b.

Using the non-dimensionalization presented in Section 2.3, we can return to dimensional variables and determine the experimental conditions necessary for a STIRAP transition of the type described here. Consider a system of cold cesium atoms interacting with a system of lasers tuned near the D_2 transition (as in References [78; 80]), yielding a recoil frequency of $\omega_r \approx 1.3 \times 10^4$ Hz. For the example considered above, the traveling cosine wave is therefore generated by counter-propagating lasers with frequencies offset by $\delta\omega/2\pi \approx 10$ kHz; amplitude modulation frequencies corresponding to $\Omega_1/2\pi$ and $\Omega_2/2\pi$ are 11 and 7.7 kHz, respectively. The relationship between dimensionless time t and physical time t_{phys} for this system is

$$t_{\text{phys}} \approx [2 \times 10^{-5}\,\text{s}]\,t\,. \tag{5.54}$$

Therefore, the near-100% transition between the stationary and traveling lattices shown in Figure 5.9b, acquiring a momentum of 6 recoil momenta, would require half a second in the laboratory. The approach to adiabatic evolution can be achieved more rapidly by increasing the coupling strength λ [48], as long as the assumption of small perturbation ($\lambda << \kappa_0$) remains valid. In numerical experiments, we were able to decrease the transfer time for the preceding example (with resonant coupling) by a factor of five, while maintaining 90% efficiency, by setting $\lambda \approx 0.1$. Selection of a larger value of κ_0, i.e. deeper wells in the optical lattice, would allow for a larger value of λ and shorter transfer times.
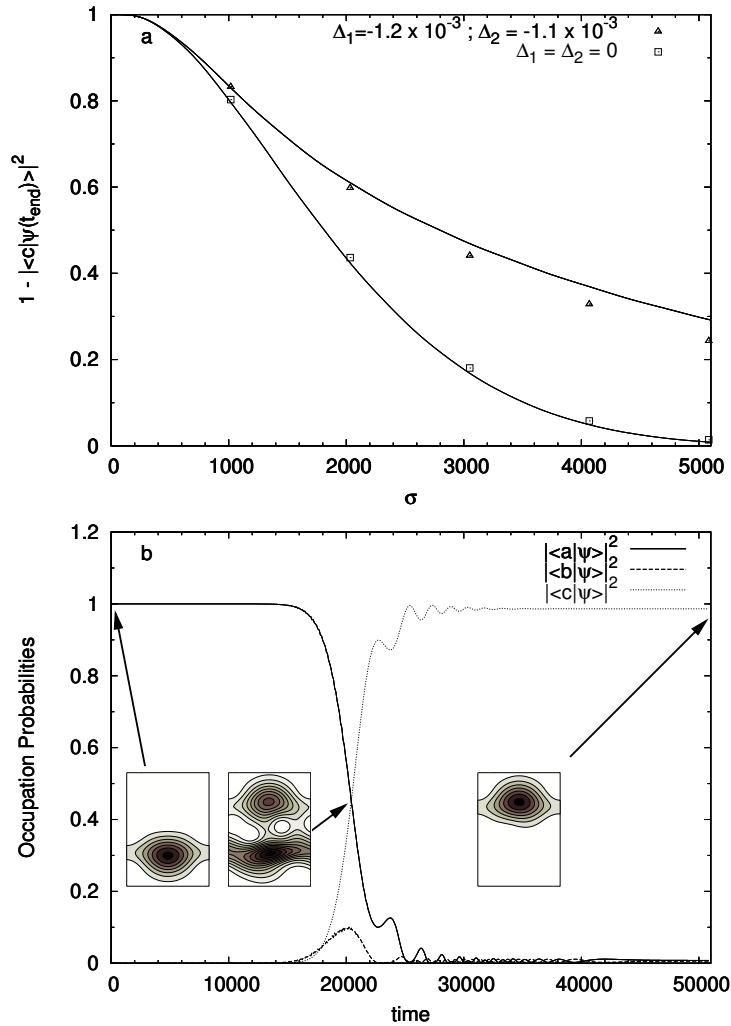
Figure 5.9: The numerical evolution of a state initially localized in the stationary cosine wave of the two-resonance system $(|\langle\phi_a^0(0)|\psi(0)\rangle|^2 = 1)$, under the influence of $\hat{V}(t)$ for the example described in the text. The probability of a transition to any state other than $|c\rangle$ is plotted versus the width of the coupling fields $\sigma = \sigma_1 = \sigma_2$ (a), with evolution under resonant coupling ($\Omega_1 = \omega_1$ and $\Omega_2 = \omega_2$) plotted with triangles and evolution under near-resonant coupling (with Δ_1 and Δ_2 as shown in Figure 5.6) plotted with squares. Solid lines are the corresponding values predicted by the numerical evolution of the three-state model. Figure (b) shows the evolution of the occupation probabilities for the case of $\sigma \approx 5000$ and resonant coupling (axes on inset Husimi functions, each taken at an integer multiple of the period $\bar{T}$, are the same as in Fig 5.7).

Appendix A

Perturbation analysis for avoided crossings

The Floquet pendulum system $\hat{H}_F^0(\kappa)$ has a two-fold degeneracy at $\kappa = \kappa_0$ where two eigenstates $|\alpha^0\rangle \equiv |n_\alpha(\kappa_0), q_\alpha\rangle$ and $|\beta^0\rangle \equiv |n_\beta(\kappa_0), q_\beta\rangle$ have eigenvalues $\epsilon_\alpha(\kappa_0) = \epsilon_\beta(\kappa_0)$. We will use a modified degenerate perturbation theory to lift this degeneracy at the κ-position of the resulting avoided crossing when $\lambda > 0$. In light of the discussion in Section 4.2.2, we write the Floquet Hamiltonian as

$$\hat{H}_F(\kappa) = \hat{H}_F^0 + \delta\hat{H}_F \, \Delta\kappa(\lambda) + \lambda \, \hat{V}, \tag{A.1}$$

where we now write $\hat{H}_F^0 \equiv \hat{H}_F^0(\kappa_0)$. The operator $\delta\hat{H}_F$ is $\frac{\partial \hat{H}_F}{\partial \kappa} = \cos\hat{\theta}$ which is diagonal in the unperturbed basis. We expand $\Delta\kappa(\lambda)$, setting $\Delta\kappa(0) = 0$, so that

$$\Delta\kappa(\lambda) = \Delta\kappa^{(1)}\lambda + \Delta\kappa^{(2)}\lambda^2 + \cdots \tag{A.2}$$

We expand the near-degenerate eigenstates and eigenvalues in powers of λ about their $(\kappa = \kappa_0, \lambda = 0)$ values:

$$|\phi\rangle = C_\alpha |\alpha^0\rangle + C_\beta |\beta^0\rangle + \lambda |\phi^1\rangle + \lambda^2 |\phi^2\rangle + \cdots$$
$$\epsilon = \epsilon^{(0)} + \lambda \epsilon^{(1)} + \lambda^2 \epsilon^{(2)} + \cdots \tag{A.3}$$

where $\hat{H}_F^0 |\alpha^0\rangle = \epsilon^{(0)} |\alpha^0\rangle$, $\hat{H}_F^0 |\beta^0\rangle = \epsilon^{(0)} |\beta^0\rangle$ and the zeroth-order eigenstates have been assumed to be a superposition of the two degenerate unperturbed states. As is usual in degenerate perturbation theory, the lowest-order near-degenerate eigenstates and the corrections to their eigenvalues will be the eigenvectors and eigenvalues of a 2×2 matrix in the basis of the two degenerate unperturbed states. At this order, we will make the distinct assignments $|\phi\rangle \to |\phi_\pm\rangle$ (corresponding to the solutions of the quadratic characteristic equation). The final expressions for $C_\alpha^\pm$, $C_\beta^\pm$, $|\phi_\pm^i\rangle$, and $\epsilon_\pm^{(i>0)}$ will depend on κ through the particular choice of the $\Delta\kappa^{(i)}$'s. The Floquet eigenvalue equation (3.12) for the near-degenerate state now takes the form

$$\left[(\hat{H}_F^0 - \epsilon^{(0)}) \; (C_\alpha |\alpha^0\rangle + C_\beta |\beta^0\rangle) \right]$$
$$+ \lambda \left[(\hat{H}_F^0 - \epsilon^{(0)}) |\phi^1\rangle + \left(\Delta\kappa^{(1)} \delta\hat{H}_F + \hat{V} - \epsilon^{(1)} \right) \; (C_\alpha |\alpha^0\rangle + C_\beta |\beta^0\rangle) \right]$$
$$+ \lambda^2 \left[(\hat{H}_F^0 - \epsilon^{(0)}) |\phi^2\rangle + (\Delta\kappa^{(1)} \delta\hat{H}_F + \hat{V} - \epsilon^{(1)}) |\phi^1\rangle \right.$$
$$\left. + (\Delta\kappa^{(2)} \delta\hat{H}_F - \epsilon^{(2)}) \; (C_\alpha |\alpha^0\rangle + C_\beta |\beta^0\rangle) \right] + \cdots = 0 . \tag{A.4}$$

A.1   First-order results

At first order in λ we have the eigenvalue equation

$$(\hat{H}_F^0 - \epsilon^{(0)}) |\phi^1\rangle + (\Delta\kappa^{(1)} \delta\hat{H}_F + \hat{V} - \epsilon^{(1)})(C_\alpha |\alpha^0\rangle + C_\beta |\beta^0\rangle) = 0 . \tag{A.5}$$

If we now act on this equation with $\langle \alpha^0 |$ and then with $\langle \beta^0 |$, we obtain

$$\begin{pmatrix} \Delta\kappa^{(1)}\delta E_\alpha + V_{\alpha\alpha} - \epsilon^{(1)} & V_{\alpha\beta} \\ V_{\beta\alpha} & \Delta\kappa^{(1)}\delta E_\beta + V_{\beta\beta} - \epsilon^{(1)} \end{pmatrix} \begin{pmatrix} C_\alpha \\ C_\beta \end{pmatrix} = \mathbf{0} . \qquad (\text{A.6})$$

where V_{ij} are the matrix elements of the perturbation in the basis of the degenerate unperturbed eigenstates,

$$\delta E_i \equiv \langle\langle n_i, q_i | \delta\hat{H}_F | n_i, q_i \rangle\rangle = \langle n_i | \cos\hat\theta | n_i \rangle , \qquad (\text{A.7})$$

and we have used the identity

$$1 = \sum_\gamma |\gamma^0\rangle\langle\gamma^0| \equiv \sum_{(n_\gamma, q_\gamma)} |n_\gamma, q_\gamma\rangle\langle n_\gamma, q_\gamma| = \sum_{n,q=-\infty}^{\infty} |n, q\rangle\langle n, q| . \qquad (\text{A.8})$$

At this point, we must consider two possible cases: $V_{\alpha\beta} \neq 0$ and $V_{\alpha\beta} = 0$. In the first case, a nontrivial solution for the C_i requires first-order corrections to the unperturbed Floquet eigenvalues

$$\epsilon_\pm^{(1)} = \frac{1}{2}\left[V_{\alpha\alpha} + V_{\beta\beta} + \Delta\kappa^{(1)}(\delta E_\alpha + \delta E_\beta) \right]$$
$$\pm \frac{1}{2}\left\{ \left[(V_{\alpha\alpha} - V_{\beta\beta}) + \Delta\kappa^{(1)}(\delta E_\alpha - \delta E_\beta) \right]^2 + 4|V_{\alpha\beta}|^2 \right\}^{\frac{1}{2}} . \quad (\text{A.9})$$

We can then write the spacing between the two Floquet eigenvalues

$$\Delta\epsilon \equiv \epsilon_+^{(1)} - \epsilon_-^{(1)} = \lambda \left\{ \left[(V_{\alpha\alpha} - V_{\beta\beta}) + \Delta\kappa^{(1)}(\delta E_\alpha - \delta E_\beta) \right]^2 + 4|V_{\alpha\beta}|^2 \right\}^{\frac{1}{2}} + O(\lambda^2) .$$
$$(\text{A.10})$$

In order to determine the particular value of $\Delta\kappa^{(1)}$ at which the minimum spacing occurs, we solve the extremal equation

$$\left(\frac{\partial\Delta\epsilon}{\partial\Delta\kappa}\right)_\lambda = \frac{1}{\lambda}\left(\frac{\partial\Delta\epsilon}{\partial\Delta\kappa^{(1)}}\right)_{\lambda,\Delta\kappa^{(m)}} = 0 \quad (m \neq 1), \tag{A.11}$$

finding that

$$\Delta\kappa_{ac}^{(1)} = \frac{V_{\beta\beta} - V_{\alpha\alpha}}{\delta E_\alpha - \delta E_\beta}. \tag{A.12}$$

If we substitute this into Eq. (A.9), we obtain first order corrections to the eigenvalues of

$$\epsilon_\pm^{(1)} = \frac{V_{\beta\beta}\delta E_\alpha - V_{\alpha\alpha}\delta E_\beta}{\delta E_\alpha - \delta E_\beta} \pm |V_{\alpha\beta}|. \tag{A.13}$$

Therefore, we find the minimum splitting to be

$$\Delta_{\alpha\beta} = 2\lambda|V_{\alpha\beta}| + O(\lambda^2). \tag{A.14}$$

In the second case ($V_{\alpha\beta} = 0$), we find that the nearest approach of the two Floquet eigenvalues is in fact a *crossing* (to first order in λ). In this case we define $\Delta\kappa_{ac}^{(1)}$ to be the offset of this crossing, i.e.

$$\Delta\epsilon = O(\lambda^2) \quad \text{at} \quad \Delta\kappa_{ac}^{(1)} \equiv \frac{V_{\beta\beta} - V_{\alpha\alpha}}{\delta E_\alpha - \delta E_\beta}. \tag{A.15}$$

The coefficients C_i remain undetermined until the degeneracy is broken.

A.2 Second-order results with remaining degeneracy

For the case $V_{\alpha\beta} = 0$, the zeroth order states must be determined from the second order equation, which takes the form

$$(\hat{H}_F^0 - \epsilon^{(0)})|\phi^2\rangle + (\Delta\kappa^{(1)}\delta\hat{H}_F + \hat{V} - \epsilon^{(1)})|\phi^1\rangle$$
$$+(\Delta\kappa^{(2)}\delta\hat{H}_F - \epsilon^{(2)})\,(C_\alpha|\alpha^0\rangle + C_\beta|\beta^0\rangle) = 0\,, \tag{A.16}$$

Following the same procedure as in first order, we obtain

$$\begin{pmatrix} \Delta\kappa^{(2)}\delta E_\alpha + v_{\alpha\alpha} - \epsilon^{(2)} & v_{\alpha\beta} \\ v_{\beta\alpha} & \Delta\kappa^{(2)}\delta E_\beta + v_{\beta\beta} - \epsilon^{(2)} \end{pmatrix}\begin{pmatrix} C_\alpha \\ C_\beta \end{pmatrix} = \mathbf{0}\,, \tag{A.17}$$

where we have used the first-order result

$$\langle\gamma^0|\phi^1\rangle = \frac{V_{\gamma\alpha}C_\alpha + V_{\gamma\beta}C_\beta}{\epsilon^{(0)} - \epsilon_\gamma^{(0)}} \qquad (\gamma \notin \{\alpha, \beta\}) \tag{A.18}$$

with $\epsilon_\gamma^{(0)} = \langle n_\gamma, q_\gamma|\hat{H}_F^0|n_\gamma, q_\gamma\rangle$, and where we have defined

$$v_{ij} \equiv \sum_{\gamma \notin \{\alpha,\beta\}} \frac{V_{i\gamma}V_{\gamma j}}{\epsilon^{(0)} - \epsilon_\gamma^{(0)}} \qquad (i, j \in \{\alpha, \beta\})\,. \tag{A.19}$$

Again we must consider two cases: $v_{\alpha\beta} \neq 0$ and $v_{\alpha\beta} = 0$. In the first case, our procedure for determining $\Delta\kappa_{ac}^{(2)}$ is identical to that of first-order and we obtain

$$\Delta\kappa_{ac}^{(2)} = \frac{v_{\beta\beta} - v_{\alpha\alpha}}{\delta E_\alpha - \delta E_\beta} \quad \text{and} \quad \Delta_{\alpha\beta} = 2\lambda^2|v_{\alpha\beta}| + O(\lambda^3)\,. \tag{A.20}$$

In the case that $v_{\alpha\beta} = 0$, we find that $\Delta\epsilon = O(\lambda^3)$ at an offset of

$$\Delta\kappa_{ac}^{(2)} = \frac{v_{\beta\beta} - v_{\alpha\alpha}}{\delta E_\alpha - \delta E_\beta}\,. \tag{A.21}$$

A.3 Third-order results with remaining degeneracy

If the conditions $V_{\alpha\beta} = 0$ and $v_{\alpha\beta} = 0$ are satisfied, we can attempt to lift the degeneracy at order λ^3. We obtain the following results

$$
\begin{pmatrix} \Delta\kappa^{(3)}\delta E_\alpha + \mathfrak{v}_{\alpha\alpha} + \bar{\mathfrak{v}}_\alpha - \epsilon^{(3)} & \mathfrak{v}_{\alpha\beta} \\ \mathfrak{v}_{\beta\alpha} & \Delta\kappa^{(3)}\delta E_\beta + \mathfrak{v}_{\beta\beta} + \bar{\mathfrak{v}}_\beta - \epsilon^{(3)} \end{pmatrix} \begin{pmatrix} C_\alpha \\ C_\beta \end{pmatrix} = \mathbf{0}\,,
$$

$$
\text{(A.22)}
$$

where we have defined

$$
\mathfrak{v}_{ij} \equiv \sum_{\gamma,\sigma \notin \{\alpha,\beta\}} \frac{V_{i\gamma}V_{\gamma\sigma}V_{\sigma j}}{\left(\epsilon^{(0)} - \epsilon_\gamma^{(0)}\right)\left(\epsilon^{(0)} - \epsilon_\sigma^{(0)}\right)} \quad (i,j \in \{\alpha,\beta\})\,, \qquad \text{(A.23)}
$$

and

$$
\bar{\mathfrak{v}}_i \equiv \sum_{\gamma \notin \{\alpha,\beta\}} \frac{\left(\Delta\kappa^{(1)}\delta E_\gamma - \epsilon^{(1)}\right)V_{i\gamma}V_{\gamma i}}{\left(\epsilon^{(0)} - \epsilon_\gamma^{(0)}\right)^2} \quad (i \in \{\alpha,\beta\})\,, \qquad \text{(A.24)}
$$

and where we have used an expression for $\langle \gamma^0|\phi^2\rangle$ (analogous to Equation A.18) determined from the second-order equation.

These equations are nearly of the same form as those at first and second order. By the same procedure we determine

$$
\Delta\kappa_{ac}^{(3)} = \frac{\mathfrak{v}_{\beta\beta} + \bar{\mathfrak{v}}_\beta - \mathfrak{v}_{\alpha\alpha} - \bar{\mathfrak{v}}_\alpha}{\delta E_\alpha - \delta E_\beta} \quad \text{and} \quad \Delta_{\alpha\beta} = 2\lambda^3|\mathfrak{v}_{\alpha\beta}| + O(\lambda^4)\,, \qquad \text{(A.25)}
$$

for the case that $\mathfrak{v}_{\alpha\beta} \neq 0$ and $\Delta_{\alpha\beta} = O(\lambda^4)$ when $\mathfrak{v}_{\alpha\beta} = 0$.

Appendix B

Non-crossing Theorem

This appendix outlines the non-crossing theorem proven by von Neumann and Wigner [84]. The theorem states that for a generic Hermitian matrix, at least three real parameters must be varied in order to bring about an eigenvalue degeneracy. In the case of a real symmetric matrix, two parameters must be varied.

The proof is as follows. An $n \times n$ Hermitian matrix can be diagonalized by unitary transformation

$$H = U^\dagger D U \,, \tag{B.1}$$

where D is a diagonal matrix of the eigenvalues and U is a unitary matrix which, in general, has n^2 real parameters. The above equation is unchanged if U is multiplied by another unitary matrix U$'$ which commutes with D. Therefore the number of free real parameters h of the matrix H can be written:

$$h = n^2 + f - v \,, \tag{B.2}$$

where f is the number of different eigenvalues and v is the number of parameters of the unitary matrix U$'$. If all of the eigenvalues are unique, then the only matrices U$'$ which commute with D are diagonal. Therefore $f = v = n$, and $h = n^2$. If

one eigenvalue is degenerate, however, U$'$ is allowed an arbitrary two-dimensional unitary block in the degenerate subspace. Therefore $v = 2^2 + (n-2)$, and the number of free parameters in the degenerate Hermitian matrix is $h = n^2 + (n-1) - (n+2) = n^2 - 3$. We see then, that *three real parameters must be varied* in a general Hermitian matrix in order to bring about a degeneracy of eigenvalues. If the matrix H is real symmetric, a similar argument shows that at least two parameters must be varied.

Appendix C

Coherent interactions between atoms and light

In this appendix we review some of the important theoretical ideas behind modern laser cooling and trapping techniques. In particular, we derive the effective Hamiltonian for a more general system than that considered in Chapter 2. Here, we consider a two-level system, but allow for magnetic sublevels. This allows us to include multiple state behavior responsible for such effects as cooling below the recoil limit. The experimental application of such techniques in alkali atoms often involves the hyperfine splitting of a two-level system, but the model considered here will be an adequate representation.

The material in this chapter is drawn from a number of sources. In deriving the dipole approximation we follow Stenholm's book on laser spectroscopy [81]. The discussion on the rotating wave approximation and the $|j, m\rangle$ formulation of the light-atom interaction relied on Henkel and Eisert's lecture notes [34] for their Theoretical Quantum Optics class at Universität Potsdam. The discussion of effective Hamiltonians (for the ground state of a two level system) and spatially dependent light-shifts was aided by Henkel and Eisert, in addition to the papers of Graham,

Schlottman and Zoller [27], Mouchet and Delande [62], and Steck's dissertation [79].

C.1 Approximations

Before considering the two-level atom, we briefly review the origins of two common tools in simplifying such calculations: the electric dipole and rotating wave approximations.

C.1.1 Electric Dipole Approximation

We will consider an atom, described by the electron wavefunction, interacting with a monochromatic light source. The Schrödinger equation for this interaction is written in terms of the vector and scalar potentials $(\vec{A}, \varphi)$ as [81]

$$i\hbar \frac{\partial}{\partial t} \psi(\vec{r}, t) = \left[\frac{1}{2m} (\vec{p} - q\vec{A})^2 + q\varphi \right] \psi(\vec{r}, t) \qquad (C.1)$$

where $\vec{p} = -i\hbar \nabla$. A gauge transformation of the potentials by the gauge function $\chi(\vec{r}, t)$

$$\vec{A} \rightarrow \vec{A}' = \vec{A} + \nabla \chi \qquad (C.2)$$

$$\varphi \rightarrow \varphi' = \varphi - \frac{\partial \chi}{\partial t} \qquad (C.3)$$

is equivalent to the transformation of the wavefunction

$$\psi(\vec{r}, t) \rightarrow \psi' = \exp\left[\frac{iq\chi(\vec{r}, t)}{\hbar} \right] \psi(\vec{r}, t). \qquad (C.4)$$

After this transformation, Equation (C.1) becomes

$$i\hbar \frac{\partial}{\partial t} \psi'(\vec{r}, t) = \left[\frac{1}{2m} (\vec{p} - q\vec{A} - q\nabla\chi)^2 + q\varphi - q\frac{\partial}{\partial t}\chi \right] \psi'(\vec{r}, t). \qquad (C.5)$$

In order to simplify the interaction, we now make the electric dipole approximation. The fields in question are due to monochromatic radiation, so the vector potential will have harmonic form

$$\vec{A}(\vec{r}, t) = \vec{e} \cos(\vec{k} \cdot \vec{r} - \omega t)$$
$$= \frac{\vec{e}}{2} \left[e^{i(\vec{k} \cdot \vec{r} - \omega t)} + e^{-i(\vec{k} \cdot \vec{r} - \omega t)} \right]$$

(C.6)

where $\vec{e}$ is the polarization vector and the magnitude of the wave vector satisfies $k = 2\pi/\lambda = 2\pi\omega/c$. For optical light, the wavelength of the light ($\sim 10^{-7}m$) will be much larger than the size of the atom ($\sim 10^{-10}m$) and we can expect that the spatial variation of the radiation will be small around the atom. More precisely, the product $|\vec{k} \cdot \vec{r}|$ will be of order 10^{-2} and we can reasonably expand the exponential

$$e^{\pm i\vec{k} \cdot \vec{r}} \approx 1 \pm i\vec{k} \cdot \vec{r} \mp \frac{1}{2}(\vec{k} \cdot \vec{r})^2 \dots ,$$

(C.7)

and keep only the first term. Thus we make the *Electric dipole approximation*: $\exp[\pm i\vec{k} \cdot \vec{r}] \approx 1$, from which it follows that the vector potential is spatially independent:

$$\vec{A}(\vec{r}, t) = \vec{A}(\vec{R}_{atom}, t).$$

(C.8)

Armed with this simplification, we can make a gauge transformation to eliminate the vector potential entirely from the Schrödinger equation:

$$\chi(\vec{r}, t) = -\vec{A}(\vec{R}_{atom}, t) \cdot \vec{r}.$$

(C.9)

Plugging this into Equation (C.5) we find

$$i\hbar \frac{\partial}{\partial t} \psi(\vec{r}, t) = \left[\frac{\vec{p}^2}{2m} + q\varphi + q\frac{\partial \vec{A}}{\partial t} \cdot \vec{r} \right] \psi(\vec{r}, t).$$

(C.10)

If we further assume that the fields are source-free, and therefore $\varphi = 0$ and $\frac{\partial \vec{A}}{\partial t} = \vec{E}(t)$, we can write the new Schrödinger equation as:

$$i\hbar \frac{\partial}{\partial t} \psi(\vec{r}, t) = \left[\frac{\vec{p}^2}{2m} - q\vec{r} \cdot \vec{E}(t) \right] \psi(\vec{r}, t),$$

(C.11)

where we can define the dipole moment operator $\vec{d} \equiv q\vec{r}$.

C.1.2   Rotating wave approximation

The rotating wave approximation (RWA) is made to simplify many calculations in studying the interaction of atoms and single-frequency laser light. The essence of the RWA is that terms with large frequency complex exponential terms lead to small corrections in the calculations and can be neglected. These "large frequency" terms result from the multiplication of one exponential from the electric field and another from the energy separation of the two levels. Here we show, by perturbation analysis, the efficacy of this approximation and present a general rule for its application.

n-level atomic system

We consider an atomic system $H_A = \sum_n E_n |n\rangle\langle n|$ under the influence of a monochromatic laser with electric field:

$$
\begin{aligned}
\vec{E}(\vec{r}, t) &= \vec{E}(\vec{r})e^{-i\omega_L t} + \vec{E}^\star(\vec{r})e^{i\omega_L t} \\
&= 2\vec{E}_R(\vec{r}) \cos \omega_L t + 2\vec{E}_I \sin \omega_L t
\end{aligned}
$$

(C.12)

where ω_L is the laser frequency, and $\vec{E}(\vec{r}) = \vec{E}_R(\vec{r}) + i\vec{E}_I(\vec{r})$ is the complex valued electric field amplitude. The full Hamiltonian in the dipole approximation is then

$$
\begin{aligned}
H = H_A + H_{AF} &= \sum_n E_n |n\rangle\langle n| - \vec{d} \cdot \vec{E}(\vec{r}, t) \\
&= \sum_n E_n |n\rangle\langle n| - \vec{d} \cdot \left(\vec{E}(\vec{r}) e^{-i\omega_L t} + \text{ c.c.} \right) \qquad \text{(C.13)} \\
&\equiv \sum_n E_n |n\rangle\langle n| + \left(V e^{-i\omega_L t} + V^\dagger e^{i\omega_L t} \right)
\end{aligned}
$$

We now move to the interaction picture by writing

$$
|\psi(t)\rangle = \sum_n c_n(t) e^{-iE_n t/\hbar} |n\rangle \qquad \text{(C.14)}
$$

which reduces the Schrödinger equation to a set of ODEs

$$
i\hbar \dot{c}_n = \sum_m \langle n|H_{AF}|m\rangle e^{-i\omega_{mn} t} c_m(t) \qquad \text{(C.15)}
$$

where $\hbar\omega_{mn} = E_m - E_n$.

Perturbation solution of these equations are now performed by assuming $c_n(0) = \delta_{na}$.

$$
\text{Zeroth Order}: \quad \dot{c}_n^{(0)} = 0 \qquad \text{(C.16)}
$$

$$
\text{First Order}: \quad i\hbar \dot{c}_n^{(1)} = \langle n|H_{AF}|a\rangle e^{-i\omega_{an} t} \qquad \text{(C.17)}
$$

Integrating the first order equation, we find

$$
c_n^{(1)}(t) = c_n^{(1)}(0) - \frac{i}{\hbar} \int_0^t \langle n|H_{AF}(\tau)|a\rangle e^{-i\omega_{an} t} d\tau . \qquad \text{(C.18)}
$$

Using the above form for the electric field we can integrate the second term

$$\frac{i}{\hbar}\int_0^t \langle n|H_{AF}(\tau)|a\rangle = \langle n|V|a\rangle\frac{1-e^{-i(\omega_{an}+\omega_L)t}}{\hbar(\omega_{an}+\omega_L)} + \langle n|V^\dagger|a\rangle\frac{1-e^{-i(\omega_{an}-\omega_L)t}}{\hbar(\omega_{an}-\omega_L)} \quad \text{(C.19)}$$

Let's first consider the case of absorption, where the laser is tuned close to a particular transition, i.e. $E_n - E_a \approx \hbar\omega_L$, and therefore $\to \omega_{an} + \omega_L \approx 0$). The first term is then *resonant* and dominates the first order effect. The small denominator in this term will lead to a large value of $c_n^{(1)}(t)$, effecting a transition from $|a\rangle \to |n\rangle$ ($E_n > E_a$). The second term has a relatively large denominator ($\sim 2\omega_L$), is non-resonant and can be neglected. This approximation, neglecting the negative frequency component of the electric field ($E^\star e^{i\omega_L t}$ or $V^\dagger e^{i\omega_L t}$) is called the rotating wave approximation. In the case of emission ($E_a > E_n$), the second term is resonant and leads to a large $c_n^{(1)}(t)$, effecting an emission of a photon and transition to a lower energy state. The positive frequency component can be neglected here.

Application to the two-state model: Rabi revisited

We now reduce the atomic system to two states $|g\rangle$ and $|e\rangle$ with energy difference $\hbar\omega_A$. Subtracting off their average energy, we write the atomic Hamiltonian as

$$H_A = \frac{\hbar\omega_A}{2}|e\rangle\langle e| - \frac{\hbar\omega_A}{2}|g\rangle\langle g| \quad \text{(C.20)}$$

If we identify the two-dimensional Hilbert space with $\mathbb{C}^2$, making the associations $(1,0)^T \leftrightarrow |e\rangle$ and $(0,1)^T \leftrightarrow |g\rangle$, we can write

$$H_A = \frac{\hbar\omega_A}{2}\begin{pmatrix} 1 & 0 \\ 0 & -1 \end{pmatrix} = \frac{\hbar\omega_A}{2}\sigma_3 \quad \text{(C.21)}$$

117

where σ_3 is one of the Pauli spin matrices:

$$\sigma_1 = \begin{pmatrix} 0 & 1 \\ 1 & 0 \end{pmatrix} \qquad \sigma_2 = \begin{pmatrix} 0 & -i \\ i & 0 \end{pmatrix} \qquad \sigma_3 = \begin{pmatrix} 1 & 0 \\ 0 & -1 \end{pmatrix} . \tag{C.22}$$

The interaction Hamiltonian will be assumed to be off-diagonal

$$\begin{aligned}
\langle e|V(t)|g\rangle &= \langle e|V|g\rangle e^{-i\omega_L t} + \langle e|V^\dagger|g\rangle e^{i\omega_L t} \\
&\equiv \frac{\hbar\Omega}{2} e^{-i\omega_L t} + \frac{\hbar\Omega'}{2} e^{i\omega_L t}
\end{aligned} \tag{C.23}$$

where we have defined the *Rabi flopping frequency* $\Omega = 2\langle e|V|g\rangle/\hbar$. Thus we can write

$$H_{AF} = \frac{\hbar}{2} \begin{pmatrix} 0 & \Omega e^{-i\omega_L t} \\ \Omega^\star e^{i\omega_L t} & 0 \end{pmatrix} + \frac{\hbar}{2} \begin{pmatrix} 0 & \Omega' e^{i\omega_L t} \\ \Omega'^\star e^{-i\omega_L t} & 0 \end{pmatrix} \tag{C.24}$$

where we have used the fact that this matrix is Hermitian.

To simplify this model, we use the RWA. Referencing the previous section's perturbation approach, we see that

1. **Absorption** ($|g\rangle \to |e\rangle$) corresponds to $\{a = g, n = e\}$. In that case, we neglect the first term of Eq. (C.19), i.e. $\langle e|V^\dagger|g\rangle \to 0$.

2. **Emission** ($|e\rangle \to |g\rangle$) corresponds to $\{a = e, n = g\}$. In this case, the second term of Eq. (C.19) dominates and we neglect the first term, i.e. $\langle e|V^\dagger|g\rangle \to 0$.

Thus we see that the RWA amounts to setting $\Omega' = 0$. Put another way, we first eliminate the negative frequency part of $\langle e|V(t)|g\rangle$ and then use Hermiticity to determine $\langle g|V(t)|e\rangle$.

We can now write the full Hamiltonian for the two-level system as

$$H = H_A + H_{AF} = \frac{\hbar\omega_A}{2}\sigma_3 + \frac{\hbar\Omega}{2}\left(\sigma_1 \cos\omega_L t + \sigma_2 \sin\omega_L t\right) . \tag{C.25}$$

C.2 Alkali atoms interacting with lasers

The experiments we consider in this dissertation involve the interaction of neutral alkali atoms and optical lasers. The single electron in the outer shell of these atoms allows for a relatively simple energy level structure (see cesium's energy structure in Figure 2.1). Additionally these atoms have a strong transition in the optical frequency regime, making them ideal for such experiments.

Consider such and alkali atom interacting with a monochromatic laser. We will treat these atoms as effectively two-level systems (i.e. atoms in which all but a pair of levels can be neglected in the presence of an optical laser) but allow for a magnetic subsystem in each level. This picture involves the coupling of a ground state with total angular momentum j, and therefore $2j + 1$ magnetic (Zeeman) sub-levels that we denote $|j, m\rangle$ and an excited state $|J, M\rangle$. The electric dipole transition between these states is $\langle J, M | \vec{d} \cdot \vec{E}(\vec{r}, t) | j, m \rangle$, where the electric field will be treated classically.

C.2.1 Rotating wave approximation

The dipole operator has vanishing matrix elements between sub-levels of a given (total) angular momentum state, so we will write the dipole operator as

$$\vec{d} \cdot \vec{E} = P_e \vec{d} \cdot \vec{E} P_g + P_g \vec{d} \cdot \vec{E} P_e \,, \tag{C.26}$$

where $P_{g,e}$ are the projection operators onto the Zeeman subspaces of the ground and excited states, respectively. To make the RWA, we notice that the excitation part of the dipole operator $P_e \vec{d} \cdot \vec{E} P_g$ will only have a significant contribution from the positive frequency component of the electric field (see previous section). Therefore,

we can write the interaction Hamiltonian in the rotating wave approximation as

$$H_{int} = -P_e \vec{d} \cdot \vec{E}(\vec{r}) P_g e^{-i\omega_L t} - P_g \vec{d} \cdot \vec{E}^\star(\vec{r}) P_e e^{i\omega_L t} \tag{C.27}$$

where $\vec{E}(\vec{r})$ now denotes the (time-independent) complex amplitude of the electric field.

The dipole matrix elements are related to the Clebsh-Gordon coefficients known from angular momentum addition. These formulas will take the simplest form if the electric field is expanded in the eigenstates of the angular momentum operator. Choosing quantization along the z-axis, we write the unit eigenvectors for the electric field as

$$\hat{e}_0 = \hat{e}_z \quad \hat{e}_{\pm 1} = \mp \frac{\hat{e}_x \pm i\hat{e}_y}{\sqrt{2}} . \tag{C.28}$$

Thus the electric field can be written

$$\vec{E} = \sum_{q=-1,0,1} E_q \hat{e}_q \tag{C.29}$$

where we have suppressed the spatial dependence and where $E_q = \hat{e}_q^\star \cdot \vec{E}$. The matrix elements of the field then follow from

$$\langle J, M | \vec{d} \cdot \hat{e}_q | j, m \rangle = D(j, J) \langle J, M | j, m1, q \rangle \tag{C.30}$$

where the "reduced matrix element" $D(j, J)$ is independent of Zeeman level, and $\langle J, M | j, m, 1, q \rangle$ are the Clebsch-Gordon coefficients. These have the following properties:

- They are non-zero only when $m + q = M$

- They are unity for $J = j + 1$

The Rabi frequency corresponding to a particular transition can then be written

$$\Omega_{JMjm} = \frac{-2D(J,j)}{\hbar} \sum_q E_q \langle J, M | j, m, 1, q \rangle \tag{C.31}$$

C.2.2   Effective ground state Hamiltonians by adiabatic elimination

In this section we show how a far detuned laser field can induce transitions between sub-levels of the ground state. This process involves the "adiabatic elimination" of the excited state(s).

Transformation to the rotating frame

We use a unitary operator

$$U(t) = \exp\left[\frac{i\omega_L t}{2}(P_e - P_g)\right] \tag{C.32}$$

to transform to the rotating frame of the laser field, and thereby eliminate the explicit time-dependence from the Hamiltonian. The Schrödinger equation

$$
\begin{aligned}
i\hbar \frac{\partial}{\partial t}|\psi\rangle &= [H_A + H_{int}]|\psi\rangle \\
&= \left[\frac{\hbar\omega_A}{2}(P_e - P_g) - P_e\vec{d}\cdot\vec{E}P_g e^{-i\omega_L t} - P_g\vec{d}\cdot\vec{E}^\star P_g e^{i\omega_L t}\right]|\psi\rangle
\end{aligned} \tag{C.33}
$$

can be written

$$U i\hbar \frac{\partial}{\partial t}|\psi\rangle = UH_A U^\dagger U|\psi\rangle + UH_{int}U^\dagger U|\psi\rangle \tag{C.34}$$

where

$$UH_A U^\dagger = H_A \quad \text{and} \quad H'_{int} \equiv UH_{int}U^\dagger = -P_e\vec{d}\cdot\vec{E}P_g - P_g\vec{d}\cdot\vec{E}^\star P_e \tag{C.35}$$

121

and we can use

$$\left[U, i\hbar\frac{\partial}{\partial t}\right]f = Ui\hbar\frac{\partial f}{\partial t} - i\hbar\left[\frac{i\omega_L}{2}\left(P_e - P_g\right)\right]Uf - i\hbar U\frac{\partial f}{\partial t}$$

$$= \left[\frac{\omega_L\hbar}{2}\left(P_e - P_g\right)U\right]f \qquad \text{(C.36)}$$

to write

$$i\hbar\frac{\partial}{\partial t}\left[U|\psi\rangle\right] = -\frac{\omega_L\hbar}{2}\left(P_e - P_g\right)\left[U|\psi\rangle\right] + H_A\left[U|\psi\rangle\right] + H'_{int}\left[U|\psi\rangle\right], \qquad \text{(C.37)}$$

or, writing the primed Hamiltonian,

$$H' = -\frac{\hbar\Delta}{2}\left(P_e - P_g\right) - P_e\vec{d}\cdot\vec{E}P_g - P_g\vec{d}\cdot\vec{E}^\star P_e \qquad \text{(C.38)}$$

where $\Delta \equiv \omega_L - \omega_A$ is the detuning of the laser from the atomic transition.

Adiabatic elimination

Writing $U|\psi\rangle \to |\psi\rangle$ we expand into the Zeeman sub-levels of the ground and excited states:

$$|\psi\rangle = \sum_m c_m|j,m\rangle + \sum_M C_M|J,M\rangle \qquad \text{(C.39)}$$

we find that the new Schrödinger equation yields

$$i\hbar\dot{C}_M = -\frac{\hbar\Delta}{2}C_M + \frac{\hbar}{2}\sum_m \Omega_{Mm}c_m \qquad \text{(C.40)}$$

$$i\hbar\dot{c}_m = \frac{\hbar\Delta}{2}c_m + \frac{\hbar}{2}\sum_M \Omega_{mM}C_m \qquad \text{(C.41)}$$

where $\hbar\Omega_{Mm} \equiv -2\langle J,M|\vec{d}\cdot\vec{E}|j,m\rangle$, and $\Omega_{mM} = \Omega^\star_{Mm}$.

We now perform the adiabatic elimination of the excited levels. By assuming that the detuning Δ is large, and that the atom is nearly in the ground state, we

122

can assume that all coefficients c_m and C_M will contain the oscillating factor $e^{-i\Delta t/2}$ characteristic to free evolution in the ground state. We then write

$$C_M(t) = \tilde{C}_M e^{-\frac{i\Delta t}{2}} \quad \text{and} \quad c_m = \tilde{c}_m e^{-\frac{i\Delta t}{2}}. \tag{C.42}$$

If we further assume that $\dot{\tilde{C}}_M = 0$ (i.e. that the excited state is approximately constant, modulo the oscillations due to the ground state evolution), we find

$$\tilde{C}_M = \sum_m \frac{\Omega_{Mm}}{2\Delta} \tilde{c}_m. \tag{C.43}$$

Plugging this into the equation of motion for the (slowly varying) ground state amplitudes

$$i\hbar \dot{\tilde{c}}_m = \frac{\hbar}{4\Delta} \sum_{m'} \left[\sum_M \Omega^\star_{Mm} \Omega_{Mm'} \right] \tilde{c}_{m'} \tag{C.44}$$

leading to an effective Hamiltonian for the ground state:

$$H_{eff} = \frac{1}{\hbar\Delta} P_g \left(\vec{d} \cdot \vec{E}^\star \right) P_e \left(\vec{d} \cdot \vec{E} \right) P_g = -\frac{P_g H_{int} P_e H_{int} P_g}{E_e - E_g - \hbar\omega_L} \tag{C.45}$$

or

$$H^{eff}_{mm'} = \sum_M \frac{\hbar \Omega_{mM} \Omega_{Mm'}}{4\Delta}. \tag{C.46}$$

We should notice here that transitions between ground state levels involves a two photon transition. This is important when we consider optical lattices formed by counter-propagating lasers: momentum can only be transferred from lattice to atom in integer multiples of $2\hbar k$.

C.2.3 Applications

Light Shifts

As an application of the effective ground state Hamiltonian, consider transitions between $|j = 0\rangle \rightarrow |J = 1\rangle$. The only matrix element of H_{eff} is

$$\langle 0, 0 | H_{eff} | 0, 0 \rangle = \sum_M \frac{\hbar \Omega_{0M} \Omega_{M0}}{4\Delta}, \tag{C.47}$$

and the Rabi frequencies are

$$\begin{aligned}
\Omega_{M0} &= -\frac{2}{\hbar} \sum_q E_q \langle 1, M | \vec{d} \cdot \hat{e}_1 | 0, 0 \rangle \\
&= -\frac{2}{\hbar} \sum_q E_q D(0, 1) \langle 1, M | 0, 0, 1, q \rangle = -\frac{2 E_M D(0, 1)}{\hbar}
\end{aligned} \tag{C.48}$$

where we have used the fact that $m + q = M$ and that the Clebsch-Gordon coefficents are unity for $J - j = 1$. The matrix element above is then simply a function of the magnitude of the electric field:

$$\langle 0, 0 | H_{eff} | 0, 0 \rangle = \sum_M \frac{D^2}{\hbar \Delta} \sum_M |E_M|^2 = \frac{D^2}{\hbar \Delta} |\vec{E}|^2. \tag{C.49}$$

This energy is called the AC Stark shift or the light shift.

Raman transition

Now we apply the effective ground state model to a degenerate ground and excited state $(j, J = 1/2)$. In this case we have three independent matrix elements between

the two ground state Zeeman levels

$$\langle -1/2|H_{eff}|-1/2\rangle = \frac{D^2}{\hbar\Delta}\left(\frac{1}{3}|E_0|^2 + \frac{2}{3}|E_{+1}|^2\right) \tag{C.50}$$

$$\langle +1/2|H_{eff}|+1/2\rangle = \frac{D^2}{\hbar\Delta}\left(\frac{1}{3}|E_0|^2 + \frac{2}{3}|E_{-1}|^2\right) \tag{C.51}$$

$$\langle -1/2|H_{eff}|+1/2\rangle = \frac{D^2\sqrt{2}}{\hbar\Delta 3}\left(E_0^{\star}E_{-1} + E_{+1}^{\star}E_0\right) \tag{C.52}$$

$$\langle -1/2|H_{eff}|+1/2\rangle = \langle +1/2|H_{eff}|-1/2\rangle^{\star}, \tag{C.53}$$

where we have used the Clebsch-Gordon coefficients (see Henkel's Chapter 2, Fig. 2.2) connecting the two Zeeman levels of both the ground and excited levels. The "Raman transition" is that between the two ground states $|+1/2\rangle$ and $|-1/2\rangle$, which will occur when the field amplitudes E_0 and E_{+1} (or E_{-1}) are simultaneously nonzero. The transition involves the absorption of a photon with polarization 0 and emission of a photon with polarization -1

$j = 1 \rightarrow J = 1$ transitions

We now consider the transitions between two triple-degenerate levels ($m = -1, 0, +1$) in the presences of a circularly polarized light field (see Henkel's Chapter 2, Fig. 2.3). In this case, the $|j = 1, -1\rangle$ state is coupled to only the $|J = 1, 0\rangle$ and $|j = 1, +1\rangle$ sub-levels, or we can say that the $m = +1, -1$ Zeeman sub-levels of the ground state are coupled by a two photon transition.

C.3   Atomic momentum considerations

We have introduced two-level atomic systems without any consideration of the center of mass motion of the atom, or the transfer of momentum involved in absorption or emission of a photon. It is precisely this interaction, however, which allows for the laser cooling and trapping of atoms, and for the optical lattice effective Hamiltonians

considered in this dissertation. In this section, we present two methods of atomic cooling – velocity selective coherent population trapping and Raman cooling – which are based on the model systems of the previous section.

Before these two methods can be applied to an experimental system, the atoms must first be cooled to very nearly zero Kelvin by the technique of doppler cooling (or optical molasses) [31; 14]. The essence of this technique is to direct a pair of counter-propagating lasers at a cloud of atoms, with frequencies slightly red-detuned from a transition in the atom. An atom with a velocity vector pointing opposite to an oncoming laser will preferentially absorb a photon, due to the doppler shifting of the laser's frequency. This absorption gives the atom a kick of momentum $\hbar k_L$ (where k_L is the wavenumber of the laser) toward zero velocity in that dimension. If the emission of the photon is assumed to be spontaneous and therefore randomly directed, the atom suffers a net loss of kinetic energy. A schematic of this process in one dimension is shown in Figure C.1. By applying three pairs of counter-propagating lasers, the method can be used in three dimensions and a cloud of atoms can be cooled to very nearly the recoil temperature, T_r, defined by

$$k_B T_r = \frac{\hbar k_L}{2M} \, , \qquad \qquad (C.54)$$

where k_B is the Boltzmann constant, k_L is the wavenumber of the lasers and M is the mass of the atom.

C.3.1 Velocity Selective Coherent Population Trapping

In 1988, Cohen-Tannoudji and coauthors [6] proposed a new method of cooling atoms into a narrow velocity distribution with width much smaller than the single photon recoil limit. This new technique is one of a few which allows for cooling below the theoretical limits of pure doppler cooling techniques.

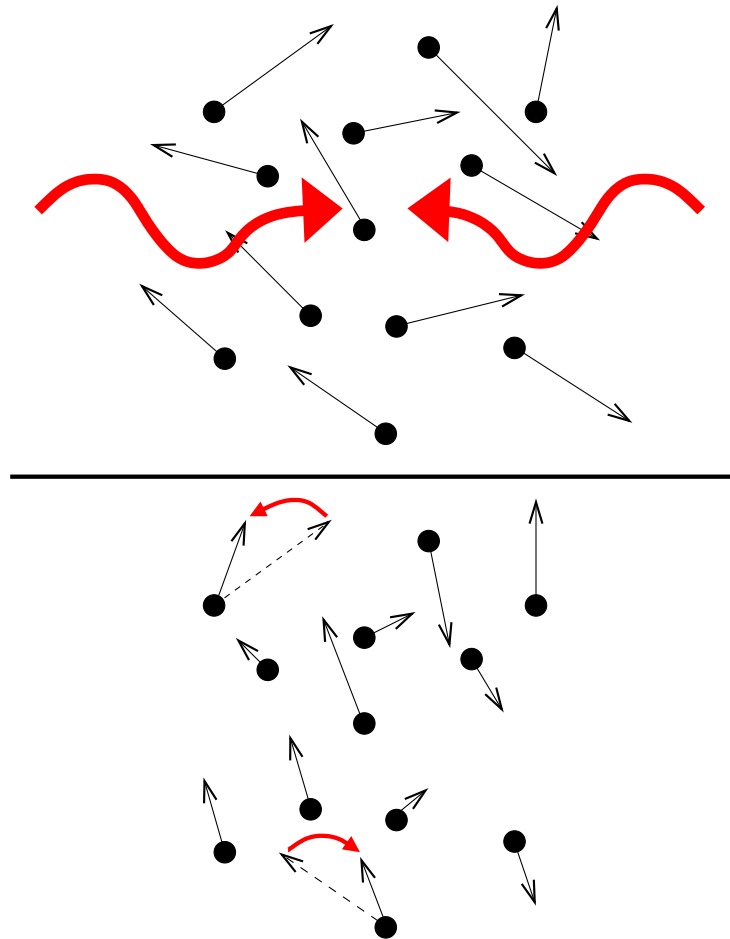The procedure was initially proposed for and experimentally demonstrated

Figure C.1: One-dimensional doppler cooling. Counter-propagating lasers impinge on a cloud of atoms with initially random thermal velocities (top). The lasers are red detuned from an optical transition in the atom, which makes absorption more likely for those atoms with velocity vectors opposing a particular beam. After application of this "optical molasses" the component of the velocity parallel to the laser beams is reduced (bottom).

on helium atom atoms with a triple degenerate ground and excited states $|g = 2^3 S_1\rangle$ and $|e = 2^3 P_1\rangle$. The atoms are first cooled to a narrow range of momentum by regular laser-cooling methods, and then subjected to two counter-propagating laser beams with the same frequency ω_L and intensities, directed along the $\pm z$-axis with σ_+ and σ_- polarizations respectively. The excited state e_0 ($m = 0$)is coupled to $g_- (g_+)$ state by stimulated emission of a σ_+ (σ_-) laser photon carrying momentum $\hbar k$ ($-\hbar k$). Thus, for each value of translational momentum p, we have a closed family of three states:

$$F(p) : \{|e_0, p\rangle, |g_+, p + \hbar k\rangle, |g_-, p - \hbar k\rangle\} \; , \qquad (C.55)$$

where the subscripts on the ground and excited states are the Zeeman values m, and $\hbar k$ is the magnitude of the laser photon, coupled by the interaction Hamiltonian

$$\langle g_\pm, p \pm \hbar k|V|e_0, p\rangle = \mp \left(\frac{\hbar \Omega_1}{2}\right) \exp[i\omega_L t] \qquad (C.56)$$

where Ω_1 is the Rabi frequency associated to each laser and the $\mp$ signs come from the Clebsch-Gordon coefficients for each transition.

Note that, for a given p, the kinetic energy difference of g_+ and g_- is $2\hbar k p/M$. One can then propose a non-absorbing, trapping state:

$$|\psi_{NA}(0)\rangle = \frac{1}{\sqrt{2}} \left[|g_-, -\hbar k\rangle + |g_+, \hbar k\rangle\right] \; . \qquad (C.57)$$

This state is stationary since the two states $|g_\pm, \pm \hbar k\rangle$ have the same kinetic and internal energies and since $\langle \psi_{NA}(0)|V|e_0, 0\rangle = 0$. Additionally, this state is radiatively stable (spontaneous emission does not effect it), so if an atom is pumped into this state, it remains trapped indefinitely. For families $F(p \neq 0)$, one can introduce

two orthogonal combinations of the ground states:

$$|\psi_{NA}(p)\rangle = \frac{1}{\sqrt{2}} \left[|g_-, p - \hbar k\rangle + |g_+, p + \hbar k\rangle \right] \tag{C.58}$$

$$|\psi_A(p)\rangle = \frac{1}{\sqrt{2}} \left[|g_-, p - \hbar k\rangle - |g_+, p + \hbar k\rangle \right] . \tag{C.59}$$

The first state is not coupled to $|e_0, p\rangle$, while the second is coupled with a Rabi frequency of $\sqrt{2}\Omega_1$. The trapping state is not stationary, however, since the kinetic energy difference of $|g_\pm, p \pm \hbar k\rangle$ is nonzero. Instead, an atom prepared in state $|\psi_{NA}(p)\rangle$ at time $t = 0$ will oscillated between $|\psi_{NA}(p)\rangle$ and $|\psi_A(p)\rangle$ with frequency $2kp/M$ (the near-degenerate tunneling mechanism). Additionally, one can show that for small values of p, the absorption rate from $|\psi_{NA}(p)\rangle$ is of the order

$$\Gamma'' = (kp/M)^2/\Gamma' \tag{C.60}$$

where $\Gamma' \approx \Omega_1^2/\Gamma$ is the absorption rate from $|\psi_A(p)\rangle$ in the case of $\Omega_1 << \Gamma$ and zero detuning, and where Γ is the spontaneous emission rate from $|e\rangle$ (see [6]). Thus, the smaller the momentum, the longer time spent in $|\psi_{NA}(p)\rangle$: velocity-selective coherent population trapping.

Thus far, only the dynamics within a given momentum family have been considered. The essential condition which allows this momentum trapping mechanism to work is that spontaneous emission redistributes atoms between different families. Along the z-axis, spontaneous emission contributes a random kick between $-\hbar k$ and $\hbar k$. Since the smaller momentum families have a longer lifetime (see previous paragraph), with longer interaction time with the lasers, atoms will accumulate into the two momentum peaks of $|\psi_{NA}(0)\rangle$ at $\pm\hbar k$ with smaller and smaller peak widths.
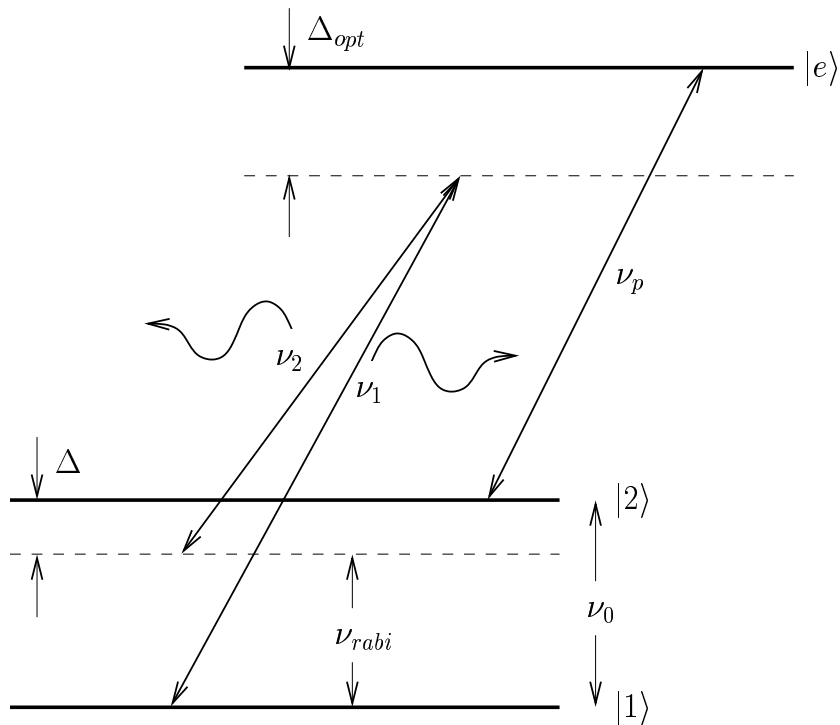
Figure C.2: The three-level Raman cooling transition (energy spacings not to scale). Counter-propagating lasers with frequencies ν_1 and ν_2 affect a Raman transition between the two ground states (effectively a Rabi system with detuning Δ). The detuning Δ of this transition allows for the velocity selection of only those atoms for which the effective transition is doppler-shifted into resonance. These atoms receive a two-photon kick toward $p = 0$. A third laser with frequency ν_p optically pumps the selected atoms back to the $|1\rangle$ state, with a fraction acquiring a velocity near zero. [Figure adapted from Kasevich & Chu [40].]

Raman Cooling

After Cohen-Tannoudji's introduction of VSCPT, Chu and Kasevich [40] proposed another multilevel method for laser cooling below the single-photon recoil limit: Raman cooling. The basic principle of this method is similar to that of Cohen-Tannoudji in that the process is velocity selective and pumps atoms into a ground state where the translational momentum of the atoms are in a very narrow band about zero. In this case, a two-level ground state is subjected to Raman transitions using a detuned optical transition to an excited level (see Figure C.2).

Considering Eqs. (C.52) and (C.53), we see that the Raman transition, resulting from adiabatic elimination of the excited level, creates an effective Rabi system between the two ground states with detuning Δ. By controlling this detuning, atoms can be velocity-selected: only those atoms for which the Rabi transition is doppler-shifted into resonance will make the transition. In Figure C.2, one can see from the orientation of the counter-propagating Raman lasers that an atom with leftward-directed velocity will be see the effective Rabi transition shifted into resonance. By reversing the direction of the two lasers, rightward-moving atoms see a resonant transition. In making the transition, the selected atoms receive a two-photon kick towards $p = 0$, while motionless atoms are unaffected. The selected atoms are then optically pumped back into the lower energy ground state by a laser with frequency ν_p, with some fraction acquiring a momentum near $p = 0$. By repeated application of such Raman pulses, with sequentially smaller detunings Δ, a large fraction of atoms will be trapped in the ground state with momentum distribution much smaller than the recoil limit.

The experimental results presented in [40] were performed on sodium atoms. The ground state of these atoms has two-level hyperfine splitting $(3S_{1/2}, F = 1, 2)$ and an excited level $3P_{3/2}$.

Appendix D

Vector spaces, linear operators and changes of basis

A vector space $\mathcal{V}$ over a field of scalars $\mathcal{F}$ is a set of elements called vectors which satisfy the property that an arbitrary linear combination of vectors

$$\sum_{i=1}^{m} f_i |v_i\rangle \quad \text{with} \quad f_i \in \mathcal{F}, |v_i\rangle \in \mathcal{V}, m \in \mathbb{N} \tag{D.1}$$

is also a vector. A set of vectors is said to span the space $\mathcal{V}$ if every vector can be written as a linear combination of the members of that set. A vector which cannot be written as a linear combination of some set of vectors is called linearly independent of that set. A set of vectors which are linearly independent and which span the space is called a basis and the number of vectors in any basis is called the dimension of the space. Thus, given a basis $\{|u_1\rangle, |u_2\rangle, ..., |u_N\rangle\}$ of an N-dimensional vector space $\mathcal{V}$, an arbitrary vector $|v\rangle \in \mathcal{V}$ can be written:

$$|v\rangle = \xi_i |u_i\rangle \tag{D.2}$$

where summation is implied over the repeated indices and the set $\{\xi_i\}$ will be called the coordinate representation of $|v\rangle$ in the basis $\{|u_i\rangle\}$. This convention, and the specification of $\mathcal{V}$ as N-dimensional, will be used throughout the rest of this section.

A transformation A which takes an arbitrary vector in $\mathcal{V}$ and returns another vector such that the operation is linear:

$$A(f|v\rangle + g|w\rangle) = fA|v\rangle + gA|w\rangle \quad (|v\rangle, |w\rangle \in \mathcal{V}) \quad (f, g \in \mathcal{F}), \qquad \text{(D.3)}$$

is called a linear transformation. The action of a linear transformation in $\mathcal{V}$ can be defined by its action on a set of basis vectors, i.e. given a basis $\{|u_i\rangle\}$, the matrix of elements a_{ij} defined by

$$A|u_i\rangle = a_{ij}|u_j\rangle, \qquad \text{(D.4)}$$

uniquely characterizes the transformation.

We can write another basis in this space in terms of the first basis

$$
\begin{aligned}
|\bar{u}_1\rangle &= R_{11}|u_1\rangle + \ldots + R_{1N}|u_N\rangle \\
|\bar{u}_2\rangle &= R_{21}|u_1\rangle + \ldots + R_{2N}|u_N\rangle \\
&\;\ldots \\
|\bar{u}_N\rangle &= R_{N1}|u_1\rangle + \ldots + R_{NN}|u_N\rangle,
\end{aligned}
\qquad \text{(D.5)}
$$

or simply

$$|\bar{u}_i\rangle = R_{ij}|u_j\rangle, \qquad \text{(D.6)}$$

where we see that R is a linear transformation from one basis to another: $|\bar{u}_i\rangle = R|u_i\rangle \, \forall i$. It can easily be shown that R has an inverse, taking each $|\bar{u}_i\rangle$ into $|u_i\rangle$. Considering an arbitrary vector which can be written

$$|v\rangle = \xi_i|u_i\rangle = \bar{\xi}_i|\bar{u}_i\rangle, \qquad \text{(D.7)}$$

we see that

$$|v\rangle = \bar{\xi}_i R_{ij}|u_j\rangle \quad \rightarrow \quad \xi_i = R_{ij}^T \bar{\xi}_j \,, \tag{D.8}$$

and $\bar{\xi}_i = R^{T-1}_{\ ij}\xi_j$.

Now consider the action of a linear transformation on two sets of basis vectors:

$$A|u_i\rangle = a_{ij}|u_j\rangle \quad \text{and} \quad A|\bar{u}_i\rangle = \bar{a}_{ij}|\bar{u}_j\rangle \,. \tag{D.9}$$

The action of this operator an arbitrary vector $|v\rangle$ can be written in either basis:

$$A|v\rangle = \xi_i A|u_i\rangle = \xi_i a_{ij}|u_j\rangle$$
$$A|v\rangle = \bar{\xi}_i A|\bar{u}_i\rangle = \bar{\xi}_i \bar{a}_{ij}|\bar{u}_j\rangle \,. \tag{D.10}$$

Rewriting the second equation, we obtain

$$\begin{aligned} A|v\rangle &= R^{T-1}_{\ ik}\xi_k \bar{a}_{ij}R_{jl}|u_l\rangle \\ &= \xi_i \left[R^{T-1}_{\ ki}\bar{a}_{kl}R_{lj} \right]|u_j\rangle \\ &\rightarrow a_{ij} = R^{-1}_{ik}\bar{a}_{kl}R_{lj} \,, \end{aligned} \tag{D.11}$$

where we recall that the transformation R is defined by $|\bar{u}_i\rangle = R|u_i\rangle$.

Appendix E

Classical dynamics and renormalization

The classical dynamical equations for the one-and-a-half degree-of-freedom (one degree-of-freedom plus time) "perturbed pendulum" system

$$H(p, \theta, t) = p^2 + \kappa \cos \theta + 2\lambda \cos \theta \cos t \,. \tag{E.1}$$

are

$$\frac{dp}{dt} = -\frac{\partial H}{\partial \theta} = \kappa \sin \theta + 2\lambda \sin \theta \sin t$$
$$\frac{d\theta}{dt} = \frac{\partial H}{\partial p} = 2p \,, \tag{E.2}$$

These two equations may be considered a subsystem of an enlarged, two degree-of-freedom system, independent of time. We can consider time to be a second angle variable, and introduce the 2 degree-of-freedom Hamiltonian

$$H_{2D}(p_1, p_2, \theta_1, \theta_2) = p_1^2 + p_2 + \kappa \cos \theta_1 + 2\lambda \cos \theta_1 \cos \theta_2 \,, \tag{E.3}$$

where we have made the association: $p \to p_1$, $\theta \to \theta_1$ and $t \to \theta_2$; and where p_2, the canonical conjugate to θ_2, has been introduced to preserve the association to time: $\dot{\theta}_2 = 1$. The dynamical equations of H_{2D} contain (E.2) as an closed subsystem.

The easiest way of visualizing a classical dynamical system with more than one degree-of-freedom is by *Poincaré section*, the intersection of the trajectories with a particular plane in phase space. A Poincaré section of the two degree-of-freedom system using the $\{p_1, \theta_1\}$ plane at $\theta_2 = 0$ is equivalent to a 2π-time strobe plot of system (E.1). Two examples of such a plot are given in Figure 3.1.

In Figure 3.1a, $\lambda = 0$ and the system is integrable. The phase space of an integrable system is sectioned into a finite number of regions foliated by nested *invariant tori* to which the dynamical trajectories are constrained [5]. In each of these regions, action-angle coordinates $\{\mathbf{J}, \mathbf{\Theta}\}$ may be introduced, the Hamiltonian can be written solely as a function of the actions $H = H(\mathbf{J})$, and the tori are labeled by the action coordinate. In our model system, we clearly have three of these regions (demarcated by the separatrices of the pendulum resonance); tori are visible in the strobe plots as a sequence of points tracing out a line. All trajectories constrained to a particular torus have the same winding number:

$$W = \frac{\omega_1(\mathbf{J})}{\omega_2(\mathbf{J})} \equiv \frac{\frac{\partial H(\mathbf{J})}{\partial J_1}}{\frac{\partial H(\mathbf{J})}{\partial J_2}} \, , \tag{E.4}$$

and we may therefore label each torus by its winding number. If the winding number of a particular torus is rational, then each orbit will be closed and will appear on the strobe plot as a finite set of points. If the winding number is irrational, the orbits constrained will never close; each will densely fill the torus. This second type of dynamics is termed *quasiperiodic motion* and will be important in the analysis of near-integrable systems. As $t \to \infty$, orbits undergoing quasiperiodic motion will appear as solid lines on a strobe plot.

136

In Figures 3.1(b), $\lambda > 0$ and the system is no longer integrable. It is visible that some of the original invariant tori have broken and the now unconstrained trajectories wander chaotically. For the parameter values shown here, this is most clearly visible near the separatrices. A number of other features in Figure 3.1 warrant comment. For each cosine term in the Hamiltonian with non-zero coefficient, there appears a pendulum-like resonance structure in the phase space. The momentum value of each of these resonances is determined by the equation

$$\frac{d\theta}{dt} = v_{phase}, \tag{E.5}$$

where, for a cosine term of the form $\cos(k\theta - \Omega t)$,

$$v_{phase} = \Omega/k. \tag{E.6}$$

Therefore, in Figure 3.1 (b), we see primary resonance structures at $p = \{0, \pm\frac{1}{2}\}$. In addition, there are visible secondary resonance structures in the phase space (for example the two-island structure at $p = \pm\frac{1}{4}$). These are the remnants of the integrable system's rational tori.

The notions of chaos and integrability illustrated in Figure 3.1 are quantified with the use of KAM theory and renormalization. KAM theorem, first proposed by Kolmogorov in 1954 [45] and subsequently proven by Arnol'd [3] and Moser [61] in the 1960's, states that most - in the sense of measure theory - of the invariant tori which foliate an integrable system will preserve under small enough perturbations. Those that survive perturbation are tori with sufficiently irrational winding numbers; those with rational winding numbers are destroyed by an arbitrarily small (generic) perturbation. In one and a half and two degree-of-freedom systems, the unbroken tori in a near-integrable state form barriers to motion in the phase space. A near-integrable one-and-a-half or two degree-of-freedom system will therefore retain much
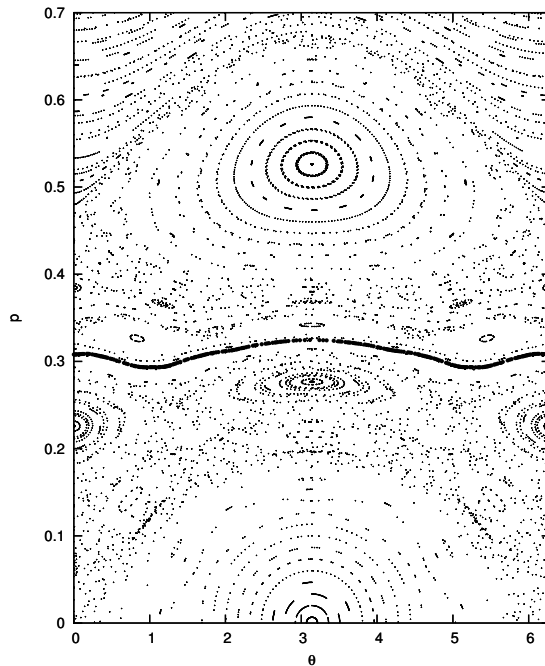
Figure E.1: A 2π-time strobed plot of system (E.1) near criticality ($\kappa = 2 \times 10^{-2}$; $\lambda = 1.0959 \times 10^{-2}$).

of the original structure of the integrable. However, as the perturbation grows larger, the invariant tori will be deformed and eventually break. As this occurs, chaotic motion will dominate in the regions between remaining tori. At some critical value of the perturbation parameters, the last of the original invariant tori will break (that with the most irrational winding number, i.e. the inverse golden mean $W = \gamma^{-1} \approx 0.618$) and global chaos will dominate the dynamics. At criticality, a given torus will break up into a cantor-like set, a *cantorus*, which will still limit the passage of trajectories. Mackay, Meiss, and Percival [57] termed this diffusion "turnstile flux".

The determination of the critical parameter values for a given Hamiltonian system is best accomplished by the methods of renormalization (see references [56; 12; 43; 42]). Following the numerical methods of [12], we can obtain the so-
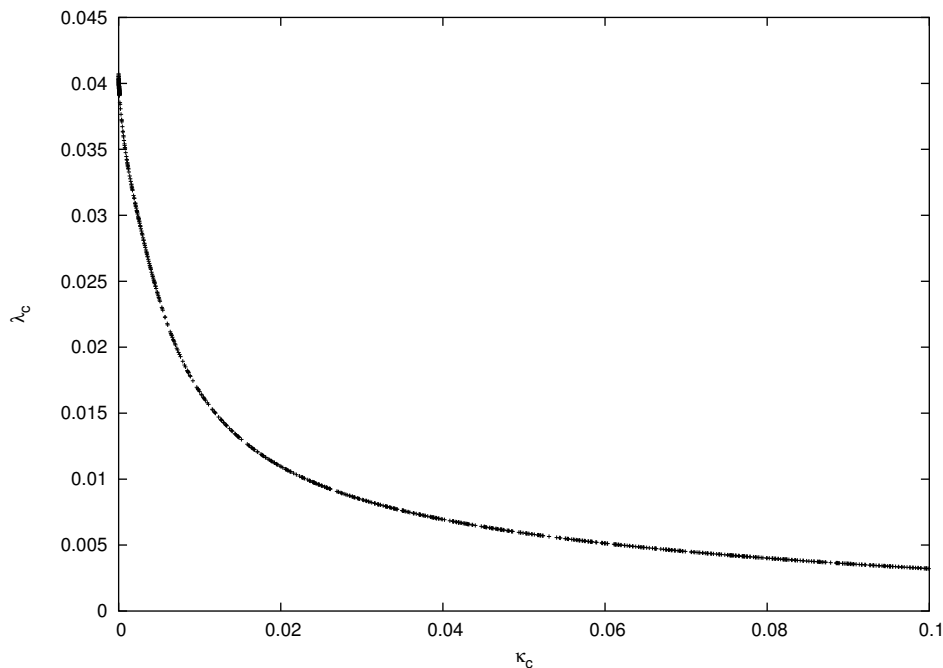
138

Figure E.2: The critical function for the model system (E.1). Each point in $\{\kappa, \lambda\}$-space represents a pair of values at which the golden torus is at criticality.

called *critical function* for the system (E.1): the set of parameter values $\{\kappa_c, \lambda_c\}$ at which the last of the original invariant tori break. For the value of κ considered in Figure 3.1, renormalization predicts a critical value of the second parameter at $\lambda_c = 1.0959 \times 10^{-2}$. A time-strobe plot of the model just below these parameter values (Figure E.1) clearly shows a phase space dominated by chaos, but divided by the remaining invariant torus (seen in bold at $p \approx 0.32$). Figure E.2 shows the set of critical parameter value pairs. For each $\{\kappa, \lambda\}$ point shown, there exists a golden torus at criticality.

We may also consider the critical parameter values at which tori of different winding numbers break. If we fix $\kappa = 0.02$, we may obtain λ_c as a function of W (Figure E.3). One can see that the most robust torus (that which has the highest value of λ_c) has winding number $W = \gamma^{-1}$. Tori with rational winding numbers
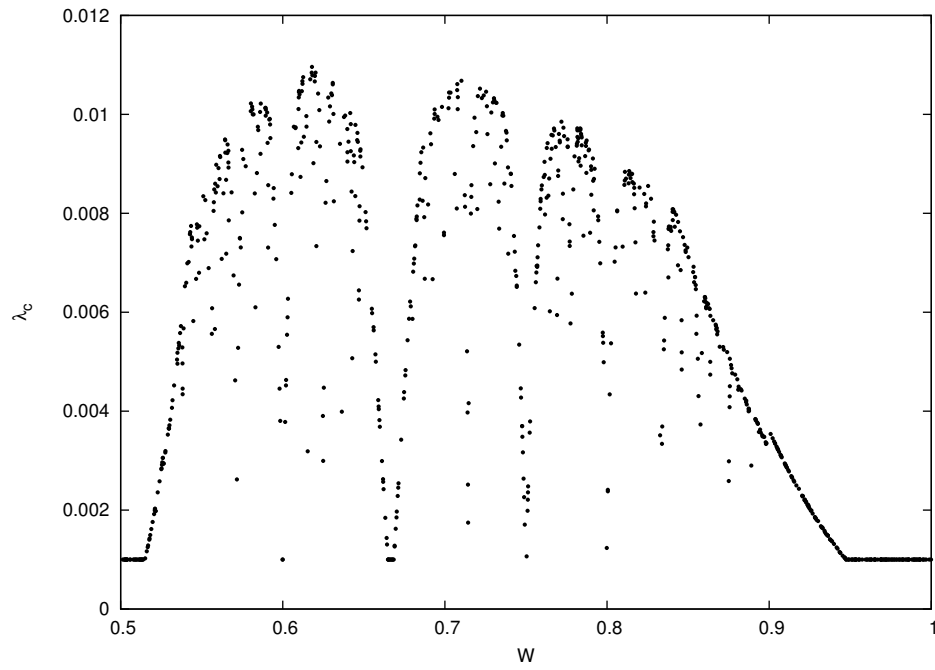
139

Figure E.3: The critical function for (E.1): λ_c as a function of winding number, with $\kappa = 0.02$.

have $\lambda_c = 0$.

Appendix F

Mathieu Functions

This Appendix reviews the process of solving the Mathieu Equation

$$\frac{d^2y}{dz^2} + (a - 2q\cos 2z)y = 0\,, \tag{F.1}$$

for the function $y(z)$ and the *characteristic value* a for a given parameter q. A primary reference on these techniques, as well as a collection of tables and figures illustrating the solutions can be found in [1]. A recent paper [29] reviews the techniques with particular emphasis on visualization techniques, while Aldrovandi and Ferreira [2] apply them to the problem of the quantum pendulum.

We will only be concerned with solutions of equation (F.1) which are periodic in z with period of π or 2π. Solutions of this type have the form

$$y = \sum_{m=0}^{\infty} A_m \cos mz + B_m \sin mz\,, \tag{F.2}$$

where B_0 can be taken to be zero. Inserting this into equation (F.1) we find

$$(a - m^2)y - 2q \sum_{m=0}^{\infty} \left[A_m \cos(2z)\cos(mz) + B_m \cos(2z)\sin(mz) \right] = 0 \tag{F.3}$$

or

$$\sum_{m=0}^{\infty} (a - m^2)(A_m \cos mz + B_m \sin mz) \qquad \text{(F.4)}$$

$$- q \left\{ A_m \left[\cos(m+2)z + \cos(m-2)z \right] + B_m \left[\sin(m+2)z + \sin(m-2)z \right] \right\} = 0 \ .$$

With a few changes of index variables and the definitions

$$A_{-m} = B_{-m} = 0 \quad \forall \, m > 0 \ , \qquad \text{(F.5)}$$

we can write

$$\sum_{m=-2}^{\infty} \left[(a - m^2)A_m - q(A_{m-2} + A_{m+2}) \right] \cos mz \qquad \text{(F.6)}$$

$$+ \sum_{m=-1}^{\infty} \left[(a - m^2)B_m - q(B_{m-2} + B_{m+2}) \right] \sin mz = 0 \ .$$

The solution (F.2) has four independent types

$$y_e = \sum_{m=0}^{\infty} A_{2m+p} \cos(2m+p)z \qquad \text{(F.7)}$$

$$y_o = \sum_{m=0}^{\infty} B_{2m+p} \sin(2m+p)z \qquad \text{(F.8)}$$

where p takes the value 0 for solutions of period π and 1 for solutions of period 2π. Using (F.6) we obtain recursion relations for the coefficients. Here we only write down those relations for $p = 0$ since the relevant solutions for the quantum pendulum problem must be of period π. For even solutions the relations are as

follows:

$$aA_0 - qA_2 = 0 \tag{F.9}$$

$$(a - 4)A_2 - q(2A_0 + A_1) = 0 \tag{F.10}$$

$$(a - m^2)A_m - q(A_{m-2} + A_{m+2}) = 0 \quad (m \geq 3) . \tag{F.11}$$

Odd solutions of period π must satisfy:

$$(a - 4)B_2 - qB_4 = 0 \tag{F.12}$$

$$(a - m^2)B_m - q(B_{m-2} + B_{m+2}) = 0 \quad (m \geq 3) . \tag{F.13}$$

In order to solve for the characteristic values a, we must collect these recursion relations into a single root-finding problem. By defining

$$G_{em} \equiv \frac{A_m}{A_{m-2}} \quad , \quad G_{om} \equiv \frac{B_m}{B_{m-2}} \tag{F.14}$$

and

$$V_m \equiv \frac{a - m^2}{q} \tag{F.15}$$

we can write equations (F.9-F.11) as

$$G_{e2} = V_0 , \tag{F.16}$$

$$G_{e4} = V_2 - \frac{2}{G_{e2}} , \tag{F.17}$$

$$G_m = \frac{1}{V_m - G_{m+2}} \quad (m \geq 3) , \tag{F.18}$$

where we write G_m when the relations are identical for even and odd solutions. For odd solutions, equation (F.18) holds in addition to

$$V_2 = G_{o4} . \tag{F.19}$$

143

Bibliography

[1] M. Abramowitz and I.A. Stegun. *Handbook of Mathematical Functions* (Chapter 20, G. Blanch), Applied Mathematics Series no. 55 (U.S. Dept. of Commerce, Washington D.C., 1972).

[2] R. Aldrovandi, P. Leal Ferreira. "Quantum pendulum," Am. J. Phys. **48**, 660 (1980).

[3] V.I. Arnol'd. "Proof of AN Kolmogorov's theorem on the preservation of quasiperiodic motions under small perturbations of the Hamiltonian," Usp. Mat. Nauk. SSSR, **18** (5) (1963), 13-40.

[4] V.I. Arnold. *Mathematical Methods of Classical Mechanics*, Grad. Texts Math. **60** (Springer-Verlag, New York, 1978).

[5] V.I. Arnold (editor).*Dynamical Systems III* (Springer, Berlin, 1988).

[6] A. Aspect, E. Arimondo, R. Kaiser, N. Vansteenkiste, and C. Cohen-Tannoudji. "Laser Cooling below the one-photon recoil energy by Velocity-Selective Coherent Population Trapping," Phys. Rev. Lett. **61**, 826 (1988).

[7] M. Ben Dahan, E. Peik, J. Reichel, Y. Castin and C. Salomon. "Bloch oscillations of atoms in an optical potential," Phys. Rev. Lett. **76**, 4508 (1996).

[8] M.V. Berry and M. Wilkinson. "Diabolical points in the spectra of triangles," Proc. Roy. Soc. Lond. **A392**, 15 (1984).

[9] O. Brodier, P. Schlagheck, and D. Ullmo. "Resonance-assisted tunneling in near-integrable systems," Phys. Rev. Lett. **87**, 064101 (2001).

[10] K.G Calkins. "Recent D1,D2 Cesium measurements," December 2006 (http://www.andrews.edu/~calkins/physics/phys699h.htm).

[11] C.E. Carroll and F.T. Hioe. "Driven three-state model and its analytic solutions," J. Math. Phys **29**, 487 (1988).

[12] C. Chandre and H.R. Jauslin. "Renormalization group analysis for the transition to chaos in Hamiltonian systems," Phys. Rep. **365**, 1 (2002).

[13] B.V. Chirikov. "A universal instability of many-dimensional oscillator systems," Phys. Rep. **52**, 264 (1979).

[14] S. Chu. "Laser manipulation of atoms and particles," Science **253**, 861 (1991).

[15] M.J. Davis and E.J. Heller. "Quantum dynamical tunneling in bound states," J. Chem. Phys. **75**, 246 (1981).

[16] A. Ya. Dzyublik. "Solution of time-dependent Schrödinger equation in a non-traditional Hilbert space," Theo. Math. Phys. **87**, 393 (1991).

[17] K. Eckert, M. Lewenstein, R. Corbalán, G. Birkl, W. Ertmer and J. Mompart. "Three-level atom optics via the tunneling interaction," Phys. Rev. A **70**, 023606 (2004).

[18] A. Einstein. "Zum Quantensatz von Sommerfeld und Epstein," Deutsche Physikalische Gesellschaft. Verhandlungen **19** (1917). [English translation in *The Collected Papers of Albert Einstein, Vol. 6*, A. Engel, trans. (Princeton Univ. Press, Princeton, 1997), p. 434.]

[19] D. F. Escande and F. Doveil. "Renormalisation method for computing the threshold of the large scale stochastic instability in two degree of freedom Hamiltonian systems," J. Stat. Phys. **26**, 257 (1981).

[20] T. Esslinger, F. Sander, M. Weidemüller, A. Hemmerich, and T.W. Hänsch. "Subrecoil laser cooling with adiabatic transfer," Phys. Rev. Lett **76**, 2432 (1996).

[21] A. Fleischer and N. Moiseyev. "Adiabatic theorem for non-Hermitian time-dependent open systems," Phys. Rev. A **72**, 032103 (2005).

[22] G. Floquet. "Sur les équations différentielles linéaires à coefficients périodiques," Ann. École Norm. Sup. **12**, 47 (1883).

[23] U. Gaubatz, P. Rudecki, M. Becker, S. Schiemann, M. Külz, and K. Bergmann. "Population switching between vibrational levels in molecular beams," Chem. Phys. Lett. **149**, 463 (1988).

[24] U. Gaubatz, P. Rudecki, M. Becker, S. Schiemann, and K. Bergmann. "Population transfer between molecular vibrational levels by stimulated Raman scattering with partially overlapping laserfields. A new concept and experimental results," J. Chem. Phys. **92**, 5363 (1990).

[25] R.M. Godun, M.B. d'Arcy, M.K. Oberthaler, G.S. Summy and K. Burnett. "Quantum accelerator modes: A tool for atom optics," Phys. Rev. A **62**, 013411 (2000).

[26] L.S. Goldner, C. Gerz, R.J.C Spreeuw, C.I. Westbrook, W.D. Phillips, P. Marte, and P. Zoller. "Momentum transfer in laser-cooled cesium by adiabatic passage in a light field," Phys. Rev. Lett. **72**, 997 (1994).

[27] R. Graham, M. Schlautmann, P. Zoller. "Dynamical localization of atomic-beam deflection by a modulated standing light wave," Phys. Rev. A **45**, R19 (1992).

[28] F. Grossmann, T. Dittrich, P. Jung, and P. Hänggi. "Coherent destruction of tunneling," Phys. Rev. A **67**, 516 (1991).

[29] J.C. Gutiérrez-Vega, R.M. Rodríguez-Dagnino, M.A. Meneses-Nava, S. Chávez-Cerda. "Mathieu functions, a visual approach," Am. J. Phys **71**, 233 (2003).

[30] M.C. Gutzwiller. "Periodic orbits and classical quantization conditions," J. Math. Phys. **12**, 343 (1971).

[31] T.W. Hänsch and A.L. Schawlow. "Cooling of gases by laser radiation," Opt. Commun. **13**, 68 (1975).

[32] W.D. Heiss and A.L. Sannino. "Avoided level crossing and exceptional points," J. Phys. Math. A **23**, 1167 (1990).

[33] W.D. Heiss and W.H. Steeb. "Avoided level crossings and Riemann sheet structure," J. Math. Phys **32**, 3003 (1991).

[34] Henkel, Eisert. Lecture Notes for Theoretical Quantum Optics II, Chapter 2, 2004 (www.quantum.physik.uni-potsdam.de/teaching/ss2004/henkeleisert.ss2004.q02.html).

[35] W.K. Hensinger, H. Häffner, A. Browaeys, N.R. Heckenberg, K. Helmerson, C. McKenzie, G.J. Milburn, W.D. Phillips, S.L. Rolston, H. Rubinsztein-Dunlop, and B. Upcroft, Nature **412**, 52 (2001).

[36] F.T. Hioe. "Theory of generalized adiabatic following in multilevel systems," Phys. Lett A **99**, 150 (1983).

[37] B.P. Holder and L.E. Reichl. "Avoided crossings in driven systems," Phys. Rev. A **72**, 043408 (2005).

[38] B.P. Holder and L.E. Reichl. "STIRAP-like transitions in a harmonically-modulated optical lattice," Phys. Rev. A, *in press*; quant-ph/0702232 (2007).

[39] K. Husimi. "Some formal properties of the density matrix," Proc. Phys. Math. Soc. Japan **22**, 264 (1940).

[40] M. Kasevich, and S. Chu. "Laser Cooling below a Photon Recoil with Three-Level Atoms," Phys. Rev. Lett. **69**, 1741 (1992).

[41] J. B. Keller. "Corrected Bohr-Sommerfeld quantum conditions for nonseperable systems" Ann. Phys. (N.Y.) **4**, 180 (1958).

[42] H. Koch and S. Kocic. "Renormalization of Vector Fields and Diophantine Invariant Tori," math-ph/02-220 (2007).

[43] S. Kocic. "Renormalization of Hamiltonians for Diophantine frequency vectors and KAM tori," Nonlinearity **18** 2513 (2005).

[44] S. Kohler, R. Utermann, P. Hänggi, and T. Dittrich. "Coherent and incoherent chaotic tunneling near singlet-doublet crossings," Phys. Rev. E **58**, 7219 (1998).

[45] A.N. Kolmogorov. "On the conservation of quasiperiodic motions under small perturbations of the Hamiltonian," Dokl. Akad. Nauk. SSSR, **98**, 527-530 (1954).

[46] E. Korsunsky. "Laser cooling during velocity-selective adiabatic population transfer," Phys. Rev. A **54**, R1773 (1996).

[47] A. Knauf and Y.G. Sinai, *Classical Nonintegrability, Quantum Chaos* (Chapter 4), DMV Seminar Band 27 (Birkhäuser Verlag, Basel, 1997).

[48] J.R. Kuklinski, U. Gaubatz, F.T. Hioe, and K. Bergmann. "Adiabatic population transfer in a three-level system driven by delayed laser pulses," Phys. Rev. A **40**, R6741 (1989).

[49] S. Kulin, B. Saubmea, E. Peik, J. Lawall, T.W. Hijmans, M. Leduc, and C. Cohen-Tannoudji. "Coherent manipulation of atomic wave packets by adiabatic transfer," Phys. Rev. Lett. **78**, 4185 (1997).

[50] L.D. Landau. "Non-Adiabatic Crossing of Energy Levels," Phys. Z. Sowjetunion 2, 46 (1932). (or "The theory of energy exchange in collisions" Vol. 1, p 88).

[51] M. Latka, P. Grigolini, and B.J. West. "Chaos and avoided level crossings," Phys. Rev. A **50**, 596 (1994).

[52] M. Latka, P. Grigolini, and B.J. West. "Chaos-induced avoided level crossing and tunneling," Phys. Rev. A **50**, 1071 (1994).

[53] M. Latka, P. Grigolini, and B.J. West. "Control of dynamical tunneling in a biochromatically driven pendulum," Phys. Rev. E **50**, R3299 (1994).

[54] R. Luter and L.E. Reichl. "Floquet analysis of atom-optics tunneling experiments," Phys. Rev. E **66**, 053615 (2002).

[55] R. Luter and L.E. Reichl. "Tunneling between Floquet states using a Bose-Einstein condensate," J. Phys. Soc. Jpn. **72**, Suppl. C, 134 (2003).

[56] R.S. MacKay. *Renormalisation in area preserving maps*, (World Scientific, Singapore, 1993).

[57] R.S. MacKay, J.D. Meiss, I.C. Percival. "Transport in Hamiltonian systems," Physica D **13**, 55 (1984).

[58] P. Marte, P. Zoller and J.L. Hall. "Coherent atomic mirrors and beam splitters by adiabatic passage in multilevel systems," Phys. Rev. A **44**, R4118 (1991).

[59] D. Martinez. "Floquet theory and continued fractions for harmonically driven systems," Ph.D. Dissertation, University of Texas at Austin, 2003.

[60] F.L. Moore, J.C. Robinson, C. Bharucha, Bala Sundaram, M.G. Raizen. "Atom optics realization of the Quantum δ-kicked rotor," Phys. Rev. Lett. **75**, 4598 (1995).

[61] J. Moser. "On invariant curves of area-preserving mappings of an annulus," Nach. Akad. Wiss. Gött., II, Math. Phys. **K1**, 1-20 (1962).

[62] A. Mouchet, C. Miniatura, R. Kaiser, B. Gremaud, D. Delande. "Chaos-assisted tunneling with cold atoms," Phys. Rev. E **64**, 016221 (2001).

[63] A. Mouchet and D. Delande. "Signatures of chaotic tunneling," Phys. Rev. E **67**, 046216 (2003).

[64] K. Na and L.E. Reichl. "Chaos-assisted adiabatic passage," Phys. Rev. A **70**, 063405 (2004).

[65] K. Na and L.E. Reichl. "Chaos-assisted adiabatic passage of molecular rotation," Phys. Rev. A **72**, 013402 (2005).

[66] K. Na, C. Jung and L.E. Reichl. "Dynamics of radiation induced isomerization for HCN – CNH," J Chem. Phys. **125**, 034301 (2006).

[67] M.K. Oberthaler, R.M. Godun, M.B. d'Arcy, G.S. Summy and K. Burnett. "Observation of quantum accelerator modes," Phys. Rev. Lett. **83**, 4447 (1999).

[68] J. Oreg, F.T. Hioe, and J. Eberly. "Adiabatic following in multilevel systems," Phys. Rev. A **29**, 690 (1984).

[69] U. Peskin and N. Moiseyev. "The solution of the time-dependent Schrödinger equation by the (t,t') method: Theory, computational algorithm and applications," J. Chem. Phys. **99**, 4590 (1993).

[70] W. Phillips and C Cohen-Tannoudji. "New mechanisms for laser cooling," Phys. Today **43**, 33 (1990).

[71] V.I. Podolskiy and E.E. Narimanov. "Semiclassical description of chaos-assisted tunneling," Phys. Rev. Lett. **91**, 263601 (2003).

[72] M. Raizen, C. Salomon and Q. Niu. "New light on quantum transport," Phys. Today **50** (7), 30 (1997).

[73] M.G. Raizen. Private communication.

[74] L.E. Reichl, *Transistion to Chaos in Conservative Classical Systems: Quantum Manifestations* (Springer-Verlag, New York, 1992).

[75] J.J. Sakurai, *Modern Quantum Mechanics* (Addison-Wesley Pub., Reading MA, 1994).

[76] H. Sambe. "Steady States and Quasienergies of a Quantum-Mechanical System in an Oscillating Field," Phys. Rev. A **7**, 2203 (1973).

[77] J.H. Shirley. "Solution of the Schrödinger equation with a Hamiltonian periodic in time," Phys. Rev. B **138**, 979 (1965).

[78] D.A. Steck, W.H. Oskay, M.G. Raizen. "Observation of chaos-assisted tunneling between islands of stability," Science **293**, 274 (2001).

[79] D. Steck. "Quantum chaos, transport and decoherence in atom optics," Ph.D. Dissertation, University of Texas at Austin, 2001.

[80] D.A. Steck, W.H. Oskay and M.G. Raizen. "Fluctuations and decoherence in chaos-assisted tunneling," Phys. Rev. Lett. **88** , 120406 (2002).

[81] S. Stenholm. *Foundations of Laser Spectroscopy*, John Wiley & Sons, New York, 1984.

[82] S. Tomsovic and D. Ullmo. "Chaos-assisted tunneling," Phys. Rev. E **50**, 145 (1994).

[83] N.V. Vitanov, T. Halfmann, B.W. Shore, and K. Bergmann. "Laser-induced population transfer by adiabatic passage techniques," Ann. Rev. Phys. Chem. **52**, 763 (2001).

[84] J. von Neumann and E. Wigner. "On the behavior of eigenvalues in adiabatic processes," Physik. Zeitschr. **30**, 467 (1929). [English translation in: R.S. Knox and A. Gold, *Symmetry in the solid state* (W.A. Benjamin, New York, 1964).]

[85] I. Vorobeichik and N. Moiseyev. "Tunneling control by high-frequency driving," Phys. Rev. A **59**, 2511 (1999).

[86] J.R. Walkup, M. Dunn, D.K. Watson, and T.C. Germann. "Avoided crossings of diamagnetic hydrogen as functions of magnetic field strength and angular momentum," Phys. Rev. A **58**, 4668 (1998).

[87] J.R. Walkup, M. Dunn, and D. K. Watson. "Branch-point structure and the energy level characterization of avoided crossings," J. Math. Phys **41**, 218 (2000).

[88] M. Wilkinson and M.A. Morgan. "Nonadiabatic transitions in multilevel systems," Phys. Rev. A **61**, 062104 (2000).

[89] S.R. Wilkinson, C.F. Bharucha, K.W. Madison, Q. Niu and M.G. Raizen. "Observation of atomic Wannier-Stark ladders in an accelerating optical potential," Phys. Rev. Lett. **76**, 4512 (1996).

[90] M. Weitz, B.C. Young and S. Chu. "Atom manipulation based on delayed laser pulses in three and four-level systems: Light shifts and transfer efficiencies," Phys. Rev. A **50**, 2438 (1994).

[91] M. Weitz, B.C. Young and S. Chu. "Atomic interferometer based on adiabatic population transfer," Phys. Rev. Lett. **73**, 2563 (1994).

[92] C. Zener. "Non-Adiabatic Crossing of Energy Levels", Proc. Roy. Soc. Lond. A **137**, 696 (1932).

Vita

Benjamin Peirce Holder was born in Schenectady, NY on February 10, 1976 to Christopher and Rebecca Holder. After graduating from Burnt Hills - Ballston Lake High School in upstate New York in 1994, he attended Wesleyan University where received a B.A. in Physics and Astronomy in May 1998. Before attending graduate school, he spent two years working in astronomy, first at the Smithsonian Observatory in Cambridge, MA and then at Maria Mitchell Observatory on Nantucket, MA. He enrolled in the physics graduate program at the University of Texas at Austin in the Fall of 2000.

Permanent Address: 14663 West Lake Rd.

Hammondsport, NY 14840

This dissertation was typeset with $\text{\LaTeX}\,2_\varepsilon$[1] by the author.

---

[1] $\text{\LaTeX}\,2_\varepsilon$ is an extension of $\text{\LaTeX}$. $\text{\LaTeX}$ is a collection of macros for $\text{\TeX}$. $\text{\TeX}$ is a trademark of the American Mathematical Society. The macros used in formatting this dissertation were written by Dinesh Das, Department of Computer Sciences, The University of Texas at Austin, and extended by Bert Kay, James A. Bednar, and Ayman El-Khashab.